Flow transformations, mud partitioning and the variable stratigraphic architecture of basin-floor fan fringes

Arnau Obradors-Latre[1,2], Peter D.W. Haughton[1] Colm S. Pierce[3], Patrick M. Shannon[1], Anthea R. Lacchia[1], Simon P. Barker[4], Ole J. Martinsen[4]

[1] UCD School of Earth Sciences, University College Dublin, Ireland, D04 V1W8

[2] Current address: Geostudi, Carrer Ter, 16, 08670 Navàs, Barcelona, Spain

[3] CASP, West Building, Madingley Rise, Madingley Road, Cambridge, CB3 0UD

[4]Equinor ASA, Sandsliveien 90, 5020 Bergen, Norway

Running title: Flow transformations and mud partitioning across submarine fan fringes

ABSTRACT

Highly efficient sediment gravity flows can bypass mid fan channels and lobes and deposit significant volumes of sand, mud and particulate organic matter in outer fan and basin plain settings. The Serpukhovian to Bashkirian fill to the Shannon Basin, western Ireland, includes deep-water fan deposits (Ross Sandstone Fm) that gradationally overlie basin floor shales (Clare Shale Fm). As part of a broader progradational succession, the upward transition from muddy basin floor to sandy fan preserves the stacked deposits of settings present prior to and outboard of mid-fan channels and lobes. Three fully cored boreholes and associated wireline data constrain the facies tracts in an 18 km long panel orientated oblique to original depositional dip. Two distal successions dominated by hybrid event beds (HEBs) are recognised, separated by a prominent condensed section. The lower Cosheen system includes m-thick, tabular HEBs with prominent linked debrites that pass down dip into much thinner sandstones overlain by sand-speckled mudstone caps that thicken distally before

thinning. The latter are interpreted as secondary mudflows released following reconstitution of more thoroughly mixed sections of the up-dip linked debrites. Significant bypass and accumulation of mud by this mechanism helped heal local topography and maintain a relatively flat sea floor promoting an overall tabular geometry for the deposits of larger volume hybrid flows reaching the distal sector of the basin. The overlying distal Ross system fringe is characterised by very fine to fine-grained sandstones and is lateral to compensationally-stacked lobes further to the west. It has a progradational (at least initially) stacking pattern, facies transitions developed over shorter length scales, and includes outsized event beds but these are thinner than those in the Cosheen system. Common banding and evidence for turbulence suppression by dispersed clay rather than entrained mud clasts indicate these were transitional flows. In this case, event beds are inferred to taper distally, with significant mud emplaced by plug flow retained as caps to sandy event beds rather than bypassing down-dip. Different flow transformation mechanisms thus impacted how mud was partitioned across the fringe of the two systems and this influenced bed geometries, larger scale bed stacking patterns and stratigraphy. Whereas the flow efficiency concept stresses the ability of flows to carry sand in a basinward direction, it is also imperative to consider the variable efficiency of mud transport given the operation of clay-induced flow transformations. These can either promote bypass or trigger premature fallout of mud with implications for how systems fill accommodation, bed -scale facies transitions and the burial and preservation of particulate organic carbon fractionated along with the clay in deep-water system fringes.

INTRODUCTION

Much attention has focussed on the role of channel-lobe systems in submarine fan construction (e.g. Piper and Normark 1983; Prélat et al. 2009; Mulder and Etienne 2010; Dennielou et al. 2017; Deptuk and Sylvester 2018; McHargue et al., 2021). Hierarchical stacking patterns have been related to avulsions driven by local deposition and elevation of the sea floor that force repeated relocation of

the flow pathways producing compensational stacking (Mutti and Sonnino 1981, Deptuck et al. 2008). The outer parts of many fan successions are thus often seen as an amalgam of thin-bedded distal lobe deposits, i.e. the lobes extend to the fan fringe where they pinch out, with the lateral and distal fringes in some cases characterised by different facies (Spychala et al. 2017a) or modified by the presence of basin floor topography (Soutter et al. 2019). Boulesteix et al. (2020) have shown how lobe hierarchies can extend beyond the sand pinch out into down-dip, thin-bedded mudstone successions and that these should also be considered part of the fan system. However, elsewhere lobes pass down-dip into sandier outer fan and basin plain sheet systems. Thus Mutti (1977; 1983) recognised that particularly efficient flows in the Eocene Hecho Group of the Jaca Basin, Spain, formed detached lobes associated with what was described as a 'virtually flat outer fan' that passed gradationally into a basin plain that also contained significant sand. Remacha and Fernández (2003) described extensive sheet-like geometries in both the lower fan lobes and basin floor in the same basin and showed that beds in the fan fringe extend onto and partly build the basin plain. More efficient flows were interpreted to pond distally to level the basin plain and compensate for the thinning of less efficient flows that dissipated before they could pond (Remacha et al. 2005). More recently, Bell et al. (2018) have questioned whether the distal Hecho Group succession is as tabular as previously inferred and point to a change in stacking from up-dip lobe compensation to less systematically stacked, down-dip and broadly sheet-like geometries. This they attribute to the presence of isolated thicker hybrid event beds (HEBs) formed by flows that interacted with and entrained mud from distal confining slopes, the idea being that the HEBs introduced local topography that prevented deposition of the normal more-organised lobe stacking patterns.

Significant questions thus remain concerning how the outer parts of submarine fans and the sandy basin plains into which they can pass distally are built, particularly in cases where flows of higher efficiency (sensu Mutti 1979) bypass sites of more proximal lobe construction, and where distal flow transformations are occurring. Turbidity currents arriving distally often do so because of a larger than average volume and/or a significant clay load (Mutti 1979; Mutti 1992). The clay is acquired by

substrate erosion (likely important in large bypassing flows) and/or inherited from the initial slope failures. Parts of the turbidity current enriched in clay will tend to undergo initial turbulence enhancement followed by turbulence damping due to an increase in near-bed cohesion (Baas et al. 2011; Baker and Baas 2020). Turbulence modulation can drive transformation from turbulent to transitional to a quasi-laminar rheology (Baas and Best 2002; Baas et al. 2009, 2011). Flow transformations will be favoured by settings where the flows are also forced to decelerate, for example at flow expansion points (e.g. downstream of avulsion nodes; Terlaky and Arnott, 2014). Where flow transformation imparts a variable rheology along and/or vertically within the flow, this can lead to complex tiered event beds including divisions emplaced by turbulent, transitional and/or laminar flow components. The resulting deposit has been termed a hybrid event bed (Haughton et al. 2009; HEB), but analogous event beds have also been referred to as slurried beds (Wood and Smith, 1958), argillaceous sandstone (Enos, 1969), slurry-flow deposits (Lowe and Guy, 2000; Sylvester and Lowe, 2004), co-genetic turbidite-debrite beds (Talling et al., 2004), tripartite beds (Muzzi Magalhaes and Tinterri, 2010), transitional flow deposits (Kane and Pontén, 2012) and matrix-rich beds (Terlaky and Arnott, 2014). Internal bed divisions often conform to a characteristic vertical pattern, ideally comprising a basal, clean (i.e. with mud matrix less than 15%), graded structureless or dewatered sandstone (H1), a banded sandstone (H2) made up, of alternating darker and paler bands, a complex mudclast-rich argillaceous sandstone and or sandy mudstone (H3) forming a 'linked debrite' (sensu Haughton et al., 2003), a thin well-structured parallel and/or ripple laminated sandstone/siltstone (H4) and a mudstone cap (H5; bed division terminology after Haughton et al., 2009).

Two aspects of the flow transformations that can occur in distal fringe settings are important. Firstly, the extent to which the hybrid event beds, either isolated or when stacked, build local topography that can then drive compensational stacking or the less organized stacking envisaged for the distal Hecho Group by Bell et al. (2018). Secondly, the fate of the mud in terms of how it is partitioned across the fan fringe will impact the wider stratigraphic architecture and distal facies tracts. Mud can fall out prematurely if flow turbulence is extinguished or it may picked up and transported further

basinward in cases where it is entrained via substrate erosion and carried in linked debris flows (sensu Haughton et al. 2003). There could therefore be significant departures from systems where lobe fringes extend to the distal fan fringe and mud ends up in very thinly bedded facies. Understanding how mud is partitioned is also important for tracing the fate of other components fractionated with it. Terrestrial organic carbon is often strongly coupled to clay (Baudin etal. 2010; Stretten et al. 2015; Blattmann et al.2019) and the mechanism whereby the carbon is carried and buried is important to the efficiency of natural carbon sequestration in deep water. Phyllosilicates can encapsulate and protect the carbon and flow transformation may result in rapid burial in thicker deposits that help limit remineralisation (Hussain et al. 2021; Hussain and Al Ramadan 2022).

The study reported here focuses on the bed types, facies tracts and inferred flow transformation processes operating across the distal fringe of Early Pennsylvanian deep-water deposits in the Shannon Basin, western Ireland (Fig. 1A,B). The Ross Sandstone Formation (hereafter Ross Fm) is part of a broader progradational succession involving an upward transition from distal basin starved shales (Clare Shale Fm) to a sandy turbidite system (Ross Fm), a muddy slope and stacked delta cycles, the whole over 2.2 km thick (Collinson et al. 1991; Martinsen et al. 2000, 2003, 2017; Wignall and Best 2000; Best and Wignall 2016). Previously, the critical upward transition from starved basin shales to an advancing sandy basin-floor fan system was known from only a single and not easily accessed section in the basin axis at Ballybunion (Fig. 1A). It has now been fully cored in three behind-outcrop boreholes; one behind the cliffs at Ballybunion, and two on Loop Head to the north and west (Fig. 1C). New stratigraphic and sedimentological constraints from these three boreholes permit a reanalysis of the arrival of the distal fringe to sandy deep-water deposits in the outer Shannon area at a level beneath the better known mid- and upper parts of the succession that represent mid and inner submarine fan environments, respectively.

Key aims of the study are to: (1) document and quantify the lateral and vertical facies relationships in the mid- to upper Clare Shale and basal/lower Ross formations over a c.18 km long transect oblique

to original depositional dip using three fully-cored boreholes and a reanalysis of the foreshore outcrop north of Ballybunion; (2) reconstruct the flow transformations taking place at a level known to be dominated by thick (m-scale) hybrid event beds (Barker 2005; Haughton et al. 2009, Pyles and Jennette 2009); (3) address how mud was partitioned across the distal fringe up-and down-dip of the sand pinch outs as a result of these flow transformations, and (4) consider the wider implications for bed stacking and the stratigraphy of outer fan and basin floor successions containing significant sand.

GEOLOGICAL CONTEXT

The mid-Carboniferous Shannon Basin in the west of Ireland (also known as the Clare Basin and the West Clare Namurian Basin; Croker 1995; Wignall and Best 2000; Sevastopulo 2009; Naylor and Shannon 2011; Martinsen et al. 2017) has a current onshore footprint of 70 by 110 km. It is particularly well known from cliff and foreshore exposures in counties Clare and Kerry around the mouth of the Shannon Estuary (Fig. 1A,C). The eastern limit of the outcrop is erosional, and the basin extends offshore to the west although its geometry here is less certain.

Basin subsidence commenced in the early Mississippian, initially with the accumulation of a thick shelfal carbonate succession, but during a rifting phase that affected much of NW Europe in the Mississippian, fault-controlled subsidence outpaced carbonate production and the Shannon area became a Viséan deep-water trough oriented approximately WSW-ENE (Leeder 1982; Strogen 1988; Strogen et al. 1996). Slumps, debris flows and calciturbidites were subsequently emplaced by resedimentation from the surrounding carbonate shelves (Dolan 1984; Somerville 2016). Whereas slopes to the north formed a low angle ramp (Hodson and Lewarne, 1961) steeper slopes to the south (Kelk 1960) likely reflect a more important underlying structural control (Martinsen *et al.* 2003). An influx of silicate clay became increasingly important in the late Visean with many of the calciturbidites including prominent fine-grained clay-rich capping divisions (Dolan 1984), culminating in the demise of carbonate production and the onset of a thick Serpukhovian-Bashkirian progradational clastic succession fed by river systems draining from the west and south-west. The

basin at the time was located in the tropics and was part of a more extensive seaway closing to the west in eastern Canada where conditions were increasingly marginal. It had an intermittent connection to the open ocean to the east (Cope et al. 1992), and to the south, the rising trans-equatorial Variscan mountains provided a topographic barrier (Bresser and Walter 1999), while their extension to the west likely provided the dominant sediment source. Syn-depositional subsidence has been linked to thermal relaxation during an early post-rift phase (Leeder 1976, 1982; de Morton *et al.* 2015). Alternatively, there may have been an element of distal flexural subsidence considering that the Variscan compressional deformation was already underway to the south (Fraser and Gawthorpe 1990; Maynard et al. 1997; Wignall and Best 2000, 2016), or further active extension may have been accommodated by local reactivation of basement structures continuing the Lower Carboniferous pattern (Martinsen and Collinson 2002; Martinsen *et al.* 2003). Deposition overlapped with a phase of glacial conditions related to the Late Paleozoic Ice Age with the expansion and contraction of multiple ice centres at high southern latitudes driving sea level fluctuations at a range of frequencies (Fielding et al. 2008; Rygel *et al.* 2008; Montañez and Poulsen 2013; Fielding 2021; Montañez 2022). Periods of high sea level were associated with reduced sediment input and the development of extensive condensed sections also referred to as marine bands (Ramsbottom 1977). These contain an ammonoid fauna that provides critical biostratigraphic control (Fig. 2).

The muddying-upward carbonate succession is overlain by the first of the main clastic formations, the Clare Shale Formation (Hodson 1951; 1954a,b; Lewarne 1959; Kelk 1960; Hodson and Lewarne 1961; Rider 1974; Figs 1B, 2). This is a unit of organic-rich, anoxic to dysoxic shales. Similar shales occur in mid-Carboniferous basins throughout NW Europe (England, Wales, Belgium and Germany; Hodson, 1957). They record a major switch from carbonate to dominantly clastic deposition which is not the same age everywhere and likely reflects a change in climate to wetter conditions and a switch in sediment supply to major hinterland river systems. The thickest development of the Clare Shale Fm in the outcrop occurs at Inishcorker (230 m; Lewarne 1959; Hodson and Lewarne 1961; Fig. 1A) from where it thins both to the north and south (10-12 m in North Clare; Hodson 1951; 1954a; 10

m in Cork; Morton 1965). Biostratigraphy shows that the top of the Clare Shale Fm is older in the axial outer Shannon area than on the flanks of the basin to the north and south where it is thinner, and a depositional hiatus is present at the base (O'Sullivan et al. 2021).

The Clare Shale Formation is transitionally overlain by the Ross Sandstone Formation (hereafter Ross Fm). The boundary is generally placed at the first significant (>5 cm-thick) sandstone bed, but biostratigraphy demonstrates that the contact varies both in nature and age depending on location. Thus, at Ballybunion (Fig. 1C, 3), the uppermost Clare Shale Fm becomes siltier and lighter grey in colour (compared to the usual black/dark grey hue) above the H_{1b} condensed section (*Homercas beyrichianum*). This distinctive character was originally highlighted by Kelk (1960) as preceding the onset of sandstone deposition. Similar transitional patterns have been observed in cores from boreholes in the Loop Head area (Pierce 2016; Pierce *et al.* 2018). However, elsewhere, the top of the Clare Shale Fm passes into thin-bedded sandstones interbedded with silty shales (the 'Ribbed beds' of Hodson and Lewarne 1961) that are then sharply overlain by thicker sandstone beds or mass transport deposits (Obradors-Latre 2017).

Rider (1974) first interpreted the Ross Fm in the Loop Head area as a submarine fan composed of an intercalation of turbidite sandstones and siltstones. Since then, numerous studies have focussed on different aspects of the deep-water sedimentology of the Ross Fm. These have dealt mainly with the mid- and upper parts of the Ross Fm that are particularly well exposed in the cliffs and foreshore on either side of the Loop Head (Fig. 1C). Thus Collinson et al. (1991) described the sedimentology and larger scale architecture of the Ross Fm inferring poorly-organised, low-relief lobes and subordinate shallow channels linked to multiple shifting sediment entry points. Subsequently, Chapin et al. (1994) highlighted the alternation of amalgamated and layered sheet geometries in the mid- to upper Ross with thickening-upwards cycles attributed to lobe deposition and scoured surfaces with megaflutes to channel-lobe transition zones. Elliott (2000a,b) related the megafluted surfaces to bypass of rare high-efficiency turbidity currents that locally deflated the fan surface and seeded channels. Lien et al. (2003) suggested that the m-scale thickening-upward cycles reflected lateral spillover from channels

as opposed to terminal lobes. Subsequently, a dominance of terminal lobe deposits fed by shallow channels was invoked by Pyles (2008), MacDonald et al. (2011), Straub and Pyles (2012), Pyles et al. (2014) and Zhang and Yilong (2020). Pierce et al. (2018) showed that locally parts of the mid- and upper Ross were characterised by hybrid event beds in addition to turbidites. There is a wide-held consensus that the Ross Fm was emplaced by sediment gravity flows sourced from the south-west (Kloster, 1987; Collinson et al. 1991; Chapin et al. 1994; Elliott 2000a,b; Martinsen et al. 2000; Wignall and Best 2000; Lien et al. 2003), but Pyles (2008) inferred a more northerly flow direction, and Rider (1974) proposed transport to the east. Nauton-Fourteu et al. (2022) have shown heavy minerals and U-Pb ages for detrital zircons and apatites are consistent with derivation from the south and southwest. The Ross Fm is transitionally overlain by the 550 m-thick Gull Island Formation, a dominantly siltstone succession with soft-sediment deformation attributed to a slope and base of slope setting (Martinsen 1987; Martinsen et al. 2003).

The basal and lower Ross Fm and its transition with the underlying Clare Shale Fm in the outer Shannon area has received less attention, partly because of the more limited exposure which is restricted to a single coastal section south of Leck Point, north of Ballybunion (Fig. 1C). Collinson et al. (1991) described a systematic upward-thickening of sandstone beds above the Clare Shale Fm. Lien et al. (2003) estimated the full thickness of Ross Fm at 460 m and informally subdivided it into lower (170 m-thick) and upper (290 m) members based on distinctive facies associations. The lower Ross Fm at Ballybunion was described as devoid of channels and characterised by tabular bed geometries. Lien et al. (2003) noted a lack of the m-scale thickening-upward cycles that characterise the upper Ross Fm, as well as apparently random occurrences of thicker beds (up to a metre-thick) in the lower Ross Fm. They also pointed to a slump 10 m above the base of the formation. Subsequently, Barker (2005) and Haughton et al. (2009) showed the basal 30 m of the Ross Fm was characterised by unusually thick hybrid event beds (>1m including the slump inferred by Lien et al. 2003) capped by a prominent condensed section (*Hudsonoceras proteus–Homoceras smithii*; $H_{2a}1$ in NW European ammonoid biostratigraphic scheme; Fig. 2). These were overlain by a succession of

thinner hybrid and transitional flow banded bed-types over the succeeding 50 m before a transition to more common turbidites with partial or complete Bouma sequences.

Pyles and Jennette (2009) also examined the section north of Ballybunion. They interpreted the basal part of the Ross Fm as containing levels of convolute bedding and slumps (in contrast to the interpretation as unusually thick hybrid event beds) and inferred that these were sourced from a local slope to the east that acted to contain the basin floor deposits. The slumps were then overlain by a 51 m-thick unit characterised by what they termed co-genetic debrite-turbidite couplets and then a succession of turbidites. The co-genetic-debrite turbidite couplets were seen as the product of turbulence-dampened (at least in part) flows that had acquired clay and mud clasts by up-dip erosion and bypass. They were inferred to be physically detached from the equivalent up-dip lobes and to interfinger with local slope failures forming a distinctive distal slope-adjacent facies association (termed a transition zone) in what was inferred to be a confined mini-basin.

Pierce et al. (2018) used new behind-outcrop cores from Loop Head to re-examine the types of event bed emplaced by sediment gravity flows in the Ross Fm. Cores from two of the boreholes traversed the contact between the lower part of the Ross Fm and the underlying Clare Shale Fm. Surprisingly, the lowermost 30 m of the Ross Fm was shown to be made of thick (up to 4 m), poorly amalgamated hybrid event beds that had medium to coarse-grained sandy H1 basal divisions (terminology of Haughton et al. 2009; Fig. 4). These were sandier and more abundant than those in the basal Ross Fm at Ballybunion. As at Ballybunion they were capped by a prominent condensed section and then a succession containing finer-grained, up to m-scale, clay-rich event beds. The behind-outcrop drilling on the Loop peninsula demonstrated that the earliest thick-bedded sandstones had a very distinct low gamma log signature (Fig. 2). Hussain et al. (2020) subsequently showed that the lower sandy components of the basal thick event beds had lower clay and mica contents than the overlying Ross Fm sandstones.

DATASET AND METHODOLOGY

The analysis reported here focusses on the characterisation and analysis of a behind-outcrop borehole derived dataset acquired at Ballybunion (12-KY-UCD-09, hereafter -09) that fully cored from the lower Ross Fm through into the Clare Shale Fm. The succession in this borehole is first contrasted to the adjacent outcrop sequence. Wider correlation to stratal equivalents in 10-CE-UCD-03 and -05 boreholes on the Loop peninsula to the north and west is underpinned by a robust biostratigraphic framework (Figs 1C,2). Together these three boreholes provide an 18 km correlation panel capturing lateral relationships in the outer part of the Ross system ahead of the establishment of the channel and lobe architecture that dominates the mid- and upper Ross Fm, and by implication the mid and inner sectors of the Ross fan complex. Paleoflow data for the basal (R5 and R10) and lower (R20) Ross Fm obtained on the foreshore north of Ballybunion (see description of outcrop below) show flows travelled towards the east and north-east so the correlation panel which is oriented broadly west to east represents a low-angle oblique to dip section with Ballybunion in a down-dip position, and Loop Head in a more proximal setting. All three boreholes have a full suite of wireline log data including gamma ray, spectral gamma, caliper, sonic, neutron, density and resistivity logs as well as orientated *Televiewer*© imagery that help constrain bedding orientations.

The -09 borehole was drilled at the end of a farm track (ITM grid reference 86926 E, 144646 N; Fig. 3) 2 km north of the town of Ballybunion and c.100 m east of the local cliff edge. It reached a total depth of 200.68 m d.d. (driller's depth) having entered the top of the Clare Shale Fm at 118.20 m d.d. The borehole was cored at PQ diameter throughout (88 mm wide core) and a full suite of wireline logs was acquired shortly after the borehole was drilled. The water table in the hole was close to sea level at 32.50 m l.d. (logger's depth) when the wireline tools were run. The borehole was vertical and bed dips average 22.3° (n=915 measurements from Televiewer© imagery) to the north with little down-hole variation. Consequentially, the 200.68 m of drilled section equates to 185.7 m true thickness (including 11.8 m of Quaternary till and rubble at the top of the hole).

The -03 borehole was drilled close to the tip of Loop Head (Grid reference 69126 E, 147155 N; Fig. 1C) to a depth of 233.60 m having encountered the boundary with the Clare Shale Fm at 183.20 m. Bed dips remained sub-horizontal down to 190 m, but began to steepen towards the base of the hole (up to 50˚ dip north) due to the subsurface projection of a Variscan fold pair exposed in the sea cliffs to the north of the drill site. The -05 borehole was drilled just to the east of Kilbaha Bay (Grid reference 77030 E, 147485 N; Fig. 1C), c.6 m from the cliff edge, and 7.9 km due east of the -03 borehole at Loop Head and 10.5 km north-west of the -09 borehole at Ballybunion. The -05 borehole was drilled to a total depth of 149.76 m. It started coring in the lower mid-Ross Fm on the western end of Kilcloher cliff and cored the boundary with the underlying Clare Shale Formation at 131.6 m. Bed dips remain at a shallow angle throughout the core (5˚ to 20˚ to the north, occasionally reaching 25˚).

Detailed 1:50 scale graphic core logs were created for -09 and the relevant parts of -03 and -05 boreholes. The graphic logs record the lithology, grain size (using a grain size comparator calibrated with thin sections), sedimentary structures, Munsell rock colour, fossil content, diagenetic features and tectonic structures including the bed dip. The nature of the bed contacts, internal event bed boundaries and event bed types (Table 1; Fig. 4) were also captured. All observations were made on clean cut core halves, both dry and wet. The core logs were then matched at 1:200 scale to a suite of wireline logs (Fig. 5). The cores were logged as along-hole thicknesses (AHT) as marked up by the driller's depths but calibrated subsequently to the *Televiewer* imagery. The gamma ray (c.32 cm vertical resolution) and spectral gamma logs were particularly useful in determining and correcting for core-to-log shifts. Dip data from the *Televiewer* were used to correct interval thicknesses to true vertical thickness to allow detailed correlation between boreholes in true vertical depth.

A modified version of the Pierce et al. (2018) Ross bed-type scheme was used to classify the different bed types (Fig. 4; details summarised in Table 1). The bed classification focusses on bed thicknesses, overall sand content and proportions of the internal divisions within different classes of event bed >

1 cm thick. Both turbidites (TB) and hybrid event beds (HEB) are defined and are grouped into four facies tracts (Fig. 4) based on stratigraphic occurrence, stacking patterns and the inferred proximal to distal trends evident in the borehole correlations detailed below. Event beds are separated by either barren 'background' siltstones (Bk) reflecting hemipelagic deposition including very thin, muddy sediment gravity flow deposits, or black, organic-rich and fossiliferous shales interpreted as times of condensed deposition (CS). Mudstones emplaced as part of an event bed can generally be distinguished on the basis of their lighter colour, the presence of suspended sand grains, and a lack of lamination or fine scale bedding. They can also be distinguished geochemically using XRF core scanning (Hussain et al. 2020). Core description was accompanied by petrographical study of targeted thin sections acquired from both outcrop samples and core plugs. These provided additional information on texture including grain size and clay content, fabrics and grain components (see also Hussain et al. 2020). In addition, bed-types, base and tops of event beds and thickness of event beds and intervening background deposits were tabulated for all the cored sections. These data were used to construct moving averages of the bed-type proportions (using a one metre sliding window) to highlight stratigraphic variations and document lateral changes in bed make-up between boreholes. Percentages cited below refer to the proportion of bed types by thickness relative to the overall thickness of each unit or subunit. Lobe hierarchy (bed, lobe element, lobe, lobe complex) follows Prélat et al (2009).

The core data were tied to the local cliff and foreshore exposures using additional outcrop logs, marker beds and photomontages constructed using oblique helicopter aerial imagery courtesy of Ordnance Survey Ireland (OSI) and web-sourced aerial images (Bing maps, Microsoft©). Mapping and structural measurements helped relate the core to adjacent outcrop sections. Field-based graphic logging at Ballybunion involved the same methodology as the core description with the addition of paleoflow measurements.

Correlation framework

A parallel reanalysis and expansion of the ammonoid biostratigraphy underpins the correlations between the boreholes studied here (Lacchia 2016; Lacchia et al. 2016). This work combined sampling of ammonoids from the cores and resampling of both previously studied and new condensed sections from 37 outcrops in the outer Shannon area. Nearly all the ammonoids were preserved as moulds of flattened shells. A relatively small number of ammonoids preserved in three dimensions were extracted from diagenetic concretions (bullions) and these specimens augmented the collections of similarly preserved material in museums. The three-dimensional specimens were used to examine and document changes in ornament with ontogeny, which then facilitated identification of flattened and fragmentary specimens.

The biostratigraphy underpins a wider ten-fold subdivision (Fig. 2) that splits the Ross Fm using the variably expressed condensed sections into units typically 70-80 m-thick and labelled R5 to R90, from base to top (Pierce et al. 2018). These are grouped as follows: basal Ross (units R5 and R10), lower Ross (R20), mid-Ross (R30 and R40) and upper Ross (R50 to R90). Many but not all the main condensed sections are characterised by a distinctive association of ammonoids and in some cases a dominant ammonoid species that can be related to the wider NW European regional scheme. The latter is the case for three main condensed sections (CS) that bracket the studied section (Fig. 2): (1) the *Homoceras beyrichianum* condensed section of $H_{1b}1$ age (late Chokierian) is the youngest CS within the Clare Shale Fm in the outer Shannon area. It is only seen on the foreshore north of Ballybunion and in the -09 borehole; the -03 and -05 boreholes did not extend deep enough to intersect it. (2) the *Hudsonoceras proteus-Homoceras smithii* CS of $H_{2a}1$ age (early Alportian) marks the top of R10 and occurs in all three boreholes, and (3) the *Homoceratoides prereticulatus* CS of $H_{2c}2$ age (late Alportian) marks the top of R20 and is again present in the two Loop boreholes. The -09 borehole entered the Ross Fm just below this level but the CS crops out both at Ballybunion and directly to the west and east of Kilbaha Bay on the south side of the Loop peninsula (Fig. 1C). In addition to the main condensed sections, subordinate condensed sections are used to split R10 and R20, respectively.

The main condensed sections are associated with unusually high gamma ray values (usually between 200 and 400 API), corresponding to high U concentrations (8 to 15 ppm) on spectral gamma logs (see Supplementary Figure) . As some of the condensed sections (e.g. at the top of R10) are several metres-thick, unit tops are placed at the most U-rich level based on the highest spectral gamma peak. Where no log data are available (for example in the outcrop), unit tops are placed at the darkest coloured, finest grained interval with the highest abundance of ammonoids. Subordinate gamma ray peaks are associated with less significant intra-unit condensed sections that aid higher resolution subdivision of R10 and R20.

The overall wireline log signature also helps support the borehole correlations. The upper part of the Clare Shale Fm has relatively low gamma API values as it is dominantly siltstone. The R10 sandstones have an unusually low gamma and a blocky log response compared to the more serrate overlying Ross sandstones, and the lower third of unit R20 shows a cleaning-upward gamma trend (Fig. 1C).

CHARACTER OF THE STACKED DEEP-WATER SYSTEMS

A series of detailed correlation panels have been constructed linking the main depositional units identified in the -09 borehole with equivalent units in the -03 and -05 boreholes guided by the correlation framework discussed above. In the following sections, the bed types and sedimentology of each of five main units identified in the -09 core (Fig. 5) are described in stratigraphic order. The five units are as follows: (1) the hot Mid-Clare Shale Fm characterised by stacked condensed sections separated by thin siltstone intervals; (2) the Upper Grey Clare Shale Fm that is dominated by stacked sand-speckled muddy event beds; (3) the basal Ross Fm containing the first sandy event beds and referred to as R5; (4) an overlying unit dominated by thick and unusually coarse grained HEBs that makes up R10, and (5) a unit of hybrid event beds and subordinate turbidites (R20) composed of fine to very fine grained sandstones, the lower part of which is characterised by a prominent sandying-upward profile. For each unit, details of the wireline log expression, the character of the unit on the

adjacent cliffs and foreshore outcrops where low tide allows beds to be followed up to several hundred metres, and the evidence for larger-scale lateral changes between equivalent sections in the -09, -05 and -03 boreholes. The key observations are then interpreted in terms of the flow processes that operated. Later sections then assess the wider system evolution, the types of flow transformation, the way in which mud was partitioned and the implications for distal stacking patterns. All depths cited below are along hole from the surface based on matching the cores to the *Televiewer* images. All thicknesses are true thicknesses corrected for tectonic dip. Percentages cited below refer to the proportion of bed-types by thickness for each of the units or subunits.

'Hot' mid-Clare Shale Formation

-09 Core: The lower part of the Clare Shale succession cored in the -09 borehole (200.60 m to 155.20 m) is characterised by an alternation of dark grey, barren, organic-rich and mostly structureless silty mudstones (Bk 56.9%; Munsell colour N2-3) with rare early carbonate or pyrite concretions and dark grey to black (N1), laminated mudstones (CS 38.1%) with abundant ammonoids which mostly occur as compressional casts but locally are pyritised and preserved in 3D (Figs 6, 7A,B). The dark mudstones contain several ammonoid species that have not been identified in the core, but which have been described on the adjacent foreshore by Kelk (1960). They also contain bivalves (*Dunbarella*), broken shell material and common carbonaceous organic matter. Both types of mudstone are interbedded with minor siltstone beds speckled with floating sand grains (distal HEB8 2.2%). These beds have rare basal, mm-scale, laminated very fine-grained sandstones overlain by siltstone caps a few cm-thick. In addition, a distinctive package (2 m-thick), comprising a series of thin carbonate-rich beds (2.8%; Fig. 7A) contains sparse thin-shelled ostracods and ammonoid shell fragments. These beds are mm- to cm-thick and they have loaded bases and show grading towards the top where they are capped by a thin mudstone. The frequency and scale of the calcareous beds increases upward, and they contain abundant carbonaceous matter. Petrography reveals they have a very fine-grained texture with a bimodal association of paler coloured (N7-8) bioclastic bands with a

coarser dolomite cement and darker coloured (N4-5) bands mostly composed of a micritic matrix with scattered larger calcareous bioclasts partially replaced by dolomite.

Log response: Overall, the unit has a very high and serrate gamma ray response (Fig. 5) that drifts to slightly lower values upwards, paralleled by an increase in siltstone content and proportion of silty mudstones (Bk facies), but averages c.220 API with peaks rising to over 350 API associated with elevated U concentrations of 10 to 15 ppm and very low Th on the spectral gamma log (Supplementary Figure). In contrast, the calcareous package stands out as having very low gamma ray values down to less than 50 API and an associated reduction in the U content (Fig. 5).

Link to adjacent outcrop: In the cliffs and on the foreshore c.300 m south of the borehole (Fig. 3), the unit comprises the same alternation of barren (Bk) and ammonoid-rich mudstones (CS) with six ammonoid-bearing levels together with a prominent package of dolomitic calcareous sandstones similar to that encountered near the base of the cored section (Fig. 6). Kelk (1960) recognised ammonoids extending from *Cravenoceratoides nitidus* (E_{2b}) biozone at the level corresponding to the base of the core, to *H. beyrichianum* (H_{1b}) at the top of the unit . Overall, the unit shows a significant lateral variation in thickness, from 26 m in the cliff and foreshore, to 46.7 m in the -09 borehole (Fig. 6).

Correlation to -03 and -05 boreholes: Neither of the two boreholes on the Loop peninsula reached to this level in the stratigraphy or encountered ammonoid-rich shales within the Clare Shale Fm. Both reached total depth (TD) in siltstones correlated with the overlying Upper Grey Clare Shale Fm (see below).

Interpretation: This unit comprises an alternation of ammonoid-bearing and barren mudstones interpreted to reflect changing water column conditions. The high gamma response, U content and pelagic fauna concentrated in the dark mudstones suggests these were times of relatively condensed deposition and correspond to times of marine flooding. The Kelk (1960) ammonoid biostratigraphy suggests the unit extends from the Arnsbergian to the Chokierian and given the time calibration

reported by Waters and Condon (2012) this would correspond to approximately 5 Myr of deposition. The condensed sections are separated by barren mudstones (Bk) that are relatively thin so these must also be condensed. They are interpreted as hemipelagic deposits, but silty event beds (HEB8) some with floating silt and sand grains, appear intermittently suggesting some of the mud was emplaced by muddy sediment gravity flows (cf. Emmings et al. 2020). The northward increase in overall thickness between the outcrop and where the equivalent deposits were cored suggests a possible north- to north-west facing slope draped by the condensed sections but with enhanced accumulation of muddy event beds from flows rarely sweeping the base of slope. The bundle of dolomitised carbonate beds may represent calciturbidites transported down the local slope. The overall thickness of the unit in the borehole is not dissimilar to the thickness (24 m) between the *Nuculoceras nuculum* ($E_{2c}2$) and *H. beyrichianum* ($H_{1b}1$) condensed sections in the GSI 09/04 borehole in the axis of the basin at Inishcorker in the inner Shannon 50 km to the east (Obradors-Latre 2017; Fig. 1A) implying a period of widespread condensed deposition in the basin at this time.

Upper Grey Clare Shale Formation

-09 Core: This 34.4 m thick unit is distinguished from that beneath it by the absence of well-expressed ammonoid-bearing high-gamma mudstones, and a switch to increasingly common bedded siltstones, many of which have floating sand grains, and in the upper part of the unit, more abundant very thin basal sandy divisions (HEB8). The base of the unit is placed just above the *H. beyrichianum* (H_{1b}) condensed section (at 155.20 m), and the top at the base of the first sandstone >5 cm-thick corresponding to the base of the Ross Fm (at 117.95 m). The unit is split into lower and upper subunits by a prominent thick (1.6 m) muddy event bed (HEB2b), the base of which is at 131.80 m. This has a mm-thick fine-grained sandstone base, a thick sand-speckled central muddy division and a thick structureless mudstone cap. The base to this event bed marks a step change in event bed scale and expression, and in the overall sand content of the succession (although this is still low <5%).

The lower subunit is 21.6 m-thick and dominated by dark coloured (N3), commonly black (N1) mudstones that are largely barren (Bk 80.5 %). Pyrite concretions are rare, but carbonate concretions are regularly distributed every few centimetres to decimetres. Towards the top of the sub-unit, sporadic siltstone-rich beds speckled with floating sand grains appear (HEB8; 19.5%; Fig. 7C). These have rare basal mm-scale, laminated very fine-grained sandstones overlain by speckled siltstone caps a few cm-thick.

The upper subunit is 13.6 m-thick and has prominent stacked silty event beds (HEB8 61.6%), most of which now have very thin, very fine- to fine-grained, basal sandstones (mm-scale) and overlying decimetre-thick, silty mudstone divisions with scattered suspended sand grains up to fine sand grade (Fig. 7D). Banding and silty pseudonodules commonly occur at the interface between the basal sandstone divisions and the sand-speckled mudstones, and thin capping dark-coloured mudstones can contain ammonoids and carbonaceous woody fragments. The thickness of the basal sandstones is crudely proportional to the total event bed thickness, and sandstone divisions become more prominent upwards. These clay-rich, grey-coloured (N4) HEB8 beds are interbedded with subordinate, very dark-coloured (N2-3) barren shales (Bk 26.7%) that are faintly laminated and lack floating sand grains. Local folding of the bedding occurs at 128.1 m. HEB8 increase toward the upper part of the sub-unit. These display a subtle thickening-upward trend that is also paralleled by an increase in siltstone.

Wireline log response: The gamma log profile (Fig. 5) picks out the two subunits clearly. The lower subunit has a less variable response that shows a gentle upward decline in values to around 200 API. The upper subunit is more variable with higher values (up to 275 API) coinciding with thick and faintly laminated mudstone caps to some event beds.

Link to outcrop: Kelk (1960) recognised that the upper part of the Clare Shale Fm on the foreshore is a paler grey colour (N5-6) and referred to this interval as the Grey Clare Shale. The paler siltstones form a slightly elevated wave-cut platform extending further seaward than the units below and

above (Fig. 3), emphasising they are mechanically more resistant on account of the silty texture and reduced amount of clay. The thin sandy basal laminae and laminae sets, and the sand-speckled and pseudonodular mudstone caps, are not as obvious on the foreshore, partly on account of near surface weathering. There is a significant variation in the thickness of the unit over the 250 m from the borehole to the foreshore exposure. The lower subunit thins from 21.6 m in the -09 core to 7.2 m in the outcrop (Fig. 6). A trend towards a gradual change from well-laminated to more structureless mudstones over the cored section of this sub-unit is not as obvious in the outcrop on account of weathering. The upper subunit thins from 12.6 m in the core to 7.7 m in the outcrop (Fig. 6).

Correlation to -03 and -05 boreholes: The wireline log character suggests the subdivision into a lower more homogenous and upper more variable subunit separated by a thick, muddy event bed (HEB2b) that can be followed laterally to the -03 and -05 boreholes (Fig. 8). The lower subunit has more abundant HEB8 in -03 (71.7%) compared to -09 where Bk mudstones dominate, and a higher proportion of the HEB8 have a basal sandstone in the up-dip -03 borehole. The latter have laminations (both parallel and rare ripple lamination), overlain by silty pseudonodules and scattered sandstone grains floating in darker mudstone matrix. Darker Bk mudstones account for only 27.9% in the case of -03. The number of HEB8 in the -03 and -09 boreholes is similar (52 event beds in each core) but the subunit is not fully cored in -03 so this is a minimum value. The overall thickness of the lower subunit is at least 28.4 m in -03 (the base is not cored) compared to 21.6 m for the full subunit in -09. HEB8 at Loop Head in the west are thus thicker, sandier and likely more numerous. The -05 core only drilled an estimated 4.4 m into the Lower Grey Shale and shows broadly similar bed mix and proportions to the -03 core, but there is insufficient core to be conclusive at this level. The event beds in the -09 and -03 sections preserve a subtle thickening-upward trend that is also paralleled by an increase in siltstone. Sandstone percent also increases upward in the -03 core (c.5%), but this is much less obvious in the -09 borehole where the basal sandstone divisions are rare at this level.

The upper subunit continues the overall sandying-upward trend in all three boreholes. It is 14.9 m-thick in the -03 core, 13.5 m in -05 and 12.8 m in -09. As in -09, this unit initiates with an unusually

thick (>1.5 m) HEB2b, the base of which is at 199.80 m in -03 and at 145.10 m in -05 (Fig. 8). The basal division of this event bed is very fine-grained sandstone up to only a cm-thick, followed by distorted mudstone laminations and silty pseudonodules. The remainder of the subunit consists of a similar interleaving of deposits to the -09 core, although HEB8 is now more important than Bk mudstones. The total number of event beds is similar in all three boreholes (27-29 beds, Fig. 8) which given the thickness changes reflects a gradual thinning of the beds east to Ballybunion. The mudstones rarely contain ammonoids (e.g. 185.6 m in -03 and 122.20 m in -09; Fig. 8). Thin basal sandstones to HEB8 are well developed in the -03 core (cm-scale) and to a lesser extent in the -05 and -09 boreholes (mm-scale) with 29, 19 and 15 sandy bases in each borehole, respectively, and a tendency in all three boreholes for these to be best developed towards the top of the subunit. The thickness of the basal sandstones is crudely proportional to the total bed thickness, with pseudonodules and mudstone clasts and coarser floating sand grains common at the base of the dominant upper siltstone divisions. In contrast, a few sandier though still overall muddy, m-thick HEB2 (31.1%) occur interbedded within the Upper Grey Clare Shale in -03, and these show large pseudonodules decreasing in size upwards and deformed sandstone clasts within an organic-rich silty matrix, above cm-thick and fine-grained basal sandstones. Local folding and rotation of bedding occurs from 194.50 m to 191.30 m in -03 at a level where diagenetic concretions are also developed. Similar features occur in analogous stratigraphic positions at 141.90 m in -05 and at 128.1 m in -09, although the intensity of the bed disruption diminishes from west to east.

Interpretation: The distinctive HEB8 indicate flows that had some turbulent component to emplace basal sandy divisions with current-generated structures, or transitional rheology (i.e. intermediate between turbulent and laminar rheology) in cases where the basal sand is structureless or banded. It is possible some of the thinner structureless basal sandstones settled through a weak fluid mud suspension (Sumner et al. 2008). The events beds (HEB8) are dominated by sand-speckled silty mudstone divisions indicating laminar flow and emplacement as a debris flow. Hussain et al. (2020) showed the sand-speckled mudstones can have variable grading patterns indicating they had a range

of rheology; poorly graded examples had higher strengths to the extent sand grains were unable to settle vertically. The darker mudstones sometimes cap the sand-speckled siltstones (Fig. 7D), and locally form thicker stand-alone beds that may represent periods of background settling but could also be more rapidly emplaced mudflows.

The lateral trends in the lower sub-division with the eastward loss of the basal sandstone laminae and the transition from siltstone to increasing proportions of mudstone suggest the turbulence in even the front of the flows eventually was dampened. Except for the thicker HEB2b, the event beds are relatively thin, and the bed numbers and overall thickness decline eastwards suggesting gentle tapering of both the unit as a whole and the event beds within it. This indicates the flows were relatively fluid, despite the clay content, and that they were able to spread and travel at least 18 km. There is no sense of compensational stacking patterns generated by local depositional relief. The more rapid thinning evident between the -09 borehole and the outcrop 250 m to the south is interpreted as passive onlap onto a slope previously draped by the older condensed sections. The absence of condensed sections within the unit is consistent with an increase in the rate of deposition. HEB8 are thus interpreted to have healed subtle topography so that when the thicker lowermost Ross event beds were emplaced (units R5 and R10), the base of slope was levelled. The gradual decrease in the gamma ray response in the boreholes is consistent with gradual outbuilding of a silty fringe and overall progradation or growth of the system from the west or southwest.

Basal Ross Formation - Unit R5

-09 Core: This first unit of the Ross Fm (R5) is 10.5 m-thick in the -09 borehole (Fig. 5) and contains two isolated HEB2b (16.1%) separated by common HEB8 (64.7%) resembling those in the underlying Upper Grey Clare Shale Fm together with subordinate Bk mudstones. The base of R5 and of the Ross Fm is placed at the base of a 0.6 m-thick, isolated HEB2b with a clay-rich basal fine-grained sandstone (Fig. 7E). The top is marked by a switch to a package with a more restricted grain size profile and an

alternation of barren (Bk) and fossiliferous (CS) mudstones (19.2%), the latter with abundant ammonoids and carbonaceous organic matter and minor interbedded thin sandstone beds. The lower sandier event bed (base at 117.95 m) comprises a fine-grained, dewatered sandstone (H1) sharply overlain by highly argillaceous sandstone with basal banding (H2) and scattered pseudonodules set in a sand-speckled muddy sand matrix (H3) and capped by a mm-thick laminated very fine-grained sandstone (H4) and a structureless mudstone cap (H5). A second thicker HEB2b (1.3 m-thick) occurs in the upper part of the unit (base at 109.85 m; Fig. 9). This is again a clay-rich sandstone, the basal part of which reaches medium-sand grade; its structure resembles that of the lower sandy event bed.

Wireline log response: The gamma ray log has a serrate response with low peaks of c.120 API coinciding with the lower sandy parts of the pair of thicker event beds (117.95 m and 109.85 m). There are also higher peaks of 230 API that coincide with rare thin and ammonoid-bearing CS mudstones (at 113.60 m; Fig. 5).

Link to outcrop: The pair of thicker event beds crop out in the cliffs and on the foreshore 200 m south of the borehole with little change in thickness, spacing or character. The overall thickness of the unit measured in the outcrop matches that in the -09 core, in contrast to the underlying Clare Shale Fm units that are thinner in the outcrop (Fig. 6). The CS mudstones with sparse ammonoids marking the top of R5 are also found in the outcrop (Fig. 9). Paleoflow directions from groove and flute marks in the outcrop, with sense of flow from flutes, indicate flow towards the NE for the lowermost Ross (vector mean 35˚, n=17).

Correlation to -03 and -05 boreholes: When traced to the west, a cluster of three thicker sandy event beds occur in the -03 borehole at Loop Head; a central thicker HEB2a (2 m-thick) with thinner and muddier HEB2b above and beneath (Fig. 8). The base of the Ross is placed a little deeper at a HEB2a with a basal sandstone 5 cm-thick at 183.20 m. The base of R5 in the -05 borehole 8 km to the east is a HEB2b similar to that in -09, albeit a little thicker, and this is tentatively linked to the 2 m-

thick HEB2a above the base of the unit in -03 (Fig. 8). R5 is capped by a mudstone-dominated CS facies with abundant ammonoids and carbonaceous organic matter, and minor interbedded thin sandstone beds in all three boreholes (Fig. 10).

Sandy HEB2a and 2b make up a significant part of the R5 unit (41.1%) in -03, with reduced proportions of HEB8 (43.9%), now invariably with basal sandstone laminae, and relatively uncommon Bk mudstones (12.1%). The central and thicker HEB2a in -03 has a lower medium-grained, dewatered basal sandstone (H1), sharply overlain by deformed sandy mudstones with common mudstone chips and larger clasts (H3), capped by homogeneous mudstones (H5). The underlying HEB2b includes a thin laminated sandstone H4 division. When traced laterally, just a single HEB2b is present in -05 (62 cm-thick) and no sandstone thicker than 5 cm occurs beneath this level. As in -09, stacked HEB8 (65.5%) continue to isolate the thicker event beds (20.6%) and are more abundant than Bk silty mudstones (10.8%) in -05.

The younger of the two thicker event beds in -09 may extend through all three boreholes (169.6 m, 123.05 m and 109.85 m in -03, 05 and -09, respectively) with the gamma log expression implying a change to a thinner, muddier expression when traced to the east. While no clear vertical stacking pattern is seen in the boreholes, decreasing numbers of HEB8 are observed from west to east, with 33 event beds in -03, 26 in -05 and only 22 in -09. Consequentially, the whole unit is the thickest and has the highest net sand content in the west (18.6%), whereas overall sand content decreases to the east (13.9% in the -05 and 7.1% in the -09 borehole).

Interpretation: R5 is mostly composed of HEB8 silty event beds with thin sandy basal divisions, punctuated by occasional thick HEB2a and 2b. The HEB8 resemble those in the underlying Upper Grey Clare Shale Fm and are similarly interpreted as products of transitional and hybrid flows transformed from sandier flows up slope. The occurrence of similar silty event beds in both the basal Ross Fm and the upper Clare Shale Fm indicates the latter is genetically linked to the former and together they represent the distalmost fringe of a sandier system that lay to the southwest/west.

The diachronous base of R5 likely steps up to the east as sandstones thin in this direction (Fig. 8). The lower of the pair HEB2b in -09 is correlated with a thicker sandy event bed up-dip; the correlation is supported by a consistent thinning and a change to increasingly muddy composition from west to east. HEB3a and b are interpreted as products of hybrid flows triggered by substrate entrainment and in which the linked debris flows had evolved via mud clast disintegration and incorporation of sand from beneath to form a significant part of the event bed.

R5 is capped by a CS mudstone with abundant ammonoids and carbonaceous organic matter, and minor interbedded thin sandstone beds (TB4-6) in all three boreholes. This is interpreted as a minor condensed section containing specimens of *Homoceras*/*Hudsonoceras cf.* genus (Lacchia 2016) that heralds an important vertical step change in event bed character and overall lithology between R5 and R10.

Basal Ross Formation - Unit R10

-09 core: Unit R10 comprises a 24.0 m-thick association of medium to coarse-grained (Figs. 5, 11), unusually thick (up to 3 m) HEB1b and HEB2a (47.0%) which are interbedded with thinner HEB8 (52.6.0%) and subordinate background and condensed mudstones (8.6%; Figs 5, 12A-F).

Close to the base of the unit at 104.50 m, a 1.4 m-thick, clean (clay-poor) although rather dark-coloured medium to coarse-grained sandstone occurs at the base of the first thicker event bed (HEB1b). This is structureless to locally banded or dewatered with contorted sheets and pipes (H1/H2). The sandstone is directly overlain by a >1.5 m-thick argillaceous sandstone starting with a 1.1 m-thick clay-rich division (H3) containing cm- to dm-long sheared mudstone clasts and scattered sand clasts and pseudonodules, accompanied by sand-injections (up to a few cm across), and capped by a 45 cm-thick sand-speckled mudstone (H5). This event bed is followed by a HEB8-dominated subunit extending from 101.38 m to 92.95 m. This separates the underlying isolated HEB1b from another four similarly thick (m-scale), medium- to coarse-grained sandstone beds and associated

overlying mudclast-rich sandstones (all HEB2a) in the upper part of the unit (Figs 9,10,11). These event beds are all capped by very fine-grained banded or ripple-laminated sandstones (3.0%; H4) and thin mudstone caps (H5). The thicker event beds are separated vertically by sand-speckled HEB8 (52.6%). A particularly thick (>10 m) ammonoid-rich and carbonaceous mudstone (CS) interval straddles the top of the unit (from 82.40 m to 73.20 m; with the highest gamma and top of R10 placed at 80.65 m).

Log response: The thick sandier event beds are well picked out by a change to a more serrate gamma log response, especially above 94.00 m; Figs. 5), reaching values as low as 50 API. Such values are unusually low in the wider context of the overlying Ross Fm sandstones. In several cases, the basal (H1 and H2) and upper (H4) sandstones sandwiching muddy and mudstone-clast rich sandstones (H3) produce a distinctive doublet on the gamma log (e.g. at c.88 m; Fig. 5). In contrast, a very high gamma peak is present at the top of the interval (80.60 m) coinciding with a notable increase in the U concentration (>15 ppm; Supplementary Figure). The spectral gamma log reveals a complex internal structure with high uranium at several levels.

Link to outcrop: The cliff and foreshore sections demonstrate the broadly sheet-like nature of the R10 event beds that extend at least hundreds of metres laterally with little change in thickness (Fig. 9). Although individual event beds have a continuous tabular geometry, the internal sharp boundary between the basal H1 and H2 sandstones and the overlying H3 clast-bearing argillaceous sandstone changes elevation by several decimetres over 10s of metres laterally, to the extent that in one case the basal H1/H2 sandstone (110 cm-thick) is reduced to <10 cm and replaced by a large sand-injected and deformed mudstone raft (Fig. 12G). The outcrop shows evidence of pervasive soft-sediment deformation associated with the H3 clast-bearing argillaceous sandstones and locally sand injections penetrate vertically into the H5 mudstone cap (but no further). The H3 divisions contain large angular m-scale blocks that include bedded siltstones, in a matrix containing floating coarser sand grains in an argillaceous sandstone. Paleoflow measurements on the foreshore from groove and flute marks indicate flow to the ENE (vector mean 68˚, n=31; Fig. 9). The thick ammonoid-rich CS mudstones

capping the unit are well exposed on the coast and a reanalysis of the biostratigraphy confirms this is the *Hd. proteus-H. smithii* condensed section of H_{2a} age (Lacchia 2016).

Correlation to -03 and -05 boreholes: R10 is fully cored in both the -03 and -05 boreholes (Fig. 10); this is important as there are no outcrop constraints at the R10 level on Loop Head and the subsurface data discussed here imply marked lateral changes in the character of the R10 succession. The unit is bracketed by ammonoid-bearing mudstones top and bottom, and it has a very distinctive serrate and unusually low (compared to the rest of the Ross Fm) gamma log signature in all three boreholes. Consequently, there is high confidence in the unit-level lateral correlation at this stratigraphic level. Furthermore, the thick and mostly isolated (i.e., non-amalgamated) event beds and their outboard position given the overall progradational succession indicates likely high lateral bed continuity. A tentative bed-scale correlation acknowledging this and linking the three boreholes is shown in Figure 10.

R10 is dominated by HEBs in all three boreholes (91.6%, 89.5% and 91.4% in -03, -05 and -09 cores respectively) with only rare turbidites present (TB1, TB5 and TB6 - <3%). Significant lateral variations in bed make-up and character occur with a fall in the proportion of sandy HEB1 beds from west to east (64.8% to 43.2% to 10.9%), a corresponding increase in HEB2 beds (14.8% to 14.0% to 27.9%) and HEB8 beds (7.9% to 21.8% to 52.6%). These trends reflect a lateral change to HEBs with better developed H3 divisions down-dip to the east and thinner basal H1 sandstone divisions (Figs. 10, 12). The texture of the matrix H3 divisions is variable, in some cases predominantly sandy, but also darker and richer in mud with floating sand grains, particularly in more distal examples. Moreover, the upper fine-grained and ripple-laminated H4 divisions to HEBs are only occasionally present in -03, but occur in every thicker HEB in -09. Individual thicker HEBs are rarely amalgamated, except for the basal part of R10 in the -05 core, and another instance in the upper part of R10 in -03. The number of thicker sandy event beds decreases from west to east, from 18 in -03, to 14 in -05 and to only 5 in borehole -09 (Fig. 10). The net clean sandstone decreases laterally from 40.7% to 27.3% to 14.5%

across the same three boreholes, paralleling the lateral decrease in average thickness of the event beds. One of the thicker hybrid event beds in the -05 borehole (97.8 to 95.10 m) has a 1.7 m-thick folded mudstone forming a single contorted raft that is inferred to occupy all of the H3 division where cored (Fig. 10).

The siltstone-dominated section (101.4-93.0 m; Fig. 13) separating the lower isolated HEB1b from the upper bundle of thicker event beds in -09 borehole can be followed to a similar silty section in -05 (113.7 to 106.6 m) where sand-speckled mudstones overlying thin, medium-grained sandstones (HEB8) are split by a thicker muddy HEB2 (Fig. 13). Further up-dip to the west in the -03 borehole, the interval passes into a bundle of relatively muddy, thick HEBs with well-developed debritic facies with only minor interbedded siltstones (161.2 to 150.1 m; Fig. 13). The lateral changes in bed make-up expressed by this part of R10 are important in that they capture the transition from thicker to thinner HEBs. R10 has a strongly bimodal expression in terms of event bed thickness; thick HEB1 and HEB2 are interleaved with thin HEB8. The latter show a significant change in motif from W to E. Sandy basal divisions occupy a greater proportion of the thin event beds in -03 but pass down depositional dip into thicker event beds dominated by prominent sand-speckled siltstones with only minor sandy basal divisions, if present (Fig. 14).

Interpretation: Unit R10 is dominated by various types of hybrid event beds. Common, and in some cases very large, mudstone clasts segregated in well-developed H3 divisions imply energetic sediment gravity flows that locally entrained abundant substrate clasts (Haughton *et al.* 2003; Talling et al. 2004, 2012; Kane and Pontén 2012; Patacci et al. 2014; Fonnesu et al. 2016; Dodd et al. 2022). The flows carried sand of an unusually coarse grade, depositing this first in graded and clay- and mica-poor basal H1/H2 divisions (hence the low gamma) implying important turbulence and fractionation of components. Then, parts of the flow enriched in mudstone clasts were emplaced as a linked debris flow (H3). The latter interacted with the basal sand, locally ploughing into and mixing with it, driving sand injections, soft-sediment deformation and dewatering and accounting for the complex and heterogeneous texture of the H3 divisions (Fig. 12G,H); complex enough in the more

distal examples for the event beds to have previously been interpreted as local slumps (Lien et al. 2003; Pyles and Jennette 2009). The flows entrained a range of mud lithologies, including bedded sand-speckled siltstones similar to those on this sector of the basin floor, but also darker and more carbonaceous mudstones that may have been entrained further up-slope. Finally, a dilute tail emplaced an upper finer grained banded to laminated sandstone (H4) and a capping mudstone division (H5), but only atop some of the thicker and more distal event beds.

Lateral changes evident across the correlation panel in terms of the character and number of the thicker event beds are consistent with HEB facies tracts elsewhere (Haughton et al. 2003; 2009; Talling et al. 2007; 2010; 2012; Kane et al. 2017). Thus, the change from more common H1/H2 divisions up-dip (to the W) to more important H3 debrite divisions down-dip (to the E) is a motif both documented and inferred in many systems (Davis, 2009; Hodgson 2009; Southern et al. 2015; 2017; Hansen et al. 2019). The thicker event beds tend not to taper until close to their distal pinch out and this is partly because thinning of the H1 sandstone is compensated by the distal expansion of the H3 linked debrites. Significant sand entrained in the linked debrites was carried further distally than might have occurred in the absence of flow transformation, and this and the entrained mud clasts contributed to maintaining the bed tabularity. The linked debris flows in this case extend many km with examples on the correlation panel suggesting H3 divisions extending >10 km laterally.

The thicker event beds are isolated in stacks of silty HEB8 and these are interpreted as the toes to sandier event beds up-dip but of smaller volume and hence of lower efficiency, such that they were unable to reach as far out into the fringe of the system. The result is a strongly feathered wedging geometry for the R10 unit, with only the largest volume event beds extending as far as the -09 borehole. The finer grained section that splits R10 in the distal -09 borehole corresponds to a time when flows had a more restricted run out, at least in the plane of the correlation panel. It is not clear whether this was a temporary step back due to a reduction in flow efficiency, or a lateral offset of the flow pathway meaning the panel no longer coincides with the axis of the system. Whatever the origin, the bed transitions at this level indicate that thicker event beds interfinger and potentially

pass laterally down-dip into the much thinner and muddy HEB8 beds and then thicken again further down-dip by expansion of the sand-speckled silty divisions. The latter are remarkably extensive although dominated by thin (a few 10s cm-thick) debritic facies.

Lower Ross Formation - Unit 20

-09 Core: This 62.8 m-thick cored interval stands out in that the lower third of the unit is characterised by a distinctive sandying-and thickening-upward trend (Fig. 5). This style of vertical organisation above condensed sections is not seen at other levels in the Ross Fm. Most of R20 is cored in the -09 borehole with correlation to the adjacent cliff section (Fig. 9) suggesting just ~7 m of the top of the unit up to the *Ht. prereticulatus* ($H_{2c}2$) condensed section is uncored, making the full thickness of R20 ~70 m at Ballybunion. R20 sandstones are predominantly very fine-grained, in contrast to the medium-grained sandstones with common coarse sand grains that dominate R10. Like R10, sand-on-sand amalgamation is rare in this unit in the -09 borehole, mainly on account of thick silty mudstone capping divisions on many of the event beds.

The cored R20 interval can be divided into three subunits (Fig. 5). The lower (80.60 – 59.63 m), a 19.4 m-thick, generally siltstone-dominated, sandying- and thickening-upward sub-unit, directly overlies the *Hd. proteus-H. smithii* condensed section (with condensed mudstones with ammonoids accounting for 32.2% of the subunit). Above the condensed facies, the subunit comprises dominantly silty event beds (a combination of HEB3b, HEB6 and HEB7; 44.7%), the definition of which improves upwards on account of the appearance of thin (mm-scale) very fine-grained sandstone basal divisions, in some cases with ripple lamination, but also banded examples. Subtle soft-sediment deformation features and silty pseudonodules occur in the lower parts of what are prominent mudstone caps. Some minor thin ripple-laminated sandstones (TB6; 5.8%) with cm-thick black (N1) fossiliferous mudstones appear intercalated with the basal HEBs. The younger of the silty event beds have more obvious fine-grained sandstone bases with overlying clay-rich sandstone divisions. The

subunit is capped by a pair of thicker (m-scale) HEB3a (12.5%) distinguished by well-developed banded divisions (H2) comprising alternating paler and darker coloured (N7 and N4 respectively) sandstones with cross-cutting dewatering sheets and variable clay concentrations. The banding becomes more contorted upwards and transitions into deformed/soft-sediment sheared silty and then structureless mudstone capping divisions (Fig. 16A).

The central subunit extending from 59.63 m to 31.50 m is dominated by a bow-shaped vertical grain size and bed thickness profile (Figs 5, 15). The subunit is characterised by abundant HEB3 (48.4%) together with subordinate HEB4 (6%) and HEB6 and HEB7 (together 11.5%). Turbidites (mainly TB6) account for 11%, and background mudstones (Bk) 11.2%. The component bed-types change upwards from stacked mud-rich faintly-banded sandstones (HEB3b, HEB6 and HEB7) with scattered mudstone chips and pseudonodules interbedded with mudstones, to isolated dcm-thick well-banded and fine-grained argillaceous sandstones (HEB3a and HEB4; Fig. 16A-C) that are locally interleaved with cm-thick either poorly structured or ripple-laminated very fine-grained sandstones (TB3, TB5, and TB6). The thicker banded event beds (HEB3a) commonly show internal convolution and soft sediment deformation, whereas mudstone clast-rich argillaceous sandstone divisions (H3) are rare and generally thin (Fig. 16B). Injected mudstones are observed at 54.10 m and 49.50 m. Towards the mid-part of the subunit, a combination of structureless sandstones with high clay content (HEB5,6) and banded clay-rich sandstone beds (HEB3a) occur with thick mudstone caps. Minor ammonoid-bearing mudstones occur amongst the ripple-laminated sandstones (e.g., 57.60 m, 56.20 m, 38.20 m and 37.40 m). The upper part of the subunit is marked by a 1.6 m-thick HEB3a that has a dewatered basal sandstone and a prominent overlying m-thick banded sandstone division (Fig. 5).

An upper subunit (31.50 m – 12.80 m) which is at least 17.3 m-thick is distinguished by more important turbidites (TB1 to TB6; 45.%, dominantly TB6) together with subordinate hybrid event beds (HEB3 to HEB7, 16.3%) and common background siltstones (32.9%). The unit commences with an alternation of dark grey (N3), barren and laminated mudstones (and thin-bedded, commonly ripple-laminated very fine-grained sandstones; TB% and TB6) with siltstone-rich caps (Fig. 5). These

thin beds gradually increase in thickness upward developing subordinate, occasionally banded, argillaceous fine-grained basal sandstones (HEB3b,5,6,7 typically 20-40 cm-thick) and forming a sandying- and thickening-upward bed stack. Thick silty mudstone caps occur throughout the subunit but are best developed in the basal muddier part. Despite the change in bed character, the mixed nature of the bed-types results in a rather low but overall increasing net sand content (from 10.4% to 27.1%) towards the top of the core. Many of the beds in the upper part of the unit have well-developed parallel and ripple lamination, either dominating the sandy part of the bed, or overlying basal structureless sandstones (Fig. 16D).

Wireline log response: A progressive reduction in gamma ray values mirrors the sandying-upward trend in the lower subunit peaking at 100 API. The pair of sandy event beds at the top of the lower subunit marks a change to a more serrate gamma ray response. The bow-shaped central unit stands out on the gamma log with a bimodal pattern associated with basal clean sandstones (relatively low API values c.50-100) and muddy banded sandstones and thick mudstone caps (high API values c.180-220). The gamma log for the upper subunit highlights a pair of the thickening- and sandying-upward cycles.

Link to outcrop: Representatives of the thicker HEB3a and HEB3b can all be found on the foreshore c.100 m west of the borehole where they can be seen to have a sheet-like geometry extending c.100 m laterally in the cliffs and across the foreshore (Figs. 3, 9). The thicker event beds have prominent basal grooves and tool marks indicating paleoflow towards the east (75˚, n=18, sense of flow from ripples and rare flutes). As in the core, mudstone clast-rich sandstone divisions are uncommon and thicker laminated or banded sandstones pass transitionally upwards into thick siltstone caps. The uncored upper section of R20 comprises thin-bedded ripple-laminated turbidite sandstones (TB5,6) and background fines (Bk) at the base overlain by thicker HEBs and sandy turbidites towards the top (TB3; Fig. 9). Both sections show an overall sandying-upward trend BOVE the *Hd. proteus-H. smithii* condensed section and isolated event beds with little sand on sand amalgamation. *Ht. prereticulatus*

ammonoids ($H_{2c}2$ age; Lacchia, 2016) are encountered in a CS shale a short distance (~7 m) above the uppermost section cored in -09.

Correlation to Loop boreholes: Unit R20 is bound top and base by well-developed ammonoid-bearing mudstones and the lower third of the unit has a similar and distinctive upward-decreasing gamma response in all three boreholes (Fig. 15). The unit is 74.9 m-thick in the -03 borehole, 65.4 m in the -05 and c.70 m accounting for the short uncored section in -09. A subordinate condensed section with ammonoids and a high gamma response (38.95 m) splits R20 in the -05 borehole (and this is tentatively linked to relatively 'hot' mudstones in a similar position the -03 and -09 boreholes (78.60 and 31.50 m, respectively), albeit lacking ammonoids (Fig. 15).

There is an obvious lateral change in character at R20 level between the three boreholes; it is not possible to correlate individual beds at this level due to these lateral changes. The thicker up-dip section in -03 is sandier overall and includes amalgamated sandstones in the central to upper part of the unit. The -05 borehole is less sandy particularly in the upper part above the subordinate condensed section. Silty mudstone capping divisions to HEB3a and HEB3b only occur in the lower parts of -03 and -05 but are developed throughout much of R20 in the -09 borehole and as a result, -09 has a relatively low overall sand content (45%, 34% and 27% for -03, -05 and -09, respectively). Parallel and ripple laminated sandstones (TB2,3,5), sometimes overlying structureless sandstones, appear at a deeper level in -03 and -05, whereas they only become common in the upper part of R20 in -09.

Interpretation: R20 records a step-change in bed thickness, the bed-type mix, the input grain size and depositional trends and shows little in common with the underlying R10 system. The presence of argillaceous and well-banded HEB3, particularly in the -09 borehole where they dominate, indicates deposition from transitional flows that evolved from weakly turbulent to laminar behaviour, hence the poor development of tractional structures and common banding (Lowe and Guy 2000; Lowe et al. 2003; Barker et al. 2008; Southern et al. 2017). The flows lacked abundant entrained mud clasts but

had high dispersed clay concentrations suggesting they may have entrained loose clay and mud flocs rather than larger substrate clasts (Pierce et al. 2018), with significant mud concentrated in thick caps with evidence for internal shearing suggesting *en masse* emplacement rather than settling from a suspension cloud. Gradients must have been low to arrest the trailing mud flows. The upward change to better structured sandstones with greater preservation of Bouma sequences towards the top of R20 implies a change to more turbulent flows and to deposition mainly from turbidity currents.

The borehole correlation shows the basal third of R20 across the outer Shannon area has a distinctive sandying-upward signal, consistent with build out. The muddier lower part of the cycle is relatively thin in the -03 borehole but thickens eastwards in the direction of the paleoflow via -05 to -09. Although HEB3 beds are developed, these are restricted to just the lower part of -03 and -05, and both boreholes show an upward transition, best developed in -03, to alternations of m-scale amalgamated bed sets of largely structural sandstone, with thinner bedded layered turbidites and clast-rich HEBs in the upper part of R20. This distinctive association is typical of many parts of the younger Ross Fm and has been interpreted as characteristic of lobe development (e.g., Pyles, 2008; MacDonald et al. 2011; Pierce et al. 2018). The amalgamated sandstones are interpreted as proximal or axial lobe deposits, the better bedded sections as off-axis, and the interleaving of one and the other to compensational stacking. The implication is that R20 in the west records the establishment of a fan system with depositional lobes fed by channels, although there is no evidence that channels extended this far east at this time (shallow fan channels appear for the first time in R30 in the Loop area). However, the borehole correlation implies the lobe elements pass down-dip to the east into the thick event beds with silty caps seen in the -09 borehole implying the lobes were lateral to sheets emplaced by turbulence suppressed muddy flows. Hence, an outer fan fringe built by more efficient flows occurred outboard of the lobes and at least at this level, lobes may not have extended to the fan fringe, an inference also made by Pyles and Jennette (2009).

CONTRASTING DISTAL SYSTEM TERMINATIONS

The lateral constraints provided by the three boreholes together with the outcrop section north of Ballybunion help better understand the processes operating prior to, and outboard of, the stacked lobes that built the main fan system represented by the mid- and upper levels of the Ross Fm. Although the panel is just 18 km long, deposition stepped north-eastwards in time such that each of the five units described above provide snapshots of increasingly proximal parts of the outboard environments, ranging from condensed deposition remote from the sediment input (Hot mid-Clare Shale Fm), to a fringe of stacked silty hybrid event beds (Upper Grey Clare Shale) to increasingly sandy outsized outer fan or basin-floor sheet deposits (R5 and R10) to the advance of a separate finer grained fan system, initially with distinctive outer fan deposits (R20) down-dip from the first fan lobes.

Age calibration of Pennsylvanian ammonoid biozones based on the UK Pennine Basin (Waters and Condon, 2012) suggests the pair of prominent condensed sections ($H_{1b}1$ and $H_{2a}1$) that together bracket the Upper Grey Clare Shale, R5 and R10 may represent a single long-eccentricity cycle (i.e., c.400 kyr). The overlying R20 unit is capped by an $H_{2c}2$ age condensed section and this suggests R20 might extend over longer than a single long eccentricity cycle (perhaps 600-700 kyr; Waters and Condon, 2012), probably with significant time recorded in the prominent condensed section at the base.

The character of the five units discussed above indicates that they represent two separate deep-water systems, one stacked above the other. The lower four units (hot Mid and Upper Grey Clare Shale Fm, R5 and R10 of the Ross Fm) are interpreted as a product of an earlier system that stepped north-eastwards into the basin (Fig. 17A). A genetic relationship between these units is supported by similar sand-speckled muddy event beds in all four units, interfingering relationships between the units and component facies, a relatively coarse texture for sandstones where they occur, and bracketing by the same well-developed condensed sections top and bottom. Following Kelk (1960)

who distinguished a transitional unit between what was then referred to as the Ballybunion Shales (now the Clare Shale Fm) and the Lower Greywacke Series (now the lower part of the Ross Fm), the lower four units are here referred to as the Cosheen system. It is overlain by R20, the texture and character of which resemble younger parts of the Ross Fm (e.g. the compensational stacking of lobe axis and off-axis elements inferred in the more proximal -03 borehole). Unit R20 is thus interpreted as recording the arrival of the distal Ross system fringe in the outer Shannon area (Fig. 17B).

The boundary between the two stacked systems coincides with the well-developed $H_{2a}1$ condensed section. The Cosheen system was supplied with fine- to medium-grained, locally coarse sand whereas the overlying Ross system (and the overlying slope and delta systems) had a dominant supply of very fine- to fine-grained sand. The different grain size suggests there was a change in sediment routing. The alternative, that coarse sand was bypassed in more efficient flows across fine-grained fan systems up-dip, is deemed less likely as no coarse-sand grains are found as lags or armouring mudstone clasts in the R20 and younger parts of the Ross Fm. Also, the coarse-grained texture is encountered only in the oldest part of the Ross Fm in the depocentre around the mouth of the Shannon. The onset of the sandy deep-water deposition took place later in areas further to the east, northeast and to the south and is in all cases characterised by very fine and fine-grained sandstones indicating no bypass of coarser grained sand at these younger levels (Obradors-Latre et al. 2017). Petrographically, the framework mineralogy for the R10 and younger R20 to R90 Ross sandstones is similar and dominated by quartz with subordinate lithic grains (Hussain et al. 2020), so it appears the provenance was broadly similar despite the switch in texture. A reorganisation of the drainage, either by lengthening via river capture (it must be rapid) to fractionate more efficiently the coarser grains and sequester them within the river system, or a drainage diversion to tap finer grained source lithologies, seems likely (Bishop, 1995).

The following sections consider the character of the two systems in more detail with an emphasis on linking the flow transformations that operated to stacking patterns straddling the distal sand pinch outs.

Cosheen System

Scale and stacking pattern: The stacking of separate units and their correlation across the boreholes place constraints on the minimum length scale of the different elements, and of the wider system assuming each of the correlated units now stacked vertically represent facies associations that were originally spread out laterally and contemporaneous with one another (i.e., a 2D application of Walther's Law). The Upper Grey Clare Shale extends across the panel thinning and containing less sand eastwards, suggesting muddy hybrid flows were able to spread as relatively thin (decimetre-scale) sheets for at least 18 km across the basin floor prior to the arrival of significant sand. These then interfinger with occasional thicker sandy hybrid event beds (unit R5), some of which feather out and some of which continue across the correlation panel. This low net-sand fringe follows gradationally from the underlying Upper Grey Shale and would have also been >18 km wide. The rare sandier HEBs are interpreted as products of the most efficient flows arriving in the depocentre. A jump in the bed thickness across a subordinate condensed section at top of R5 may mean part of the reconstructed profile is missing here due to a basinward step. The overlying R10 unit is made up of very thick hybrid event beds that feather out eastwards across the panel, but with some of the thicker event beds reaching and extending beyond the -09 borehole at Ballybunion. In the western -03 borehole at Loop Head, some of these event beds have well-developed H3 debritic divisions suggesting they are already relatively distal and hence the system must have extended WSW some (unknown) distance; this sandier part of the basin floor captured in the correlation panel thus likely had a lateral extent of 20-30 km or more (Fig. 17A). Splicing the units together, the Cosheen system (including the debritic outflow sheets) may thus have extended at least 60 or 70 km laterally along the basin axis.

System character and interpretation: Unit R10 is characterised by unusually thick and coarse-grained (in the context of the remainder of the Ross Fm) hybrid event beds that are tabular on a scale of hundreds of metres on the foreshore, between the cliffs and the -09 borehole north of Ballybunion, and on longer length scales (kms) between the boreholes. However, the decline in the number of thicker event beds from west to east implies they wedge out or pass into thinner beds at larger length scales (10s km). Those that do persist in the east are only marginally thinner than those encountered 18 km to the west, although they have thicker H3 debrite divisions, and have developed upper H4 divisions that are lacking in the up-dip boreholes. This suggests that they are broadly tabular until close to where they either pinch out or become very much thinner and pass in to HEB8 and the debritic outflow sheets. The wider stratigraphic context in the lowermost Ross Fm implies a distal site and the character of the succession is reminiscent of oversupplied basin plains and confined basin floors elsewhere e.g., Marnoso Arenacea (Ricci Lucchi and Valmori 1980; Talling et al. 2004; Amy and Talling 2006; Sumner et al. 2008; 2012; Muzzi Magalhaes and Tinterri 2010; Tinterri & Muzzi Magalhaes; 2011), Hecho Group (Mutti 1977,1983; Remarcha and Fernández 2003; Remarcha et al. 2005), Tabernas (Haughton 1994, 2000, 2001), Gottero (Fonnesu et al. 2018). Ponding has been invoked to account for the maintenance of a flat basin floor in many of these examples and confinement can lead to higher bed tabularity (Liu et al. 2018; Tőkés and Patacci 2018). However, there is no indication that the distal Cosheen system was contained although it may have been confined laterally given the trough-like basin along which the system advanced (and the evidence discussed above for thinning of the hot Mid- and Upper Grey Clare Shale Fm units between the -09 borehole and the equivalent outcrop section to the south). There are no ponded mudstone caps, evidence for flow reversals or basin-centred thickening of event beds that might be expected were full flow containment to have been important. The flows must have dissipated as they travelled eastwards, with variable flow efficiency and hence runout promoting a highly feathered stratal geometry. The poor vertical organisation and absence of an obvious stratigraphic hierarchy imply a

largely aggradational stacking pattern in which stratal compensation seems to have been unimportant.

Taken together, the characteristics of the Cosheen system suggest it represents either a weakly confined outer fan or basin plain sheet system; there is a continuum between 'sheet-like lobes' and basin plain successions that means distinguishing between the two is difficult (Mutti 1977; 1983; Pickering and Hiscott 2015). High flow efficiency explains the presence of some of the thickest sandy event beds in the basal Ross Fm in what must have been a distal position given the long-term progradational nature of the succession. The dominance of hybrid event beds reflects the volume of substrate incorporated in what must have been high energy flows (Pierce et al. 2018).

Flow transformations: A bimodal bed thickness is a striking feature of the Cosheen system. Pierce et al. (2018) attributed the association of thick HEB1 and HEB2 with thin HEB8 to downstream flow evolution. Substrate erosion by turbidity currents contributed abundant mud rip-up clasts, segregation and break-up of which then triggered the formation of linked debris flows. The sand-speckled siltstones deposited further outboard were interpreted as a second flow transformation involving turbulence suppression by clay in the tail of the flows, although it is difficult to explain the floating sand grains in this instance.

Recent experiments on transitional flows by Koo et al. (2020), together with the analysis of lateral facies transitions that occur in the lower part of R10 (Fig. 13), suggest an alternative mechanism that may have triggered the sand-speckled debritic outflow sheets. The experiments demonstrated how deposition from sand-mud mixtures can lead to secondary remobilisation whilst the deposit is still forming. Koo et al. (2020) showed that a clean sand emplaced by the front of a transitional flow was overlain by mud that initially stabilised but that then dewatering of the underlying sand created a decollement that allowed the upper mud division to slide, remobilise and mix, triggering additional phases of debritic flow (see fig. 12 of Koo et al. 2020).

Although the experiments were for simple sand-mud mixtures and not designed to replicate the sort of mud clast-driven flow transformations envisaged in the case of the Cosheen system, the concept of a transient deposit with evolving mechanical properties that exceed some threshold triggering secondary flowage may have wider application. The linked debris flows forming the H3 debrite following bulking of the flow with abundant mud clasts were sufficiently strong to plough through the just deposited H1 sand and to transport m-scale blocks (Fig. 12G). However, the linked debrites would have incorporated water via mixing with, and dewatered from, the underlying wet sand with disintegration of the mud clasts contributing additional matrix clay. The matrices present in H3 vary from highly heterogeneous textures with cleaner sand patches floating in argillaceous sandstone, to argillaceous sandstone through to well mixed sandy mudstones with floating sand grains implying variable and dynamic mechanical properties. Sections of the debrite can therefore evolve to become weak enough to promote reflowage or relaxation to form a thinner and more mobile mud flow that then travelled on behind what remained of the original flow front, carrying small mud clasts, coarser sand grains and some of the momentum of the linked debrite with it (Fig. 18A). The now dilute flow front had, in the meantime, separated from the triggered outflow explaining why no sand settled out on top of the thin sand-speckled siltstone divisions. Sourcing the thin debritic outflow sheets via remobilising sections of H3 cannot explain instances in which similar thin debritic caps occur on top of H4 divisions capping thicker HEB2. These only occur in the most distal section at Ballybunion and could also reflect secondary remobilisation, with mud settling out on top of the thicker sandy beds up-slope leading to destabilisation and renewed flowage in a scenario closely resembling the Koo et al. (2020) experiments.

Large volumes of mud were thus bypassed and partitioned distally beyond the sand pinch-out limit in the Cosheen system. A proportion of this mud was probably recycled in that outflow sheets from less-efficient flows were re-entrained as substrate clasts in more efficient flows, reprocessed in linked debrites, before being incorporated in new outflow sheets and dispersed further outboard again. The outflow debrites thickened distally before thinning and are several 10 cm-thick (i.e.,

medium thick bedding of Campbell 1967). The resulting muddy fringe contrasts with fan fringes built by runout of turbulent flows in which beds are typically very thin to thin. Boulesteix et al. (2020) describe bedsets of normally graded and faintly bedded mudstones with a mean thickness of ~0.2 cm forming a muddy fringe extending c. 20 km beyond the sand pinchout. The Cosheen outflow sheets were locally able to heal topography ahead of the advancing sand system, partly burying a lateral slope in the Ballybunion area, but also potentially creating subtle topography. Spychala et al. (2017b) have shown how subtle topography and lateral confinement can influence stacking patterns; the same may apply to longitudinal slopes modified by variable partitioning of mud, flow transformations and reflowage. A combination of upstream delamination by high-energy currents, and bypass and partitioning mud distally could have helped maintain a levelled basin floor and explain the high bed tabularity in the absence of ponding seen in R10. The absence of obvious compensation probably reflects a combination of the out-sized scale of the flows meaning they were probably not delivered via an up-dip distributive channel network, and deposition deep on the profile meaning the deposits could aggrade without influencing the flow field in the way that lobes building up closer to channel mouths can choke flows exiting the channels forcing relocations.

Younger Ross System fringe

Scale and stacking pattern: Unit R20 records a change in down-dip termination style, event bed type and the distances over which lateral facies transitions are expressed. The systematic upward change to increasingly proximal deposits (marked by upward sandying and increased amalgamation), particularly well expressed in the two western boreholes, implies rapid progradation that culminated in the arrival of compensationally-stacked lobes in the west (Figs. 15,17). The lobes pass down depositional dip over 10-15 km into the HEB dominated fringe documented in the -09 borehole. An expanded thickness of the mudstones and thin beds overlying the lower $H_{2a}1$ condensed section in the east suggests these are equivalent to sandier prograding lobes in the west (Fig. 15). Deposition is

inferred to have occurred on low-angle inclined surfaces equivalent to the downlapping seismic reflectors seen at the base of mounded and prograding submarine fans observed in the subsurface elsewhere (Fig. 15; Posamentier and Erskine 1991; Grundvåg et al. 2014). As the Ross system built out over the underlying Cosheen sheet system that had already levelled the basin floor, gradients were likely initially low (and this may have helped arrest trailing mud flows). Lobe style compensational stacking does not extend to the -09 borehole at R20 level suggesting progradation gave way to aggradation and then a backstep in the upper part of R20 above the internal subordinate condensed section to account for the thin beds in the lower part of Kilcloher cliff and at Ballybunion beneath the *Ht. prereticulatus* condensed section ($H_{2c}2$; Fig. 15). Thickening of the younger part of the unit towards Ballybunion (Fig. 15) suggests the latter lay in a more axial position.

System character and interpretation: The Ross system fringe represented by the lower part of R20 was built by larger than average volume flows for this system that carried sand and mud beyond where bundling of thicker and thinner beds imply lobe compensation (Fig. 17B). An outer fan to fan fringe setting is inferred dominated by HEBs and including m-thick outsized hybrid event beds. Thick hybrid event beds and transitional flow deposits in outer fan settings are known from both modern (Migeon et al. 2010; Talling et al. 2010; Fildani et al. 2018) and older systems (e.g. Talling et al. 2004, 2013; Amy and Talling 2006; Barker et al. 2008; Ito 2008; Sumner et al. 2008; Hodgson 2009; Kane and Pontén, 2012; Southern et al. 2017; Spychala et al. 2017a,b; Hansen et al. 2019).

The well-developed condensed section beneath unit R20 suggests there may have been a significant time gap between the demise of the underlying Cosheen system and the subsequent advance of the finer-grained Ross system. As there was a change in sediment supply and potentially flow efficiency, this may have induced contraction of the system that then re-advanced, hence the preservation of two stacked distal pinch-out successions embedded in the same longer term progradational trend, the implication being either the overall flow efficiency was lower in the R20 system, or that it was fed from further away. The former is consistent with the thinner beds, shorter-scale lateral facies

transitions and muddier R20 sands that were emplaced by flows that were unable to fractionate clays as effectively as those in the underlying Cosheen system suggesting a shorter transit (Hussain et al. 2020). The distinctive bed-type mix and occurrence of HEB3 characterising the progrades does not appear again in the overlying Ross Fm in the outer Shannon area despite other shutdowns and condensed sections. The toe to the Ross system thus migrated once through the outer Shannon area and then lay to the east for the remainder of the Ross Fm, arriving 50 km east at Inishcorker (Fig. 1A) close to the end of Ross deposition where similar outsized hybrid event beds are also encountered (Pyles and Jennette 2009; Obradors-Latre 2017).

Flow transformations: Many of the flows emplacing sand in the Ross system fringe also carried significant silt and clay that drove clay-induced flow transformations by damping turbulence. Event beds with mudstone clast-rich H3 divisions are present but relatively uncommon, suggesting incorporation of substrate clasts was relatively unimportant. Common banding attests to the development of transitional flow conditions with soft-sediment deformed, dewatered muddy sand demonstrating that more cohesive sectors of the flow interacted and mixed with the just deposited sand. A dominance of grooves and other tool marks on sandstone bed bases is consistent with dampened turbulence even in the front of the flows (Peakall et al. 2020). The sole marks and the evidence for banding suggest the thicker lower clean sandstone divisions did not form by vertical segregation of sand grains by settling through a cohesive flow (cf. Sumner et al. 2009). Where the event beds are dominated by upper muddy divisions overlying just thin and poorly structured sandstones, such a mechanism is possible. Both thicker and thinner event beds have thick silty mudstone caps that are interpreted as deposits of plug flows (Hussain et al. 2020). These arrested largely before they had outrun the sandy basal divisions and the resulting silty mudstones explain the vertical isolation of the sandstones beds making up the fringe. Mud in this case was not partitioned beyond the sand pinch out to the extent it was for the Cosheen system. The location of where mud was incorporated in the flow may have been important. If closer to source, longitudinal fractionation may have triggered flow transformations in the muddy rear of the current allowing a trailing debrite

to arrest on top of the sand emplaced by the flow front (Fig. 18B). Where mud was entrained as clasts via substrate delamination more distally in the system (Fonnesu et al. 2016), clast attrition and disintegration can release secondary mudflows that emplace distal outflow sheets (Fig. 18A).

The origin of the contrasting fringes to the Cosheen and Ross systems ultimately reflects the operation of particularly efficient flows capable of significant substrate entrainment in the case of the Cosheen system. Pierce et al. (2018) suggested a greater drop height from the shelf edge to the basin floor could allow flows to achieve higher velocities and thus to entrain more substrate, explaining the dominance of HEBs lower in the Ross Fm. A reduction in drop height as the basin filled could then account for the upward change to more common turbidites. However, this does not explain the sharp switch in fringe and HEB character between R10 and R20. This coincides with a prominent condensed section and a change in sand texture, suggesting a switch in sediment supply at least contributed to a change in how sediment was transferred from the shelf edge to deep water. Sediment supply is only one of a number of factors thought to control the volumes and pace of sediment delivery to deep-water, with shelf edge processes (waves, tides), shelf edge trajectory, sea level stand and slope stability all recognised as potentially playing a role (Carvajal and Steel 2009; Dixon 2012; Paumard et al. 2020; Gan et al. 2022). As the age-equivalent shelf-edge is not preserved, the extent to which these additional factors might also have played a role remains uncertain.

WIDER IMPLICATIONS

There are a number of wider implications and insights relevant to characterising the frontal parts of deep-water systems straddling sand pinch outs.

(1). Although the flow efficiency concept is expressed in terms of the distance to which sand can be carried basinwards, it is also important to consider how mud is partitioned by sediment gravity flows. This is particularly the case where flow transformations can cause the mud to either fall out

prematurely due to turbulence damping or to be re-entrained on account of substrate delamination and exported distally in linked debris flows and then secondary mud flows.

(2). There will be feedbacks between the types of flow transformation mechanism(s) operating and the stratigraphic architecture. The combination of high flow efficiency, up-dip substrate delamination and the distal triggering of secondary mudflows can help level the sea floor and promote increased bed tabularity in the absence of flow containment. Plug flows triggered in the rear of a transforming turbidity current or transitional flow (and hence further up-dip) may mean trailing mud flows do not run out beyond the sand pinch out to the same extent promoting stronger bed tapering, less tabular geometries and progradational stacking (see also Grundvåg et al. 2014). The variable properties of the substrate left by the passage of the front of the flow may also be important. The Cosheen linked debrites advanced over dewatered clean sand whereas as those in the Ross fringe travelled more cohesive banded facies. Extensive shearing and deformation in the latter case may have helped arrest the trailing linked debrites. Where mud is emplaced by plug flows, runout distances may also be impacted by the momentum they inherit from that part of the parent flow from which they form. Thus, transformations in the lower velocity rear of a turbidity current where clays have been segregated will carry less momentum than a secondary mudflow released from a fast-moving linked debrite formed closer to the erosional front of the flow. Heterogeneous release and drainage of secondary mudflows from a linked debris flow may also contribute to the fingered planform inferred for the frontal sand terminations in some systems (Prélat et al. 2009; Spychala et al. 2017a).

(3). Mudstone successions outboard of sandier basin floor successions are not necessarily very thin to thin bedded (see also Baker and Baas 2020). Where they are, this is likely because turbidity currents were able to continue distally without transforming or being overtaken by secondary mudflows. Emplacement of thicker distal outflow sheets ahead of an outbuilding system will enhance the ability of the fringe to heal topography before the arrival of the sandier part of the system.

Thicker distal event beds will also promote more efficient burial of organic matter in the muddy fringe (Hussain et al. 2021).

(4). The Cosheen system reconstruction made possible by the cores highlights the consequences of misinterpreting the significance of soft sediment deformation associated with linked debris flows close to their runout limit. Previous studies interpreted these as local slumps, and in the case of Pyles and Jenette (2009), this was used to support a contained mini-basin setting with frontal confinement. However, the borehole correlation shows that the soft-sediment deformed units are the distal expression of sandier hybrid event beds up dip and the soft-sediment deformation is related to flow emplacement and not to local gravity-driven slope deformation. Whilst thickness variations between the -09 core and the equivalent succession cropping out on the shoreline do support the presence of a slope, this is inferred to be a lateral slope passively onlapped by the Cosheen and Ross systems (the latter pinches out to the SW against a high in the Galley River section; Fig. 1A; Kelk 1960).

(5). The process inferences arising from the core and outcrop interpretations support the idea that there is a wide range of contexts and underlying mechanisms driving formation of HEBs and that they can occur widely across deep-water depositional systems (Fonnesu et al. 2018; Pierce et al. 2018; Ningthoujam et al. 2022; Fig. 19). HEBs are deposited by flows transporting sufficient quantities of clay to modulate and dampen turbulence. The clay is either derived from source failures (either slope failures or triggered by instability developed during deposition; Koo et al. 2021) and/or acquired by erosion en route; commonly the clay is hydraulically separated causing variable rheology either vertically and/or laterally either along or across the flow (Barker et al. 2008; Baas et al. 2021). The examples discussed here are interpreted as basin floor (Cosheen) and outer fan (Ross) sheets and likely formed following extensive sea floor erosion by outsized flows that acquired abundant mud clasts in the case of the Cosheen system, but dispersed clay and silt in the case of the Ross fringe. They are thus distinct from HEBs triggered by local erosion associated with submarine channel dynamics, for example on channel-lobe transition zones (Brooks et al. 2018, 2022; Baas et al. 2021)

driven by enhanced erosion directly downstream of channel mouths, on avulsion splays with deposition from vertically segregating wall jets formed as channels relocate (Terlacky and Arnott 2014; Ningthoujam et al. 2022), or on lobes forming in front of channels that are incising, sweeping sideways or lengthening by erosion (Pierce et al. 2018). Yet other HEBs are tied to interactions between flows and topography in slope marginal settings, where flows impinge on slopes or suffer accelerations due to confining topography or in ponded settings (Fig. 19; Patacci et al. 2014, 2020).

CONCLUSIONS

Behind-outcrop boreholes targeting the basal and outboard Ross Fm and its transition to the underlying Clare Shale Fm help detail the character of the distal fringes to sandier systems up dip. The analysis reveals two deep-water systems, each with a different distal expression: an early and coarser grained Cosheen system and a younger Ross system.

The older Cosheen system termination can be reconstructed from the stacking of units that step through the outer part of the system and represent a laterally confined (but not ponded) outer fan to basin plain setting built by high-efficiency flows that emplaced thick hybrid event beds charged with abundant mudstone clasts. The down-dip sand pinch-out is strongly feathered on account of variable flow runout. Event bed thicknesses are strongly bimodal; thick tabular sandy, sheet-form hybrid event beds pass down-dip into thinner, muddy debritic outflow sheets overlying (and outrunning) basal thin sandstones. The debritic outflow sheets thicken downdip before thinning and formed a muddy fringe extended >20 km beyond the loss of the thicker sandstones.

Flow transformations in the distal Cosheen system were triggered by erosional loading with mud clasts forming linked debris flows. Water and clay rich sections of the latter were then released as mobile but thin (10s cm) outflow sheets of mud with floating sand grains. Much of the mud ended up

in the distalmost fringe. The triggering of muddy outflow sheets may have been favoured by the thick and coarse-grained H1 divisions that promoted extensive dewatering.

The younger Ross termination is progradationally stacked with outsized hybrid event beds that retain thick, muddy capping divisions and with less mud bypassed distally. These were transitional flows the muddy components of which arrested before outrunning the sandy basal deposit. They bypassed compensationally-stacked up-dip lobes and built a 10-15 km wide sheet-form fringe with sandstone beds isolated vertically by mudstone caps.

Flow transformations and the range of flow efficiency play an important role in shaping outboard fan fringes which are more variable than commonly supposed and often more than simple amalgams of thin-bedded lobe fringes. Different flow transformation mechanisms can dictate the extent to which mud bypasses the sandy fringe to create outflow sheets or is retained as bed caps to thicker sandstones isolating them vertically. This in turn impacts the stratigraphic architecture.

Acknowledgements

We are grateful to Geological Survey Ireland (GSI) for a Griffith Geoscience Award that supported ALO and CP, and Equinor ASA for funding the subsurface data acquisition and the ammonoid biostratigraphy undertaken by ARL. Tom Culligan and John Kennedy provided excellent technical support. Niall Finch is thanked for field assistance in west Clare and Arif Hussain and Andrew Pulham contributed enthusiastic discussions that helped shape the ideas in this paper. Very helpful reviews of an earlier draft were provided by Megan Baker and Woong Mo Koo. This research is funded in part by a research grant from Science Foundation Ireland (SFI) under Grant Number 13/RC/2092.

References

Amy, L. A., and Talling, P. J. 2006, Anatomy of turbidites and linked debrites based on long distance (120 × 30 km) bed correlation, Marnoso Arenacea Formation, Northern Apennines, Italy: Sedimentology, v. 53, p. 161-212.

Baas, J.H. and Best, J.L., 2002, Turbulence modulation in clay-rich sediment-laden flows and some implications for sediment deposition: Journal of Sedimentary Research, v. 72, p. 336-340.

Baas, J.H., Best, J.L., Peakall, J. and Wang, M., 2009, A phase diagram for turbulent, transitional, and laminar clay suspension flows: Journal of Sedimentary Research, v. 79, p. 162-183.

Baas, J.H., Best, J.L. and Peakall, J., 2011, Depositional processes, bedform development and hybrid bed formation in rapidly decelerated cohesive (mud–sand) sediment flows: Sedimentology, v. 58, p. 1953-1987.

Baas, J.H., Tracey, N.D. and Peakall, J., 2021. Sole marks reveal deep-marine depositional process and environment: Implications for flow transformation and hybrid-event-bed models: Journal of Sedimentary Research, v. 91, p. 986-1009.

Baker, M.L. and Baas, J.H., 2020, Mixed sand–mud bedforms produced by transient turbulent flows in the fringe of submarine fans: Indicators of flow transformation. Sedimentology, v. 67, p.2645-2671.

Barker, S., 2005, Spatial and temporal evolution of deep-marine particulate gravity currents: an experimental, subsurface and outcrop investigation: [PhD thesis], University College Dublin

Barker, S.O., Haughton, P.D.W., Mccaffrey, W.D., Archer, S.G., and Hakes, B., 2008, Development of rheological heterogeneity in clay-rich high-density turbidity currents: Aptian Britannia Sandstone Member, UK Continental shelf: Journal of Sedimentary Research, v. 78, p. 45-68.

Baudin, F., Disnar, J.R., Martinez, P. and Dennielou, B., 2010, Distribution of the organic matter in the channel-levees systems of the Congo mud-rich deep-sea fan (West Africa). Implication for deep offshore petroleum source rocks and global carbon cycle: Marine and Petroleum Geology, v. 27, p. 995-1010.

Bell, D., Stevenson, C.J., Kane, I.A., Hodgson, D.M. and Poyatos-Moré, M., 2018, Topographic controls on the development of contemporaneous but contrasting basin-floor depositional architectures: Journal of Sedimentary Research, v. 88, p. 1166-1189.

Best, J. and Wignall, P.B., 2016, Introduction to the field guide. *A field guide to the Carboniferous sediments of the Shannon Basin, Western Ireland*, p.1-15.

Bishop, P., 1995, Drainage rearrangement by river capture, beheading and diversion. Progress in Physical Geography, v. 19, p. 449-473.

Blattmann, T.M., Liu, Z., Zhang, Y., Zhao, Y., Haghipour, N., Montluçon, D.B., Plötze, M. and Eglinton, T.I., 2019, Mineralogical control on the fate of continentally derived organic matter in the ocean: Science, v.366, p.742-745.

Boulesteix, K., Poyatos-Moré, M., Hodgson, D.M., Flint, S.S., and Taylor, K.G., 2020, Fringe or background: Characterizing deep-water mudstones beyond the basin-floor fan sandstone pinchout: Journal of Sedimentary Research, v. 90, p. 1678-1705.

Bouma, A. H., 1962, Sedimentology of some f!ysch deposits: a graphic approach to facies Interpretation. Elsevier, Amsterdam.

Bresser, G. and Walter, R., 1999. A new structural model for the SW Irish Variscides: the Variscan front of the NW European Rhenohercynian: Tectonophysics, v. 309, p. 197-209.

Brooks, H.L., Hodgson, D.M., Brunt, R.L., Peakall, J., Hofstra, M. and Flint, S.S., 2018, Deep-water channel-lobe transition zone dynamics: Processes and depositional architecture, an example from the Karoo Basin, South Africa: GSA Bulletin, v. 130, p. 1723-1746.

Brooks, H.L., Ito, M., Zuchuat, V., Peakall, J. and Hodgson, D.M., 2022, Channel- lobe transition zone development in tectonically active settings: Implications for hybrid bed development: Depositional Record, v. 8, p. 829-868.

Campanyà, J., Ogaya, X., Jones, A.G., Rath, V., McConnell, B., Haughton, P.D.W., ledo, J., Hogg, C., Blake, S. and Licciardi, A., 2019, Subsurface characterization of the Pennsylvanian Clare Basin, western Ireland, by means of joint interpretation of electromagnetic geophysical data and well-log data: Journal of Geophysical Research: Solid Earth, v.124, p. 6200-6222.

Campbell, C.V., 1967, Lamina, laminaset, bed and bedset: Sedimentology, v. 8, p. 7-26.

Carvajal, C. and Steel, R., 2009, Shelf-edge architecture and bypass of sand to deep water: influence of shelf-edge processes, sea level, and sediment supply: Journal of Sedimentary Research, v. 79, p. 652-672.

Chapin, M.A., Davies, P., Gibson, J.L., and Pettingill, H.S., 1994, Reservoir architecture of turbidite sheet sandstones in laterally extensive outcrops, Ross Formation, western Ireland. In Wiemer, P., Bouma, A.H. and Perkins, R.F. (eds), Submarine fans and turbidite systems, GCSSEPM Foundation 15th Annual Research Conference, p. 53-68.

Collinson, J.D., Martinsen, O., Bakken, B., and Kloster, A., 1991, Early fill of the Western Irish Namurian Basin: a complex relationship between turbidites and deltas: Basin Research, v. 3, p. 223–242.

Cope, J. C. W., Guion, P., Sevastopulo, G., and Swan, A., 1992, Carboniferous: Geological Society, London, Memoirs, v. 13, p. 67-86.

Croker, P.F., 1995, The Clare Basin: a geological and geophysical outline: Geological Society of London, Special Publications, v. 93, p. 327-339.

Davis, C., Haughton, P., Mccaffrey, W., Scott, E., Hogg, N., and Kitching, D., 2009, Character and distribution of hybrid sediment gravity flow deposits from the outer Forties Fan, Palaeocene Central North Sea, UKCS: Marine and Petroleum Geology, v. 26, p. 1919-1939.

De Morton, S.N., Wallace, M.W., Reed, C.P., Hewson, C., Redmond, P., Cross, E., and Moynihan, C., 2015, The significance of Tournaisian tectonism in the Dublin basin: implications for basin evolution and zinc-lead mineralization in the Irish Midlands: Sedimentary Geology, v. 330, p. 32-46.

Dennielou, B., Droz, L., Babonneau, N., Jacq, C., Bonnel, C., Picot, M., Le Saout, M., Saout, Y., Bez, M., Savoye, B. and Olu, K., 2017, Morphology, structure, composition and build-up processes of the active channel-mouth lobe complex of the Congo deep-sea fan with inputs from remotely operated underwater vehicle (ROV) multibeam and video surveys: Deep Sea Research Part II: Topical Studies in Oceanography, v. 142, p. 25-49.

Deptuck, M.E., Piper, D.J.W., Savoy E,B., and Gervais, A., 2008, Dimensions and architecture of late Pleistocene submarine lobes off the northern margin of East Corsica: Sedimentology, v. 55, p. 869–898.

Deptuck, M. E., and Sylvester, Z., 2018. Submarine fans and their channels, levees, and lobes: Submarine geomorphology, Springer, Cham. p. 273-299.

Dixon, J.F., Steel, R.J. and Olariu, C., 2012, Shelf-edge delta regime as a predictor of deep-water deposition: Journal of Sedimentary Research, v. 82, p. 681-687.

Dodd, T.J., Mccarthy, D.J., Amy, L., Plenderleith, G.E., and Clarke, S.M., 2022, Hybrid event bed character and distribution in the context of ancient deep-lacustrine fan models: Sedimentology, https://doi.org/10.1111/sed.12979

Dolan, J., 1984, A structural cross-section through the Carboniferous of northwest Kerry: Irish Journal of Earth Sciences, p. 95-108.

Elliott, T., 2000a, Depositional architecture of a sand-rich, channelized turbidite system: the Upper Carboniferous Ross Sandstone Formation, Western Ireland. in P. Weimer, R. M. Slatt, A. H. Bouma, and D. T. Lawrence, eds., Deep-water reservoirs of the world: Gulf Coast Section SEPM Foundation, Twentieth Annual Research Conference, p. 342–373.

Elliott, T., 2000b, Megaflute erosion surfaces and the initiation of turbidite channels: Geology, v. 28, p. 119-122.

Emmings, J.F., Davies, S.J., Vane, C.H., Moss-Hayes, V., and Stephenson, M.H., 2020, From marine bands to hybrid flows: Sedimentology of a Mississippian black shale: Sedimentology, v. 67, p. 261-304.

Enos, P., 1969, Anatomy of a flysch: Journal of Sedimentary Petrology, v. 39, p. 680–723.

Fielding, C.R., 2021, Late Palaeozoic cyclothems – A review of their stratigraphy and sedimentology: Earth-Science Reviews, v. 217, 10612.

Fielding, C.R., Frank, T.D., and Isbell, J.L., 2008, The late Paleozoic ice age—A review of current understanding and synthesis of global climate patterns: Geological Society of America Special Papers, 441, p. 343-354.

Fildani, A., Clark, J., Covault, J.A., Power, B., Romans, B.W., and Aiello, I.W., 2018, Muddy sand and sandy mud on the distal Mississippi fan: Implications for lobe depositional processes: Geosphere, v. 14, p. 1051-1066.

Fonnesu, M., Felletti, F., Haughton, P.D., Patacci, M., and McCaffrey, W.D., 2018, Hybrid event bed character and distribution linked to turbidite system sub-environments: The North Apennine Gottero Sandstone (north-west Italy): Sedimentology, v. 65, p.151-190.

Fonnesu, M., Patacci, M., Haughton, P.D., Felletti, F., and Mccaffrey, W.D., 2016, Hybrid event beds generated by local substrate delamination on a confined-basin floor: Journal of Sedimentary Research, v. 86, p. 929-943.

Fraser, A.J. and Gawthorpe, R.L., 1990, Tectono-stratigraphic development and hydrocarbon habitat of the Carboniferous in northern England: Geological Society, London, Special Publications, 55, p.49-86.

Gan, Y., de Almeida, F.N., Rossi, V.M., Steel, R.J. and Olariu, C., 2022, Sediment transfer from shelf to deepwater slope: How does it happen? Journal of Sedimentary Research, v. 92, p.570-590.

Grundvåg, S.A., Johannessen, E.P., Helland-Hansen, W., and Plink-Björklund, P., 2014, Depositional architecture and evolution of progradationally stacked lobe complexes in the Eocene Central Basin of Spitsbergen. Sedimentology, v. 61, p. 535-569.

Hansen, L.A.S., Hodgson, D.M., Pontén, A., Bell, D., and Flint, S., 2019, Quantification of basin-floor fan pinchouts: examples from the Karoo Basin, South Africa. Frontiers in Earth Science, v. 7, 12.

Haughton, P.D.W, 1994, Deposits of deflected and ponded turbidity currents, Sorbas Basin, Southeast Spain: Journal of sedimentary Research, v. 64, p. 233-246.

Haughton, P.D.W., 2000, Evolving turbidite systems on a deforming basin floor, Tabernas, SE Spain: Sedimentology, v. 47, p. 497-518.

Haughton, P., 2001, Contained turbidites used to track sea bed deformation and basin migration, Sorbas Basin, south-east Spain: Basin Research, v. 13, p. 117-139.

Haughton, P.D.W., Barker, S.P., and McCaffrey, W., 2003, “Linked” debrites in sand-rich turbidite systems – Origin and significance: Sedimentology, v. 50, p. 459-482

Haughton, P.D.W., Davis, C., McCaffrey, W., and Barker, S., 2009, Hybrid sediment gravity flow deposits – classification, origin and significance: Marine and Petroleum Geology, v. 26, p. 1900–1918.

Hodgson, D.M., 2009, Distribution and origin of hybrid beds in sand-rich submarine fans of Tanqua depocentre, Karoo Basin, South Africa: Marine and Petroleum Geology, v. 26, p. 1940-1957.

Hodson, F., 1951, The Beds Above the Carboniferous Limestone in North-West County Clare Eire: Doctoral thesis, University of Reading, Reading.

Hodson, F., 1954a, The beds above the Carboniferous Limestone in North-West Co Clare, Eire: Quarterly Journal of the Geological Society, v. 109, p. 259-283.

Hodson, F., 1954b, The Carboniferous rocks of Foynes Island, County Limerick: Geological Magazine, v. 91, p. 153-160.

Hodson, F., 1957, Marker horizons in the Namurian of Britain, Ireland, Belgium and western Germany: Association pour l'étude de la paléontologie et de la stratigraphie houillères.

Hodson, F., and Lewarne, G.C., 1961, A mid Carboniferous (Namurian) basin in parts of the counties Limerick and Clare, Ireland: Quarterly Journal of the Geological Society, v. 117, p. 307-333. doi: http://10.1144/gsjgs.117.1.0307

Hussain, A., and Al-Ramadan, K., 2022, Organic matter burial in deep-sea Fans: a depositional process-based perspective: Journal of Marine Science and Engineering, v. 10, p. 682.

Hussain, A., Haughton, P.D., Shannon, P.M., Morris, E.A., Pierce, C.S., and Omma, J.E., 2021, Mud-forced turbulence dampening facilitates rapid burial and enhanced preservation of terrestrial organic matter in deep-sea environments: Marine and Petroleum Geology, v. 130, p. 105101.

Hussain, A., Haughton, P.D.W., Shannon, P.M., Turner, J.N., Pierce, C.S., Obradors-Latre, A., Barker, S.P., and Martinsen, O.J., 2020, High-resolution X-ray fluorescence profiling of hybrid event beds: Implications for sediment gravity flow behaviour and deposit structure: Sedimentology, v. 67, p. 2850-2882. doi: http://10.1111/sed.12722

Ito, M., 2008, Downfan transformation from turbidity currents to debris flows at a channel-to-lobe transitional zone: The Lower Pleistocene Otadai Formation, Boso Peninsula, Japan: Journal of Sedimentary Research, v. 78, p. 668-682.

Kane, I. A., and Pontén, A. S., 2012, Submarine transitional flow deposits in the Paleogene Gulf of Mexico: Geology, v. 40, p. 1119-1122.

Kane, I.A., Ponten, A.S.M., Vangdal, B., Eggenhuisen, J.T., Hodgson, D.M., and Spychala, Y.T., 2017, The stratigraphic record and processes of turbidity current transformation across deep-marine lobes: Sedimentology, v. 64, p. 1236–1273

Kelk, B., 1960, Studies in the Carboniferous Stratigraphy of Western Ireland: Unpublished PhD thesis, University of Reading, 43 pp.

Kloster, A., 1987, Facies analysis of the Ross Formation: A Turbidite Sequence (Namurian H2 Age). The Western Irish Namurian Basin, Ireland: Unpublished Master Cand. Scient. Thesis, Geological Institute, University of Bergen.

Koo, W.M., Mohrig, D., Buttles, J., Sturmer, D., Pontén, A., and Hess, T., 2020, Sand–mud couplets deposited by spontaneous remobilization of subaqueous transitional flows: Sedimentology, v. 67, p. 78-95.

Lacchia, A.R., 2016, Ammonoid biostratigraphy of the Shannon Basin, western Ireland. Unpublished PhD thesis. Trinity College Dublin.

Lacchia, A.R., Sevastopulo, G.D., and Graham, J.R., 2016, Mid-Carboniferous ammonoids from the Shannon Basin, western Ireland: identification of crushed material: Swiss Journal of Palaeontology, v. 135, p. 75-85.

Leeder, M., 1976, Sedimentary facies and the origins of basin subsidence along the northern margin of the supposed Hercynian ocean: Tectonophysics, v. 36, p. 167-179.

Leeder, M., 1982, Upper Palaeozoic basins of the British Isles—Caledonide inheritance versus Hercynian plate margin processes: Journal of the Geological Society, v. 139, p. 479-491.

Lewarne, G.C., 1959, The junction of the Upper and Lower Carboniferous of County Clare and County Limerick, Eire: Unpublished PhD thesis, University of Reading

Lien, T., Walker, R.G., and Martinsen, O.J., 2003, Turbidites in the Upper Carboniferous Ross Formation, western Ireland: reconstruction of a channel and spillover system: Sedimentology, v. 50, p. 113–148. doi: http://10.1046/j.1365-3091.2003.00541.x

Liu, Q., Kneller, B., Fallgatter, C., Valdez Buso, V., and Milana, J.P., 2018, Tabularity of individual turbidite beds controlled by flow efficiency and degree of confinement: Sedimentology, v. 65, p. 2368-2387.

Lowe, D.R. and Guy, M., 2000, Slurry-flow deposits in the Britannia Formation (Lower Cretaceous), North Sea: a new perspective on the turbidity current and debris flow problem: Sedimentology, v. 47, p. 31–70.

Lowe, D., Guy, M. and Palfrey, A., 2003, Facies of slurry-flow deposits, Britannia Formation (Lower Cretaceous), North Sea: implications for flow evolution and deposit geometry. Sedimentology, v.50, p.45-80.

MacDonald, H.A., Peakall, J., Wignall, P.B., and Best, J., 2011, Sedimentation in deep-sea lobe-elements: implications for the origin of thickening-upward sequences: Journal of the Geological Society London, v. 168, p. 319-332. doi: http://10.1144/0016-76492010-036

Martinsen, O.J., 1987, Sedimentology and Syndepositional Deformation of the Gull Island Formation (Namurian R1), Western Irish Namurian Basin, Ireland - With Notes on the Basin Evolution. [MSc thesis]: University of Bergen.

Martinsen, O.J., and Collinson, J.D., 2002, The Western Irish Namurian Basin reassessed – a discussion: Basin Research, v. 14, p. 523-542. doi: http://10.1046/j.1365-2117.2002.00191.x

Martinsen, O.J., Lien, T., and Walker, R.G., 2000, Upper Carboniferous deep water sediments, western Ireland: analogues for passive margin turbidite plays, in P. Weimer, R.M. Slatt, J. Coleman, N. C. Rossen, H. Nelson, A.H. Bouma, M. J. Styzen, and D. T. Lawrence, eds., Deep-water reservoirs of the world, Gulf Coast Section-SEPM Special Publication, p. 533-555.

Martinsen, O.J., Lien, T., Walker, R.G., and Collinson, J.D., 2003, Facies and sequential organisation of a mudstone-dominated and basin floor succession: the Gull Island Formation, Shannon Basin, Western Ireland: Marine and Petroleum Geology, v. 20, p. 789-807. doi: http://dx.doi.org/10.1016/j.marpetgeo.2002.10.001

Martinsen, O.J., Pulham, A.J., Elliott, T., Haughton, P., Pierce, C., Lacchia, A.R., Barker, S., Obradors-Latre, A., Kane, I., and Shannon, P., 2017, Deep-water clastic systems in the Upper Carboniferous (Upper Mississippian–Lower Pennsylvanian) Shannon Basin, western Ireland: AAPG Bulletin, v. 101, p. 433-439.

Maynard, J.R., Hofmann, W., Dunay, R.E., Bentham, P.N., Dean, K.P., and Watson, I., 1997, The Carboniferous of western Europe: the development of a petroleum system: Petroleum Geoscience, v. 3, p. 97-115.

McHargue, Hodgson, D.M., and Shelef, E., 2021, Architectural diversity of submarine lobate deposits: Frontiers in Earth Science, 9, 697170. doi: 10.3389/feart.2021.697170

Migeon, S., Ducassou, E., Le Gonidec, Y., Rouillard, P., Mascle, J., and Revel-Rolland, M., 2010, Lobe construction and sand/mud segregation by turbidity currents and debris flows on the western Nile deep-sea fan (Eastern Mediterranean): Sedimentary Geology, v. *229*, p. 124-143.

Montañez, I.P., 2022, Current synthesis of the penultimate icehouse and its imprint on the Upper Devonian through Permian stratigraphic record: In Lucas, S. G., Schneider, J. W., Wang, X. and Nikolaeva, S. (eds) 2022. The Carboniferous Timescale. Geological Society, London, Special Publications, v. 512, p.213–245.

Montañez, I.P., and Poulsen, C.J., 2013, The Late Paleozoic ice age: an evolving paradigm: Annual Review of Earth and Planetary Sciences, v. 41, p. 629-656.

Morton, W., 1965, The Carboniferous stratigraphy of the area north-west of Newmarket, Co. Cork, Ireland: Proceedings of the Royal Dublin Society: Series A.

Mulder, T., and Etienne, S., 2010, Lobes in deep-sea turbidite systems: state of the art: Sedimentary Geology, v. 229, p. 75-80.

Mutti, E., 1977, Distinctive thin-bedded turbidite facies and related depositional environments in the Eocene Hecho Group (South-central Pyrenees, Spain): Sedimentology, v. 24, p. 107.

Mutti, E., 1979, Turbidites et cones sous-marins profonds. In: Sédimentation Détritique (Fluviatile, Littorale et Marine): vol. 1 (Ed. P. Homewood), p. 353–419. Institut Géologique Université de Switzerland, Fribourg.

Mutti, E., 1983, The Hecho Eocene submarine fan system, south-central Pyrenees, Spain: Geo-Marine Letters, v. 3, p. 199-202.

Mutti, E. 1992. Turbidite Sandstones. Agip, San Donato Milanese, 275.

Mutti, E., and Sonnino, M., 1981, Compensation cycles: a diagnostic feature of turbidite sandstone lobes. International Association of Sedimentologists, 2nd European Regional Meeting, Bologna, Italy: p. 120–123.

Muzzi Magalhaes, P., and Tinterri, R., 2010, Stratigraphy and depositional setting of slurry and contained (reflected) beds in the Marnoso-arenacea Formation (Langhian-Serravallian) Northern Apennines, Italy: Sedimentology, v. 57, p. 1685-1720.

Nauton-Fourteu, M., Tyrrell, S., Chew, D.M., Drakou, F., Pfaff, K., and Jobe, Z., 2021, Deep-versus shallow-marine sandstone provenance in the mid-Carboniferous Clare Basin, western Ireland: Journal of the Geological Society, v. 178. p.

Naylor, D., and Shannon, P., 2011, Petroleum geology of Ireland: Dunedin Academic Press Limited.

Ningthoujam, J., Wearmouth, C., and Arnott, R.W.C., 2022, Stratal characteristic and depositional origin of two-part (Mud-poor overlain by mud-rich) and associated deep-water strata: Components in a lateral depositional continuum related to particle settling in negligibly sheared mud-rich suspensions: Journal of Sedimentary Research, v. 92, p. 503-529.

Obradors-Latre, A., 2017, The large-scale architecture of the Pennsylvanian Ross Sandstone Formation, western Ireland – New insight from subsurface data and outcrop [PhD thesis]: University College Dublin.

O'Sullivan, G.J., Daly, J.S., Murray, J., Ó'Gogáin, A., Chew, D.M., Drakou, F., Guyett, P.C., Badenszki, E., Hoare, B.C., 2021, Uranium–lead phosphate chronostratigraphy: A proof of concept from the mid-Carboniferous boundary: Sedimentary Geology, v. 422, 105961, https://doi.org/10.1016/j.sedgeo.2021.105961.

Patacci, M., Haughton, P.D. and McCaffrey, W.D., 2014, Rheological complexity In sediment gravity flows forced to decelerate against a confining slope, Braux, SE France: Journal of Sedimentary Research, v. 84, p. 270-277.

Patacci, M., Marini, M., Felletti, F., Di Giulio, A., Setti, M. and McCaffrey, W., 2020, Origin of mud in turbidites and hybrid event beds: Insight from ponded mudstone caps of the Castagnola turbidite system (north-west Italy): Sedimentology, v.67, p. 2625-2644.

Paumard, V., Bourget, J., Payenberg, T., George, A.D., Ainsworth, R.B., Lang, S. and Posamentier, H.W., 2020, Controls on deep-water sand delivery beyond the shelf edge: accommodation, sediment supply, and deltaic process regime: Journal of Sedimentary Research, v. 90, p. 104-130.

Peakall, J., Best, J., Baas, J.H., Hodgson, D.M., Clare, M.A., Talling, P.J., Dorrell, R.M., and Lee, D.R., 2020. An integrated process-based model of flutes and tool marks in deep-water environments: Implications for palaeohydraulics, the Bouma sequence and hybrid event beds: Sedimentology, v. 67, p. 1601-1666.

Pickering, K.T., and Hiscott, R.N., 2015, Deep marine systems: processes, deposits, environments, tectonics and sedimentation. John Wiley and Sons.

Pierce, C.S., 2016, Development, distribution and evolution of gravity flow processes in the Pennsylvanian Ross Formation, western Ireland: University College Dublin, Unpublished PhD thesis.

Pierce, C.S., Haughton, P.D.W., Shannon, P.M., Pulham, A.J., Barker, S.P., and Martinsen, O.J., 2018, Variable character and diverse origin of hybrid event beds in a sandy submarine fan system, Pennsylvanian Ross Sandstone Formation, western Ireland: Sedimentology, v. 65, p. 952–992. doi:10.1111/sed.12412

Piper, D.J., and Normark, W.R., 1983, Turbidite depositional patterns and flow characteristics, Navy submarine fan, California Borderland. Sedimentology, v. 30, p. 681-694.

Posamentier, H.W., and Erskine, R.D., 1991, Seismic expression and recognition criteria of ancient submarine fans. In *Seismic facies and sedimentary processes of submarine fans and turbidite systems*, p. 197-222. Springer, New York, NY.

Prélat, A., Hodgson, D. M., and Flint, S. S., 2009, Evolution, architecture and hierarchy of distributary deep-water deposits: a high-resolution outcrop investigation from the Permian Karoo Basin, South Africa: Sedimentology, v. 56, p. 2132–2154.

Pyles, D.R., 2008, Multiscale stratigraphic analysis of a structurally confined submarine fan: Carboniferous Ross Sandstone, Ireland: AAPG Bulletin, v. 92, p. 557-587.

Pyles, D.R., and Jennette, D.C., 2009, Geometry and architectural associations of co-genetic debrite-turbidite beds in basin-margin strata, Carboniferous Ross Sandstone (Ireland): Applications to reservoirs located on the margins of structurally confined submarine fans: Marine and Petroleum Geology, v. 26, p. 1974-1996. doi: http://10.1016/j.marpetgeo.2009.02.018

Pyles, D.R., Strachan, L.J., and Jennette, D.C., 2014, Lateral juxtapositions of channel and lobe elements in distributive submarine fans: Three-dimensional outcrop study of the Ross Sandstone and geometric model: Geosphere, v. 10, p. 1104-1122.

Ramsbottom, W.H., 1977, Major cycles of transgression and regression (mesothems) in the Namurian: Proceedings of the Yorkshire Geological Society, v. 41, p. 261-291.

Remacha, E., and Fernández, L.P., 2003, High-resolution correlation patterns in the turbidite systems of the Hecho Group (South-Central Pyrenees, Spain): Marine and Petroleum Geology, v. 20, p. 711-726.

Remacha, E., Fernández, L.P., and Maestro, E., 2005, The transition between sheet-like lobe and basin-plain turbidites in the Hecho Basin (South-Central Pyrenees, Spain): Journal of Sedimentary. Research, v. 75, p. 798–819.

Ricci Lucchi, F., and Valmori, E., 1980, Basin-wide turbidites in a Miocene, over-supplied deep-sea plain: a geometrical analysis: Sedimentology, v. 27, p. 241–270.

Rider, M.H., 1974, The Namurian of West Co Clare: Proceedings of the Royal Irish Academy, v. 74, p. 125-142.

Rygel, M.C., Fielding, C.R., Frank, T.D., and Birgenheier, L.P., 2008, The magnitude of Late Paleozoic glacioeustatic fluctuations: a synthesis: Journal of Sedimentary Research, v. 78, p. 500-511.

Sevastopulo, G.D., 2009, Carboniferous: Mississippian (Tournaisian and Viséan): The Geology of Ireland. 2nd revised edition. Academic Press, Dunedin, p. 215–268.

Somerville, I.D., 2016, Lower Carboniferous of the Shannon Basin Region: in 'A Field Guide to the Carboniferous Sediments of the Shannon Basin, Western Ireland' (J. L. Best and P. B. Wignall Eds.): John Wiley and Sons, p. 48-78.

Southern, S.J., Kane, I.A., Warchoł, M.J., Porten, K.W., and McCaffrey, W.D., 2017, Hybrid event beds dominated by transitional-flow facies: character, distribution and significance in the Maastrichtian Springar Formation, north-west Vøring Basin, Norwegian Sea. Sedimentology, v. 64, p. 747-776.

Southern, S.J., Patacci, M., Felletti, F., and McCaffrey, W.D., 2015, Influence of flow containment and substrate entrainment upon sandy hybrid event beds containing a co-genetic mud-clast-rich division: Sedimentary Geology, v. 321, p. 105-122.

Soutter, E.L., Kane, I.A., Fuhrmann, A., Cumberpatch, Z.A., and Huuse, M., 2019, The stratigraphic evolution of onlap in siliciclastic deep-water systems: Autogenic modulation of allogenic signals: Journal of Sedimentary Research, v. 89, p. 890-917.

Spychala, Y.T., Hodgson, D.M., Prélat, A., Kane, I.A., Flint, S.S., and Mountney, N.P., 2017a, Frontal and lateral submarine lobe fringes: comparing sedimentary facies, architecture and flow processes: Journal of Sedimentary Research, v. 87, p. 75-96.

Spychala, Y.T., Hodgson, D.M., Stevenson, C.J., and Flint, S.S., 2017b, Aggradational lobe fringes: The influence of subtle intrabasinal seabed topography on sediment gravity flow processes and lobe stacking patterns: Sedimentology, v. 64, p. 582-608.

Straub, K.M., and Pyles, D.R., 2012, Quantifying the Hierarchical Organization of Compensation In Submarine Fans Using Surface Statistics: Journal of Sedimentary Research, v. 82, p. 889-898.

Strogen, P., 1988, The Carboniferous lithostratigraphy of southeast County Limerick, Ireland, and the origin of the Shannon Trough: Geological Journal: v. 23, p. 121-137.

Strogen, P., Somerville, I., Pickard, N., Jones, G.L., and Fleming, M., 1996, Controls on ramp, platform and basinal sedimentation in the Dinantian of the Dublin Basin and Shannon Trough, Ireland: Geological Society, London, Special Publications, v. 107, p. 263-279.

Stetten, E., Baudin, F., Reyss, J.L., Martinez, P., Charlier, K., Schnyder, J., Rabouille, C., Dennielou, B., Coston-Guarini, J. and Pruski, A.M., 2015, Organic matter characterization and distribution in sediments of the terminal lobes of the Congo deep-sea fan: Evidence for the direct influence of the Congo River: Marine Geology, v.369, p.182-195.

Sumner, E.J., Amy, L.A., and Talling, P.J., 2008, Deposit structure and processes of sand deposition from decelerating sediment suspensions: Journal of Sedimentary Research, v. 78, p. 529-547.

Sumner, E.J., Talling, P.J. and Amy, L.A., 2009, Deposits of flows transitional between turbidity current and debris flow: Geology, v. 37, p.991-994.

Sumner, E.J., Talling, P.J., Amy, L.A., Wynn, R.B., Stevenson, C.J., and Frenz, M., 2012, Facies architecture of individual basin-plain turbidites: Comparison with existing models and implications for flow processes: Sedimentology, v. 59, p. 1850-1887.

Sylvester, Z. and Lowe, D.R., 2004, Textural trends in turbidites and slurry beds from the Oligocene flysch of the East Carpathians, Romania: Sedimentology, v. 51, p. 945–972.

Talling P.J., 2013, Hybrid submarine flows comprising turbidity current and cohesive debris flows: Deposits, theoretical and experimental analyses, and generalized models: Geosphere, vol.9, n. 3, 460-488. doi: http://10.1130/ges00793.1

Talling, P.J., Amy, L.A., and Wynn, R.B., 2007, New insight into the evolution of large-volume turbidity currents: comparison of turbidite shape and previous modelling results: Sedimentology, 54, 737-769.

Talling, P.J., Amy, L.A., Wynn, R.B., Peakall, J., and Robinson, M., 2004, Beds comprising debrite sandwiched within co-genetic turbidite: Origin and widespread occurrence in distal depositional environments: Sedimentology, v. 51, pp. 163-194

Talling, P.J., Malgesini, G., Sumner, E.J., Amy, L.A., Felletti, F., Blackbourn, G., Nutt, C., Wilcox, C., Harding, I.C., and Akbari, S., 2012, Planform geometry, stacking pattern, and extrabasinal origin of low strength and intermediate strength cohesive debris flow deposits in the Marnoso-arenacea Formation, Italy: Geosphere, v. 8, p. 1207-1230

Talling, P.J., Weichell, D.C., Wynn, R.B., Schmidt, D.N., Rixon, R., Sumner, E., and Amy, L., 2010, How did thin submarine debris flow carry boulder sized clasts for remarkable distances across low gradients to the far reaches of the Mississippi Fan?: Journal of Sedimentary Research, v. 80, p. 829 - 851.

Terlaky, V., and Arnott, R.W.C., 2014, Matrix-rich and associated matrix-poor sandstones: avulsion splays in slope and basin-floor strata: Sedimentology, v. 61, p. 1175–1197

Tinterri, R., and Magalhaes, P.M., 2011, Synsedimentary structural control on foredeep turbidites: An example from Miocene Marnoso-arenacea Formation, Northern Apennines, Italy: Marine and Petroleum Geology, v. 28, p. 629-657.

Tőkés, L., and Patacci, M., 2018, Quantifying tabularity of turbidite beds and its relationship to the inferred degree of basin confinement: Marine and Petroleum Geology, v. *97*, p. 659-671.

Waters, C.N., and Condon, D.J., 2012, Nature and timing of Late Mississippian to Mid-Pennsylvanian glacio-eustatic sea-level changes of the Pennine Basin, UK: Journal of the Geological Society, v. 169, p. 37-51.

Wignall, P.B., and Best, J.L., 2000, The Western Irish Namurian Basin reassessed. Basin Research: v. 12, p. 59-78. doi: http://10.1046/j.1365-2117.2000.00113.x

Wignall, P.B., and Best, J.L., 2016, Basin Models in 'A Field Guide to the Carboniferous Sediments of the Shannon Basin, Western Ireland' (J. L. Best and P. B. Wignall Eds.): John Wiley and Sons, Chapter 3, 35-47.

Wignall, P.B., Somerville, I.D., and Braithwaite, K., 2016, The Clare Shales in 'A Field Guide to the Carboniferous Sediments of the Shannon Basin, Western Ireland' (J. L. Best and P. B. Wignall Eds.): John Wiley and Sons, Chapter 6, 97-111.

Wood, A. and Smith, A.J., 1958, The sedimentation and sedimentary history of the Aberystwyth Grits (Upper Llandoverian): Journal of Geological Society of London, v. 114, p. 163-195.

Zhang, L., and Yilong, L.I., 2020, Architecture of deepwater turbidite lobes: A case study of Carboniferous turbidite outcrop in the Clare Basin, Ireland: Petroleum Exploration and Development, v. 47, p. 990-1000.

Figure captions

Fig. 1: (A). Regional geological setting of the Carboniferous Shannon Basin in the west of Ireland (after Kelk (1960), Hodson and Lewarne (1961), Morton (1965), Geological Survey Ireland (GSI) Map and Martinsen et al. (2003)) with colours here and in (C) keyed to a generalised stratigraphic section (B) showing the main lithostratigraphic units and chronostratigraphy. The study area straddles the mouth of the Shannon estuary and the geology here is shown in more detail in (C) together with the locations of the behind-outcrop boreholes. The study reported here focuses on the 10-CE-UCD-03, 10-CE-UCD-05 and 12-KY-UCD-09 boreholes (abbreviated hereafter -03, -05 and -09) that intersect the base of the Ross Sandstone Fm (herafter Ross Fm), summary gamma logs for which are shown all at the same scale in red. Rose diagram is for all of Ross Fm from Pierce (2016) with additional data (Pierce unpublished) and includes a combination of sole structures, megaflutes and current ripple orientations.

Fig. 2: Composite gamma log (on left) for the Ross Sandstone Formation constructed by correlating and stacking logs from behind-outcrop boreholes from the north side of Loop Head (-01/01RE, -02, -03 and -06; see Fig. 1 for location) and highlighting subdivision of the Ross Fm using condensed sections (units R5 to R90; see Pierce et al. 2018). Detailed extract (on right) shows Clare Shale to Lower Ross Fm study interval based on stacking the -03 and -09 (for the hot Mid-Clare Shale interval) boreholes with biostratigraphy from ammonoids in the main condensed sections in the adjacent foreshore exposures from Kelk (1960) and Lacchia (2016) and link to northwest European ammonoid zones from Waters and Condon 2012.

Fig. 3: Geological map of the foreshore at Ballybunion spanning the contact between the Clare Shale and Ross formations and showing the main stratigraphic units and relationship between the coastal outcrop and the location of the -09 borehole which entered the Ross Fm close to the top of R20.

Distribution of condensed sections and associated ammonoids from Kelk (1960) and Lacchia (2016) with subdivision of the Ross Fm using condensed sections into units R5 to R50 from Pierce et al. (2018). The inset shows the gamma log from the -09 borehole, with the five main units discussed in the text distinguished by colour. Note the sub-division of the Clare Shale Fm into a lower 'hot' shale with stacked condensed sections, and an upper grey unit with a lower gamma signature.

Fig. 4: Summary of the bed type classification used to characterise the Basal and Lower Ross and Upper Grey Clare Shale formations modified after Pierce et al. (2018). Different bed types are grouped into four inferred facies tracts, with different facies tracts occurring at different stratigraphic levels. Note Facies tract 1 straddles the base of the Ross Fm (units R5 and R10) and the Upper Grey Clare Shale Fm. Kelk (1960) referred to the distinctive character of the first sandstone beds as the Cosheen system and this term is retained for the Facies tract 1 deposits. These sit beneath the Ross system (R20 and above). Facies tract 2 occurs in the lower part of R20, whereas above this level, the main part of the Ross Fm is dominated by an alternation of facies tracts 3 and 4. Codes for typical turbidite and hybrid event bed internal divisions after Bouma (1962) and Haughton et al. (2009), respectively. See Table 1 for detailed description of of bed types. TB refers to turbidite, HEB to hybrid event bed, Bk to background fines and CS to condensed mudstones.

Fig. 5: Summary core description from the -09 borehole north of Ballybunion matched to a gamma log in the borehole and distinguishing the five units (and subunits) discussed in this text. Ross Fm units defined using condensed sections R5 to R20 after Pierce et al. (2018). The depths shown and used throughout the paper are from a continuous *Televiewer* image in the borehole to which the cores have been matched. A track summarising the bed type mix is shown next to the core log and distinguishes the relative proportion of turbidites (TB), hybrid event beds (HEB), background siltstones (Bk) and condensed mudstones with ammonoids (CS). The track was created using a one metre sliding average.

Fig. 6: Comparison of the Clare Shale Fm and overlying Ross R5 unit in the -09 borehole and a measured section taken on the foreshore (Fig. 3) through the equivalent section 385 m (base of section) to 200 m (top of section) south of the borehole location. For key to graphic logs, see Fig. 5. Borehole thicknesses have been corrected for an average tectonic dip of 22.3°. Note the expansion of the Upper Grey Clare Shale Fm unit northwards from the foreshore exposure into the borehole. Ammonoid determinations on the foreshore from Kelk (1960) and these have been extrapolated into the borehole.

Fig. 7: Core photographs (from -09 borehole) illustrating the character of the Mid- to Upper Clare Shale Fm north of Ballybunion. Core photographs are annotated with depths alonghole in metres derived from matching the core to borehole *Televiewer* imagery. Location of core images shown on Figs 5 and 6: (A). Stacked thin calcareous bioclastic beds with dolomitic cement close to the base of the cored Clare Shale Fm. (B). Transition from calcareous beds in A to dark carbonaceous mudstones with locally pyritised ammonoids and *Dunbarella* bivalves representing a condensed section. (C). Light-coloured sand-speckled siltstone beds alternating with subordinate black mudstones (the latter interpreted as background). Note the very thin coarser grained sand laminae at the base of some of the paler siltstone beds, not to be confused with early diagenetic nodule at 132.72 m. (D). Thicker HEB8 with more prominent but thin sandstone (120.64 m) overlain by thick pale sand-speckled siltstone. (E). First event bed with a sandy basal unit >5 cm-thick marking the base of the Ross Formation (unit R5). Note the thick overlying graded siltstone with coarse silt pseudonodules developed over the lower 20 cm.

Fig. 8: Correlation of Upper Grey Clare Shale Fm and lower part basal Ross Fm unit R5 in an 18.15 km long panel linking the -03, -05 and -09 boreholes. Note boreholes -03 and -05 did not penetrate deep enough to intersect the 'hot' mid-Clare Shale unit beneath Loop Head. However, inversion of electromagnetic data (Campanyà et al. 2019) suggests conductive (pyrite-rich) shales are present deeper in the subsurface here. A minimum thickness of the Upper Grey Clare Shale unit in the -03

borehole exceeds the full thickness of this unit in the -09 borehole, indicating it thins to the east. Thicknesses are true thicknesses corrected for apparent bedding dip using values posted next to graphic logs. Pie charts break out the bed type mix at different stratigraphic levels (lower and upper subunits of Upper Grey Clare Shale Fm) distinguishing HEB2b and HEB8 and background dark siltstones. Histograms summarise the event bed thicknesses. Note HEB8 tend to be thicker and have more prominent basal sandstone divisions in the up dip -03 borehole. Cored hot Mid-Clare Shale Fm in -09 not shown (see Fig. 5).

Fig. 9: Corelation panel relating the Ross Fm R5 to R20 section in the -09 borehole to the equivalent section exposed on the foreshore SE of Leck Point north of Ballybunion. Borehole depths scaled to true thickness at same scale as outcrop log. Paleocurrent roses combine directions from grooves and sense of transport from flutes and ripple cross-lamination. Ammonoid determinations from Lacchia (2016). Note base of R5 not shown. See Fig. 5 for key to graphic logs.

Fig. 10: Interpreted correlation panel linking the R10 succession cored in the -03, -05 and -09 boreholes (see Fig. 1 for location) hung on the *Hudsonoceras proteus*/*Homoceras smithii* condensed section. Depths next to the core logs are along-hole matched to *Televiewer* images, but the scales have been adjusted for structural dip (8° in -03, 15° in -05 and 22° in 09) so that all boreholes are in true depth. Summary core logs are accompanied in each case by a down-hole gamma ray log (red curves). Note the finer grained interval highlighted in the lower part of R10; inferred lateral transitions at this level are shown in more detail in Fig. 13 and discussed in the text. Pie charts show bed type make-up for R5 and R10 in the three boreholes. See Fig. 5 for key to graphic logs.

Fig. 11: Example of HEB1b event bed at R10 level in the -09 core. See Fig. 5 for bed location. Core photographs to the left are annotated with along-hole core depths (derived from matching core to *Televiewer* images). The location of a series of plug samples used to cut thin sections are highlighted by the lettered red dots; these targeted matrix between mudstone clasts in the central part of the event bed. Three photomicrographs (PPL) for plugs A, I and M shown at the same scale highlight

vertical changes in texture. The H1, H3, H4 and H5 divisions (terminology from Haughton et al. 2009) of the event bed are indicated on the central Televiewer image against which to the right are tracks showing the vertical textural and compositional make-up from petrography and point counting (300 points per thin section). The mean grain size and sorting are derived from measurements of 100 grain maximum diameters with maximum grain size from an average of the diameter of the 10 largest grains.

Fig. 12: (A-F). Examples of R10 event beds in core and (G,H) and on the foreshore north of Ballybunion. (A-C). HEB1a event bed in the -03 borehole at Loop Head. Depths are along-hole derived from matching core to *Televiewer* images. The location of the event bed is shown on Figs 10 and 13. (D-F). HEB2 event bed in the -09 borehole. Depths are along-hole derived from matching core to *Televiewer* images. Note approx. 10 cm of core is missing at the rubbled interval. See Figs 5 and 10 for location. Note the well-developed H3 debritic division. (G). Outcrop of HEB2 in vertical cliff just south of Glenachoor River north of Ballybunion (see Fig. 3) approx. 125 m south of the -09 borehole. Borehole gamma log and depths superimposed on cliff. The event bed is the same as the one illustrated in (D-F). Note the large. folded clast (i), flat base to H1 (ii), irregular H1 division thickness (III) and thin sandy H4 division (iv). (H). First of the thicker event beds at the base of R10 c.150 m south of the -09 borehole (see Fig. 3 for location). This is the same event bed from the -09 borehole profiled in Fig 11.

Fig. 13: Detailed graphic logs for a short section of R10 cored in the -03, -05 and -09 boreholes that captures the lateral passage from thicker sandier event beds in the west to thinner bedded HEB8 in the east. See Fig. 10 for broader context of section. Depths shown are matched to *Televiewer* images and scales adjusted to show the same true thickness across the three boreholes. Red curves are the associated open hole gamma logs. Note change in character of thin event beds between the thicker HEBs in passing from -03 to -09 via -05. See text for discussion. See Fig. 5 for key to graphic logs.

Fig. 14: (A). Comparison of thin event bed dimensions and textural make-up for the relatively fine-grained interval shown in Fig. 13. Note event beds in the west are thinner but typically a greater proportion of the event bed comprises a well-structured basal sandstone division. Thin beds in -09 to the east are thicker but the basal sandstone is thinner or absent and they are now dominated by prominent upper sand-speckled siltstone divisions. (B-D). Representative core photographs at the same scale illustrating structure of thin beds in the -03 (B), -05 (C) and -09 (D) boreholes. Location of the core photographs shown on graphic core logs in Fig. 13.

Fig. 15: Interpreted correlation panel for the R20 Ross unit spanning the -03, -05 and -09 boreholes constrained by upper and lower condensed sections and hung on a minor condensed section in the mid-upper part of the unit. Depths on core logs are matched to *Televiewer* images and gamma logs and corrected for apparent thickness due to variable structural dip. Colours highlight interpreted depositional environments and highlight muddy (i) and sandy HEBs (ii) that dominated the outer fan down-dip from alternations of amalgamated and less well amalgamated packages (iii) related to up-dip lobe stacking. Above the internal condensed section, turbidites (iv) become more important in -05 and -09 (see Fig. 5) recording a change in system character from the initial upward-sandying, HEB dominated lower part of R20 (Ross fan system initiation and growth) to the main phase of Ross deposition dominated by alternating facies tracts 3 and 4 (see Fig. 4). Pie charts show bed type make-up for R5 and R10 in the three boreholes. See Fig. 5 for key to graphic logs.

Fig. 16: Examples of R20 event bed type in the -09 core (see Fig. 5 for location) and on the foreshore c. 200 m to the west of the borehole (Fig. 3). Depths annotated on the core photographs are along-hole from matching core to *Televiewer* images in metres from the surface. (A). HEB3a showing basal banded sandstone (to 52.5m), overlain by a central muddy sandstone with banding, dewatering an internal shearing passing upward into dark coloured mudstone cap. (B). A pair of contrasting event beds, the lower HEB6 with well-developed H1, H3, H4 (largely prolapsed into H3) and H5 internal divisions. The upper a HEB3b with reduced thickness of the basal H1 overlain by a banded H2 divison

and a thick graded mudstone cap. (C). A thick HEB3b with a prominent 'slurried' muddy sandstone division with sheared cleaner sandstone patches and mud clasts passing upwards into a mudstone cap. (D). Stacked sandstone turbidites with typical Bouma divisions in the upper part of R20; contrast these with the beds shown in A-C. (E). Typical turbidite from the upper part of R20 on the foreshore. Coin for scale. (F). HEB6 on the foreshore – this is the same event bed present in the lower part of the core stick shown in B. Note the very similar bed structure including the prolapsed H4 division to that in the core 200 m away. Coin for scale. (G). Stacked mid R20 event beds illustrating sharp bases and upward gradation into thick mudstone caps.

Fig. 17: Paleogeographic reconstructions and facies tracts for (A) the Cosheen system shown for unit R10 of the basal Ross Formation, and (B) the Ross System for unit R20 (lower Ross Fm). Red line indicates the modern coastline. Distribution of systems constrained by outcrops and boreholes in the outer Shannon area, as well as the Doonbeg, IPP-1, IPP-2 and GSI-09/04 boreholes.

Fig. 18: Schematic summarising the inferred flow transformations, flow runout and resulting distal architecture in HEB-dominated fringes associated with: (A) the early Cosheen sheet system with re-flowage of muddy and wet sections of the mudstone clast-rich linked debrites promoting runout of relatively thick mudflows for 10s km down dip from the sand pinch out, and (B) initial progradation of the younger Ross fan system with turbulence damping arresting muddy sections of the flows that largely failed to outrun the distal sand pinch outs producing distinctive sandstone-mudstone couplets that taper distally.

Fig. 19: Summary illustrating the wide context in which hybrid event beds have been identified in deep-water systems, ranging from channels (Haughton et al. 2009) and topographically-controlled constrictions (Davis et al. 2009), avulsion nodes (Terlaky and Arnott 2014), channel-lobe transition zones (Brooks et al. 2018, 2022; Baas et al. 2022), lobe fringes (Kane et al. 2017; Dodd et al. 2022), outer fan and basin plain (this study) and contained basin plain successions (Muzzi Magalhaes and Tinterri, 2010; Fonnesu et al. 2018).

Table 1: Summary of bed type and facies codes and criteria used to assign bed types.

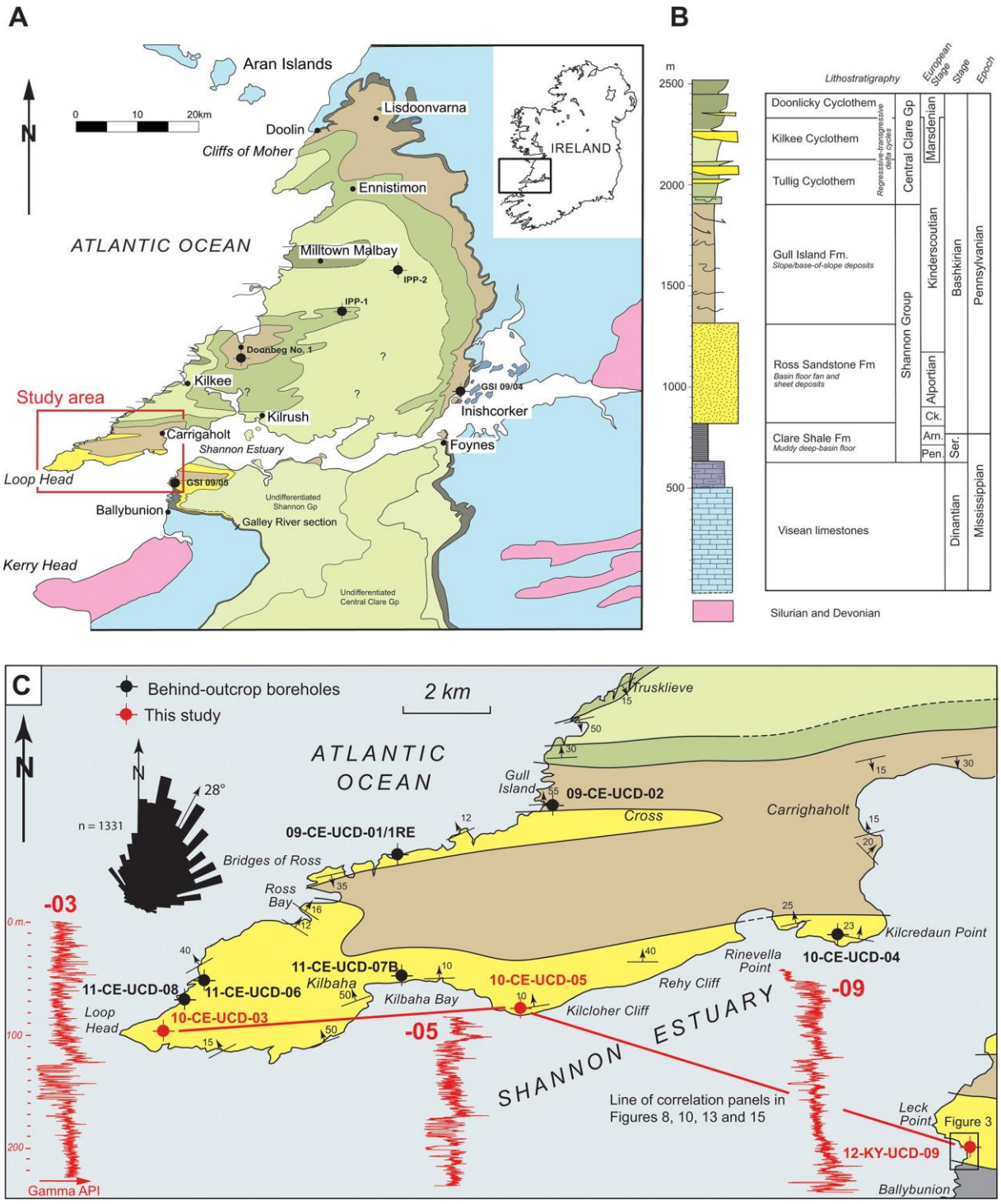
A
B
C
Aran Islands
Lisdoonvarna
Doolin
Cliffs of Moher
Ennistimon
IRELAND
ATLANTIC OCEAN
Milltown Malbay
IPP-2
IPP-1
Doonbeg No. 1
Kilkee
Study area
GSI 09/04
Inishcorker
Kilrush
Carrigaholt
Shannon Estuary
Foynes
Loop Head
GSI 09/05
Undifferentiated Shannon Gp
Ballybunion
Galley River section
Kerry Head
Undifferentiated Central Clare Gp
m
2500
2000
1500
1000
500
Lithostratigraphy
European Stage
Stage
Epoch
Doonlicky Cyclothem
Kilkee Cyclothem
Tullig Cyclothem
Regressive-transgressive delta cycles
Central Clare Gp
Marsdenian
Gull Island Fm.
Slope/base-of-slope deposits
Kinderscoutian
Bashkirian
Pennsylvanian
Shannon Group
Ross Sandstone Fm
Basin floor fan and sheet deposits
Alportian
Ck.
Clare Shale Fm
Muddy deep-basin floor
Arn.
Pen.
Ser.
Visean limestones
Dinantian
Mississippian
Silurian and Devonian
Behind-outcrop boreholes
This study
2 km
n = 1331
28°
Truskliève
Gull Island
09-CE-UCD-02
Cross
Carrighaholt
09-CE-UCD-01/1RE
Bridges of Ross
Ross Bay
-03
0 m
Kilcredaun Point
10-CE-UCD-04
11-CE-UCD-07B
Kilbaha
11-CE-UCD-08
11-CE-UCD-06
10-CE-UCD-05
Rinevella Point
Rehy Cliff
Kilbaha Bay
Loop Head
10-CE-UCD-03
-05
-09
Kilcloher Cliff
SHANNON ESTUARY
Line of correlation panels in Figures 8, 10, 13 and 15
Leck Point
Figure 3
12-KY-UCD-09
100
200
Gamma API
Ballybunion

Figure 1

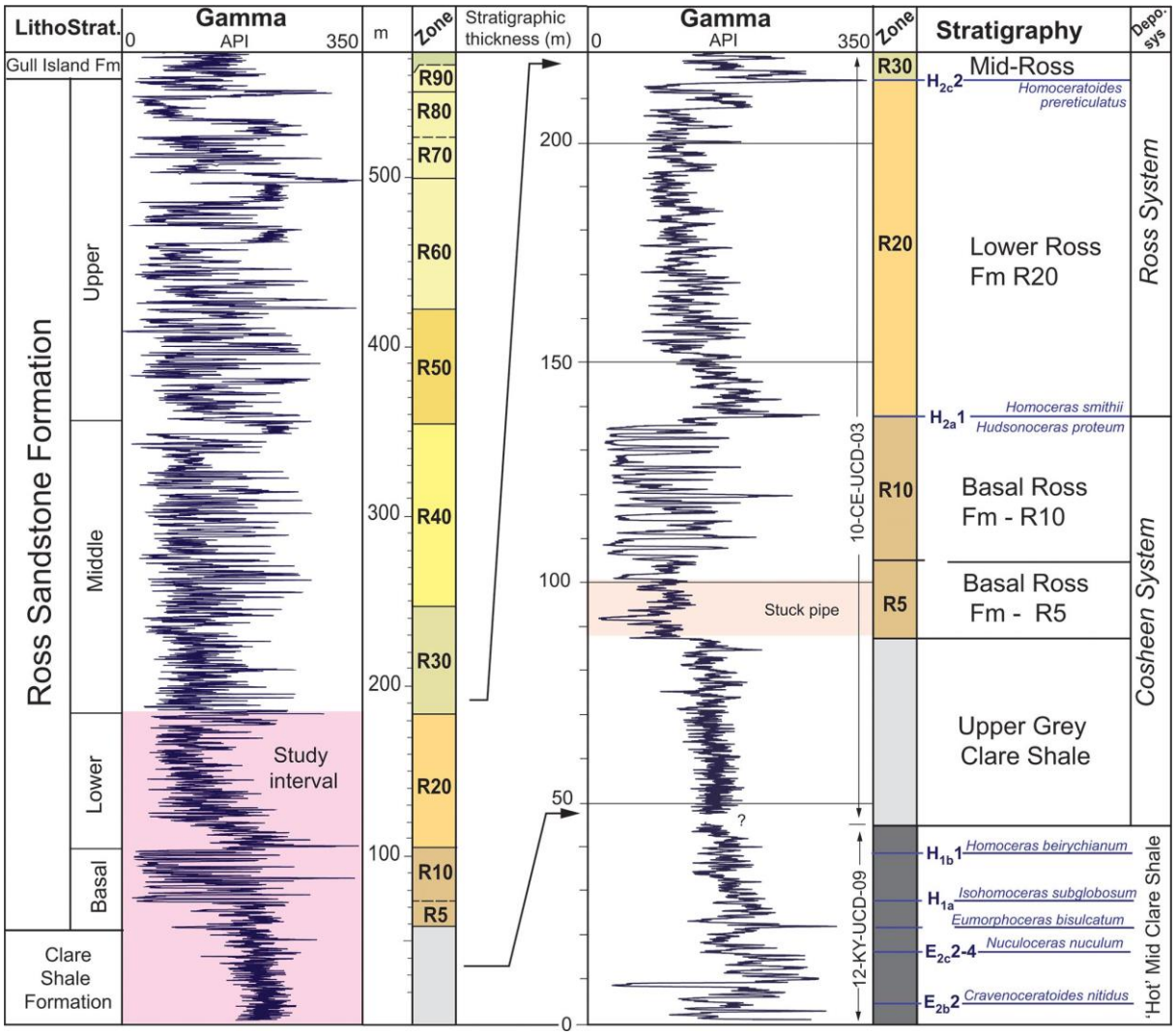
LithoStrat.
Gamma
0
API
350
m
Zone
Stratigraphic thickness (m)
Gamma
0
API
350
Zone
Stratigraphy
Depo. sys
Gull Island Fm
Ross Sandstone Formation
Upper
Middle
Lower
Basal
Clare Shale Formation
Study interval
R90
R80
R70
R60
R50
R40
R30
R20
R10
R5
500
400
300
200
100
200
150
100
50
0
Stuck pipe
?
10-CE-UCD-03
12-KY-UCD-09
R30
R20
R10
R5
H2c2
Homoceratoides prereticulatus
Mid-Ross
Lower Ross Fm R20
H2a1
Homoceras smithii
Hudsonoceras proteum
Basal Ross Fm - R10
Basal Ross Fm - R5
Upper Grey Clare Shale
H1b1
Homoceras beirychianum
H1a
Isohomoceras subglobosum
Eumorphoceras bisulcatum
E2c2-4
Nuculoceras nuculum
E2b2
Cravenoceratoides nitidus
Ross System
Cosheen System
'Hot' Mid Clare Shale

Figure 2

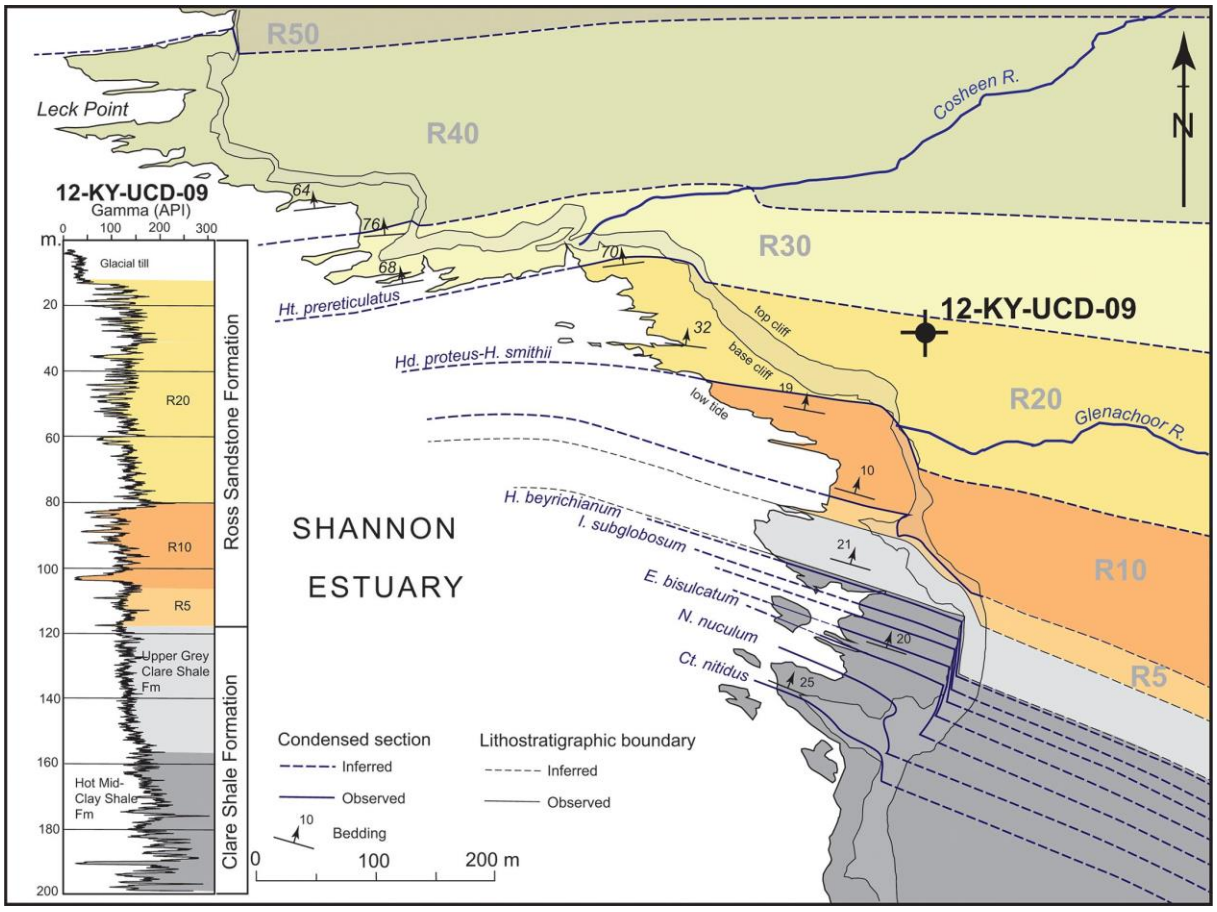
R50
R40
R30
R20
R10
R5
Leck Point
Cosheen R.
N
12-KY-UCD-09
Gamma (API)
0 100 200 300
m.
Glacial till
R20
R10
R5
Upper Grey Clare Shale Fm
Hot Mid-Clay Shale Fm
Ross Sandstone Formation
Clare Shale Formation
20
40
60
80
100
120
140
160
180
200
64
76
68
70
32
19
10
21
20
25
Ht. prereticulatus
Hd. proteus-H. smithii
top cliff
base cliff
low tide
12-KY-UCD-09
Glenachoor R.
H. beyrichianum
I. subglobosum
E. bisulcatum
N. nuculum
Ct. nitidus
SHANNON
ESTUARY
Condensed section
Inferred
Observed
Bedding
Lithostratigraphic boundary
Inferred
Observed
0
100
200 m

Figure 3

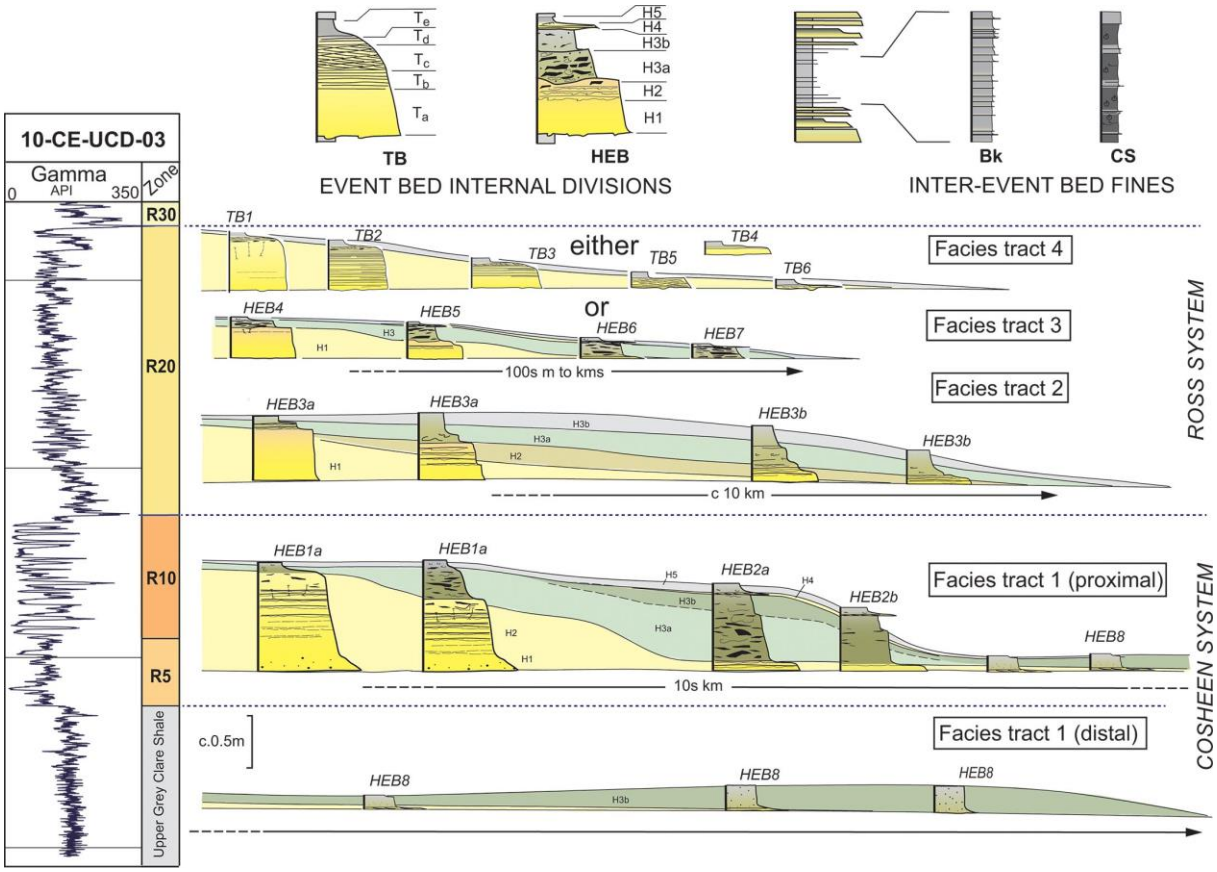
10-CE-UCD-03
Gamma
API
0
350
Zone
R30
R20
R10
R5
Upper Grey Clare Shale
Te
Td
Tc
Tb
Ta
TB
H5
H4
H3b
H3a
H2
H1
HEB
EVENT BED INTERNAL DIVISIONS
Bk
CS
INTER-EVENT BED FINES
TB1
TB2
TB3
either
TB5
TB4
TB6
Facies tract 4
HEB4
HEB5
or
HEB6
HEB7
Facies tract 3
100s m to kms
Facies tract 2
HEB3a
HEB3a
HEB3b
HEB3b
c 10 km
ROSS SYSTEM
HEB1a
HEB1a
HEB2a
HEB2b
Facies tract 1 (proximal)
HEB8
10s km
c.0.5m
Facies tract 1 (distal)
HEB8
HEB8
HEB8
COSHEEN SYSTEM

Figure 4

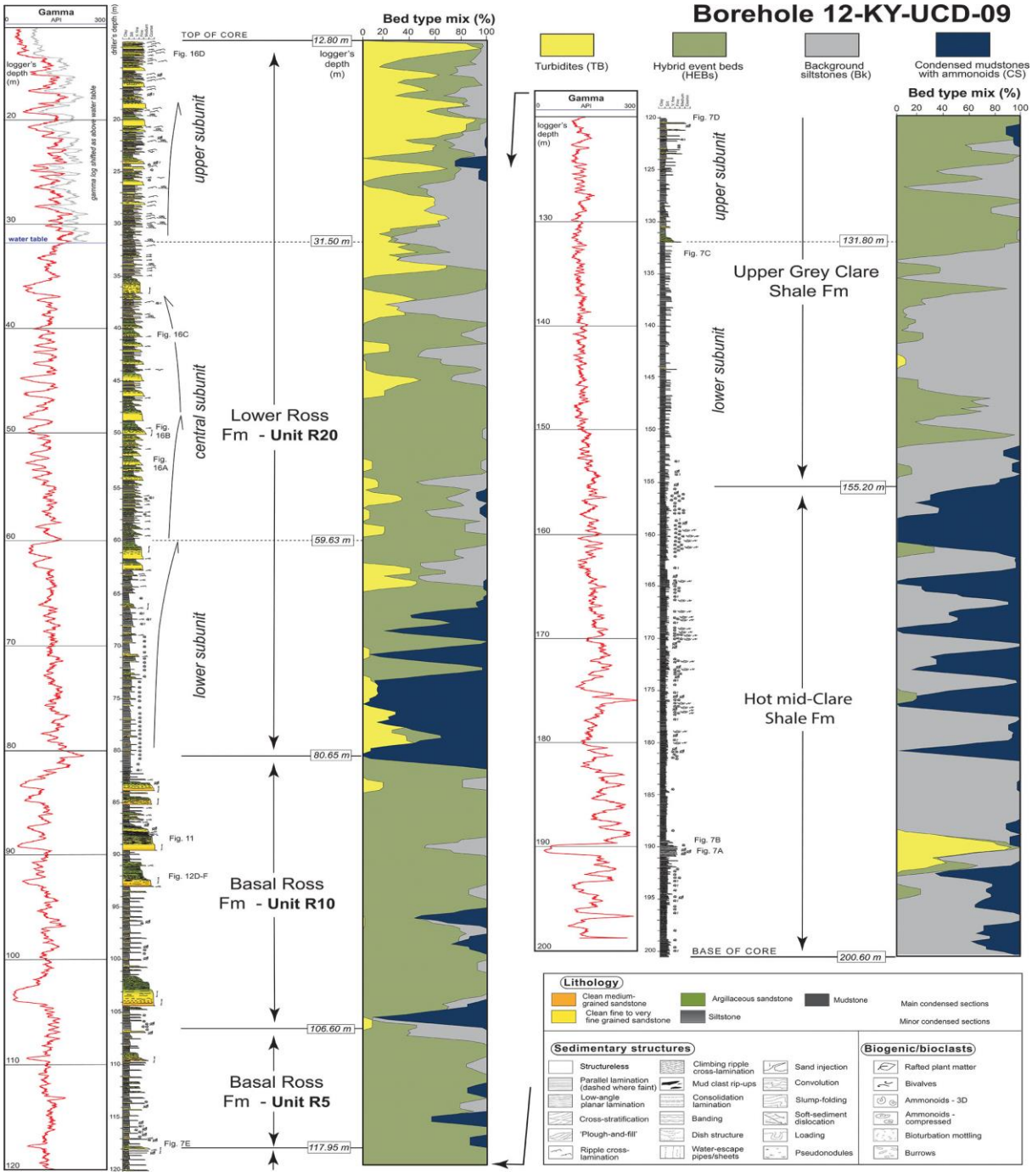
Borehole 12-KY-UCD-09
Gamma
API
Bed type mix (%)
Turbidites (TB)
Hybrid event beds (HEBs)
Background siltstones (Bk)
Condensed mudstones with ammonoids (CS)
logger's depth (m)
TOP OF CORE
12.80 m
31.50 m
59.63 m
80.65 m
106.60 m
117.95 m
131.80 m
155.20 m
200.60 m
BASE OF CORE
upper subunit
central subunit
lower subunit
Lower Ross Fm - Unit R20
Basal Ross Fm - Unit R10
Basal Ross Fm - Unit R5
Upper Grey Clare Shale Fm
Hot mid-Clare Shale Fm
water table
gamma log shifted as above water table
Fig. 16D
Fig. 16C
Fig. 16B
Fig. 16A
Fig. 11
Fig. 12D-F
Fig. 7E
Fig. 7D
Fig. 7C
Fig. 7B
Fig. 7A
Lithology
Clean medium-grained sandstone
Clean fine to very fine grained sandstone
Argillaceous sandstone
Siltstone
Mudstone
Main condensed sections
Minor condensed sections
Sedimentary structures
Structureless
Parallel lamination (dashed where faint)
Low-angle planar lamination
Cross-stratification
'Plough-and-fill'
Ripple cross-lamination
Climbing ripple cross-lamination
Mud clast rip-ups
Consolidation lamination
Banding
Dish structure
Water-escape pipes/sheets
Sand injection
Convolution
Slump-folding
Soft-sediment dislocation
Loading
Pseudonodules
Biogenic/bioclasts
Rafted plant matter
Bivalves
Ammonoids - 3D
Ammonoids - compressed
Bioturbation mottling
Burrows

Figure 5

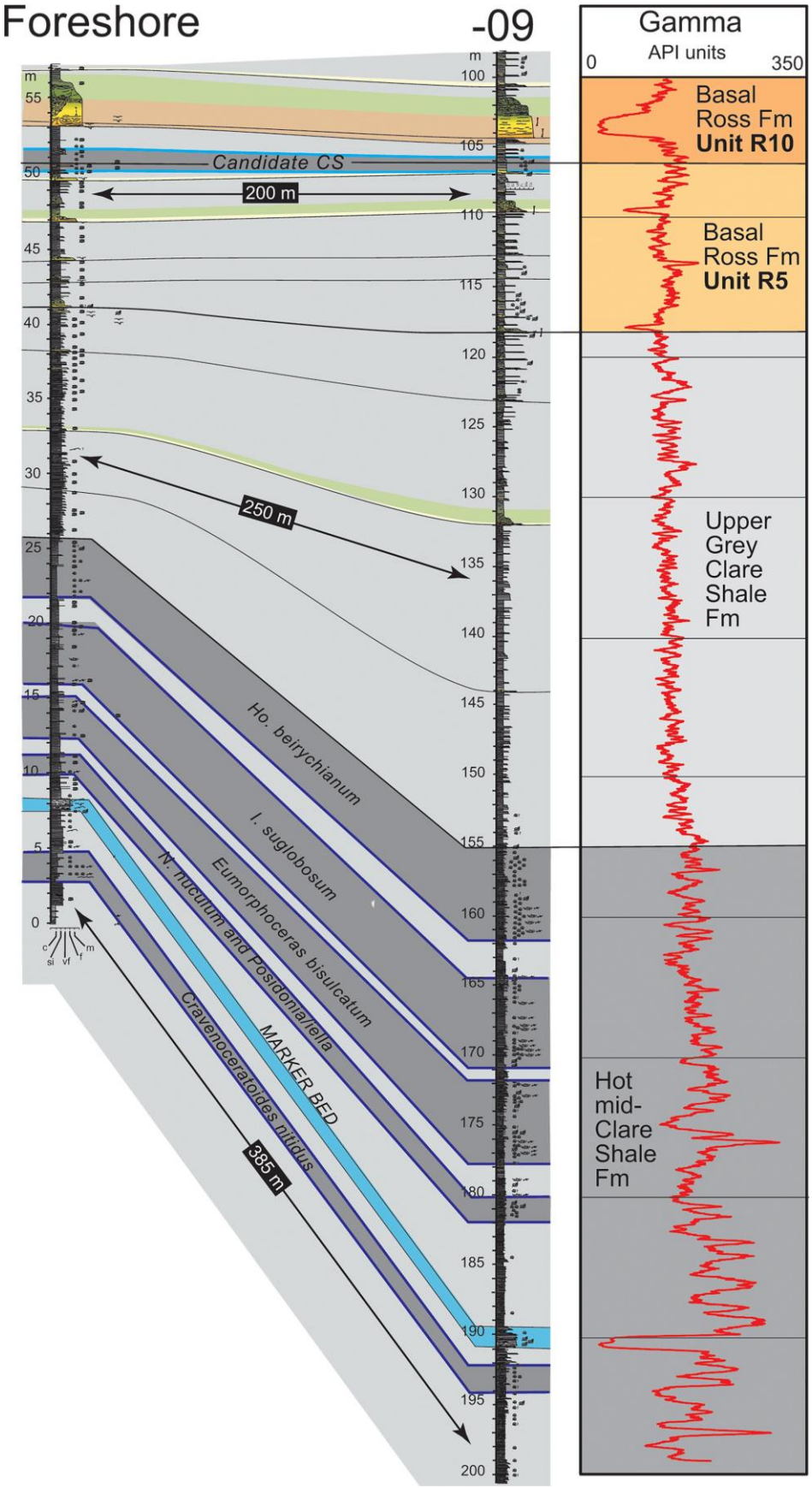
Foreshore
-09
Gamma
API units
0
350
Basal Ross Fm Unit R10
Basal Ross Fm Unit R5
Upper Grey Clare Shale Fm
Hot mid-Clare Shale Fm
Candidate CS
200 m
250 m
385 m
Ho. beirychianum
I. suglobosum
Eumorphoceras bisulcatum
N. nucumum and Posidonia/Ieilla
MARKER BED
Cravenoceratoides nitidus

Figure 6

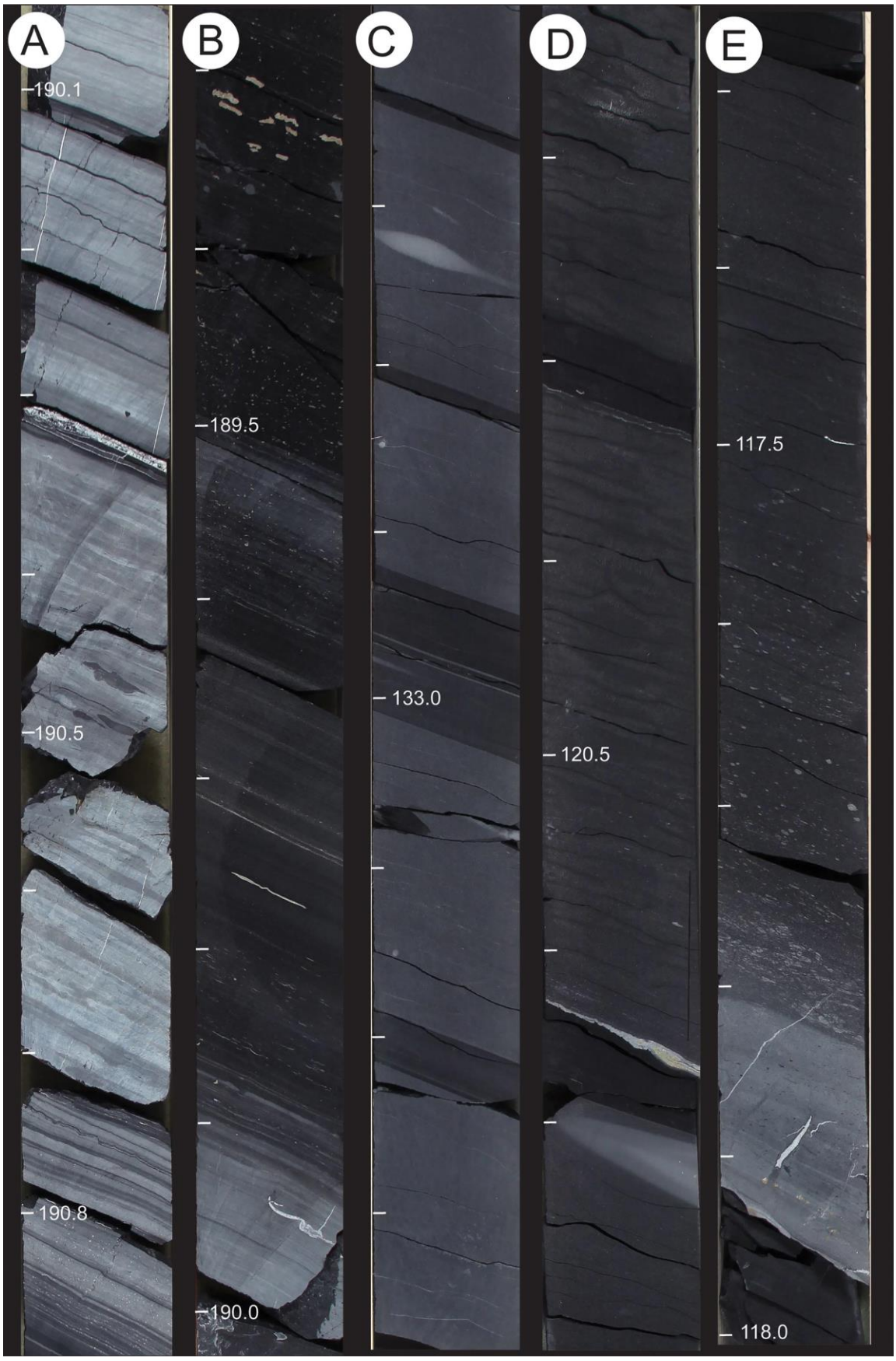

Figure 7

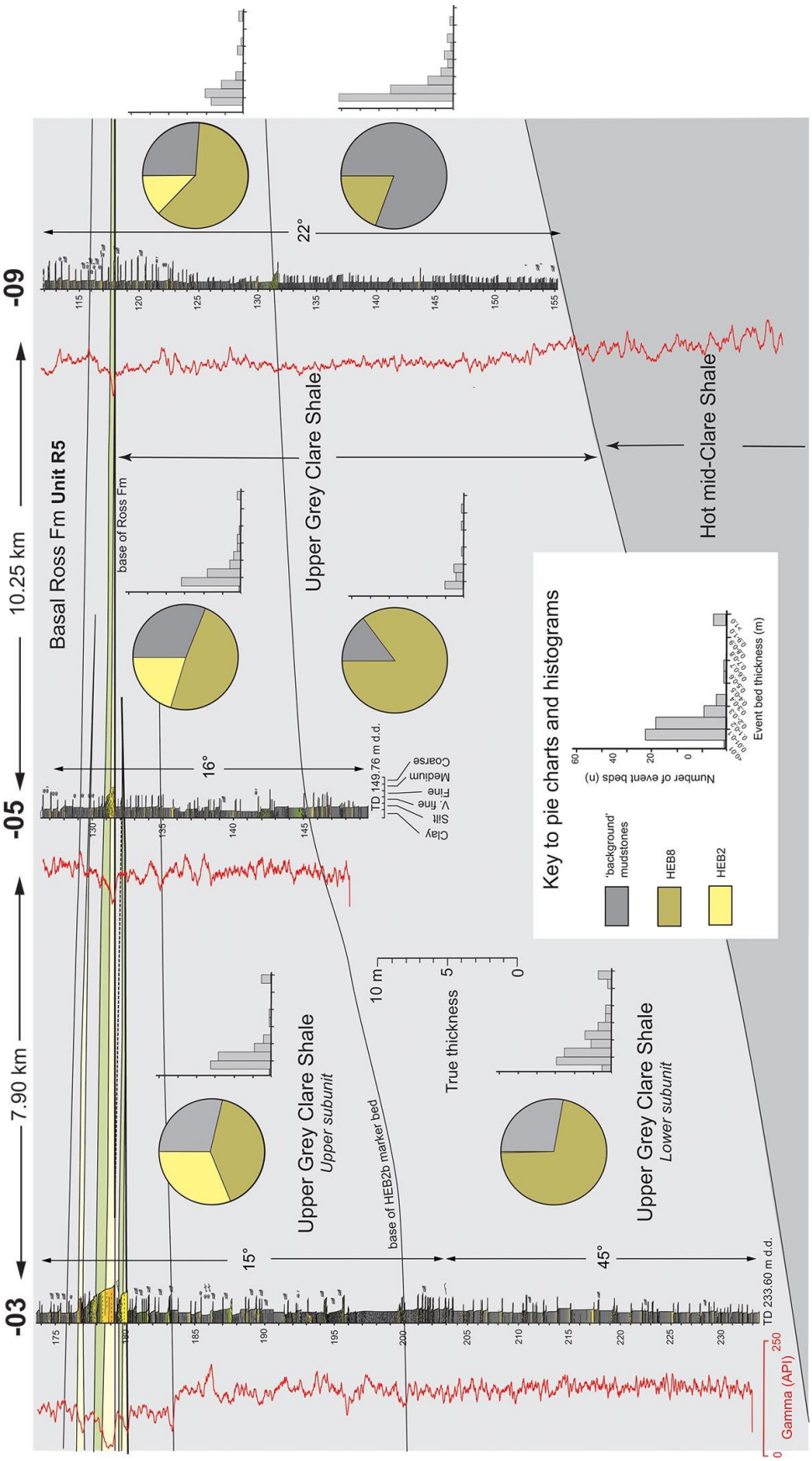
-03
7.90 km
-05
10.25 km
-09
Basal Ross Fm Unit R5
base of Ross Fm
Upper Grey Clare Shale
Hot mid-Clare Shale
Upper Grey Clare Shale
Upper subunit
base of HEB2b marker bed
Upper Grey Clare Shale
Lower subunit
15°
16°
22°
45°
TD 149.76 m d.d.
TD 233.60 m d.d.
Clay
Silt
< fine
Fine
Medium
Coarse
True thickness
10 m
5
0
Key to pie charts and histograms
'background' mudstones
HEB8
HEB2
Number of event beds (n)
Event bed thickness (m)
Gamma (API)
0
250

Figure 8

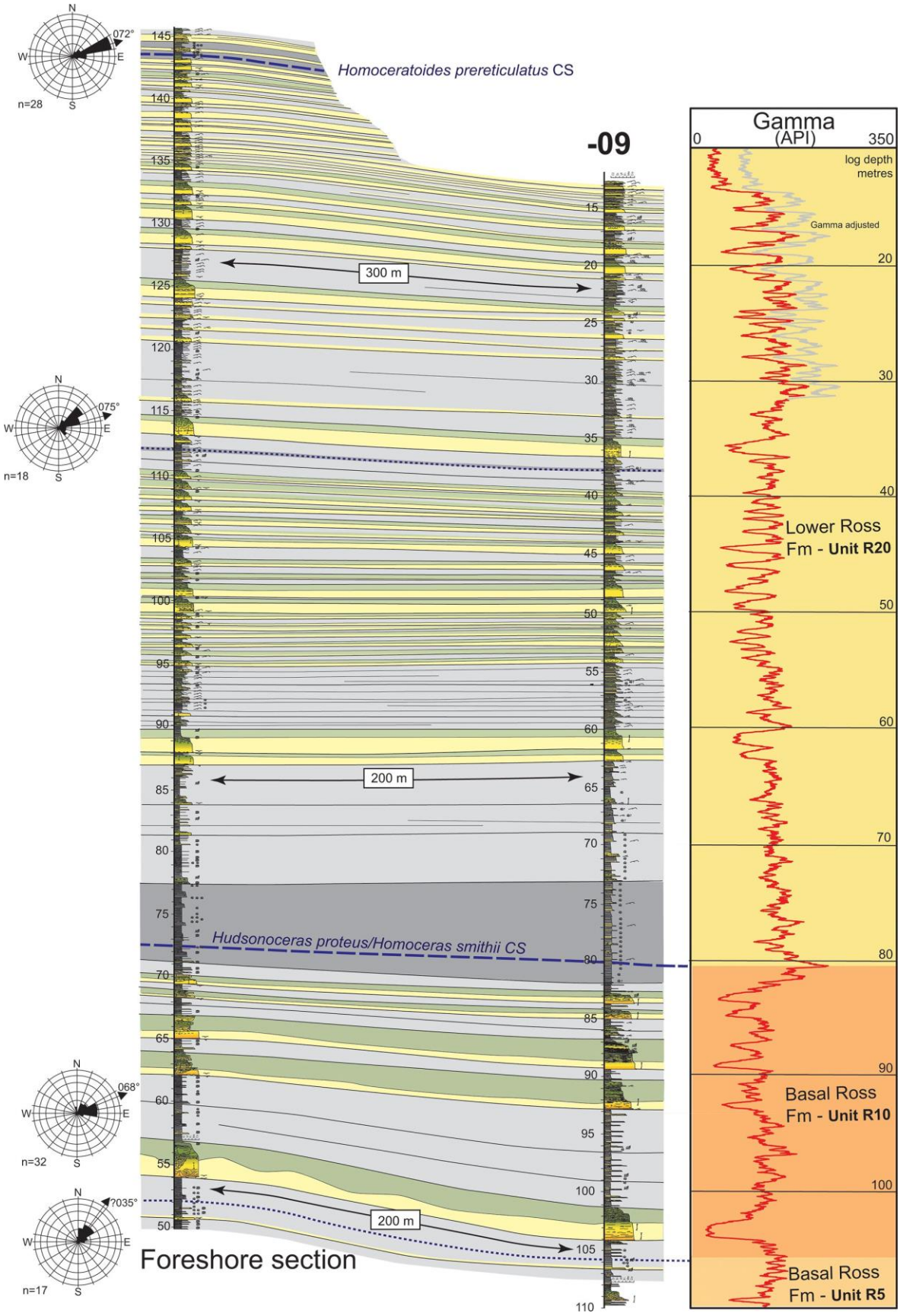
Homoceratoides prereticulatus CS
-09
Gamma
(API)
0
350
log depth
metres
Gamma adjusted
300 m
200 m
200 m
Hudsonoceras proteus/Homoceras smithii CS
Lower Ross
Fm - Unit R20
Basal Ross
Fm - Unit R10
Basal Ross
Fm - Unit R5
Foreshore section
n=28
072°
n=18
075°
n=32
068°
n=17
?035°

Figure 9

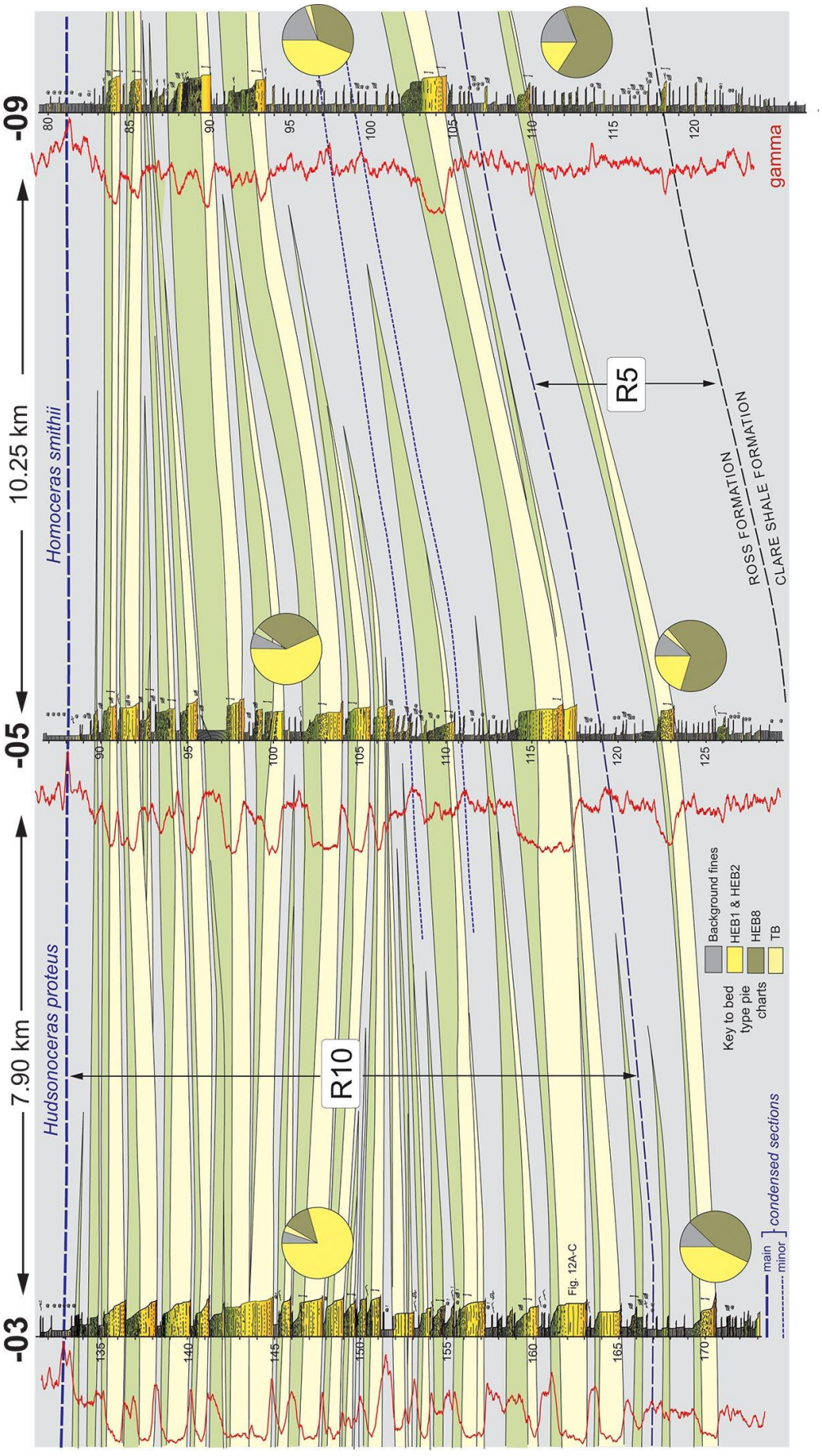
-09
-05
-03
10.25 km
7.90 km
Homoconeras smithii
Hudsonoceras proteus
gamma
R5
R10
ROSS FORMATION
CLARE SHALE FORMATION
Background fines
HEB1 & HEB2
HEB8
TB
Key to bed type pie charts
main
minor
condensed sections
Fig. 12A-C

Figure 10

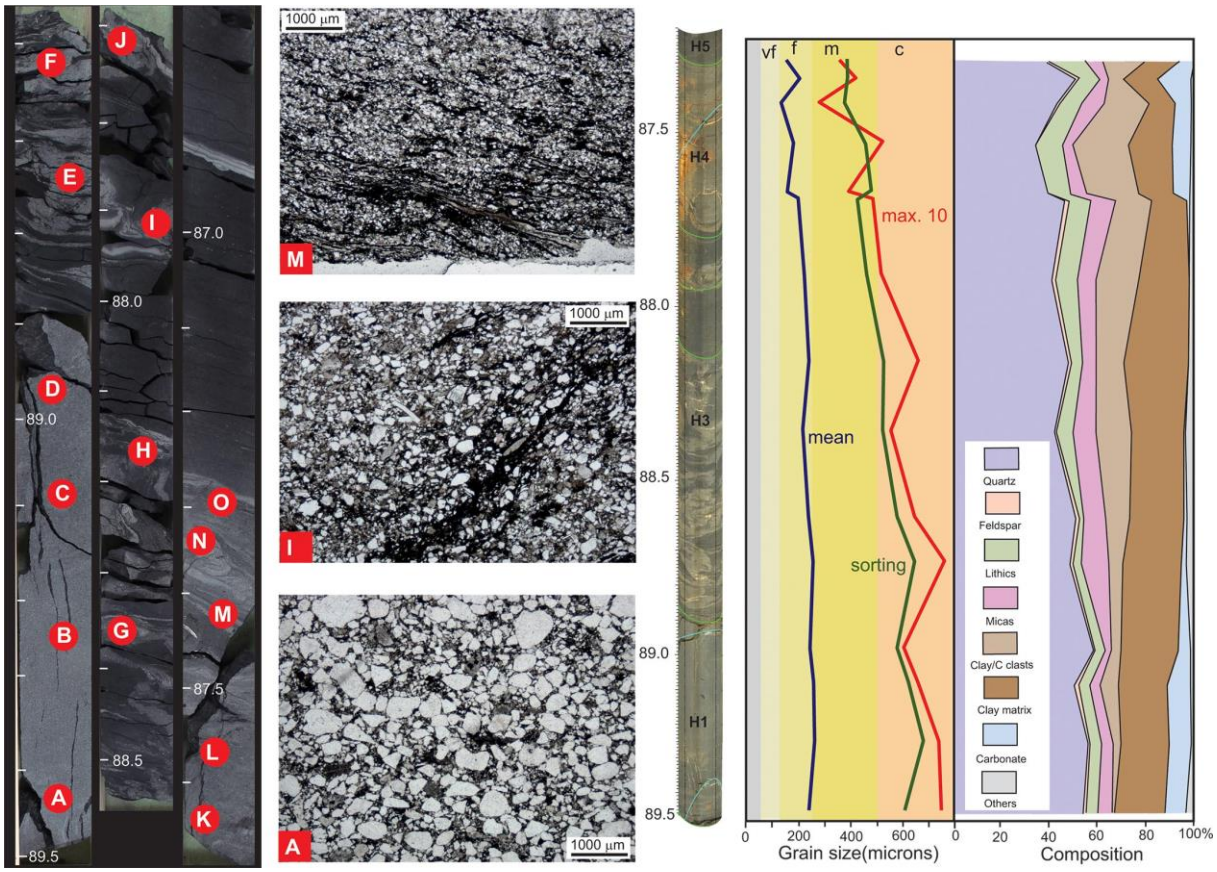
F
J
E
I
87.0
88.0
D
89.0
H
C
O
N
M
B
G
87.5
88.5
L
A
K
89.5
1000 µm
M
1000 µm
I
1000 µm
A
87.5
88.0
88.5
89.0
89.5
H5
H4
H3
H1
vf
f
m
c
max. 10
mean
sorting
Quartz
Feldspar
Lithics
Micas
Clay/C clasts
Clay matrix
Carbonate
Others
0
200
400
600
Grain size(microns)
0
20
40
60
80
100%
Composition

Figure 11

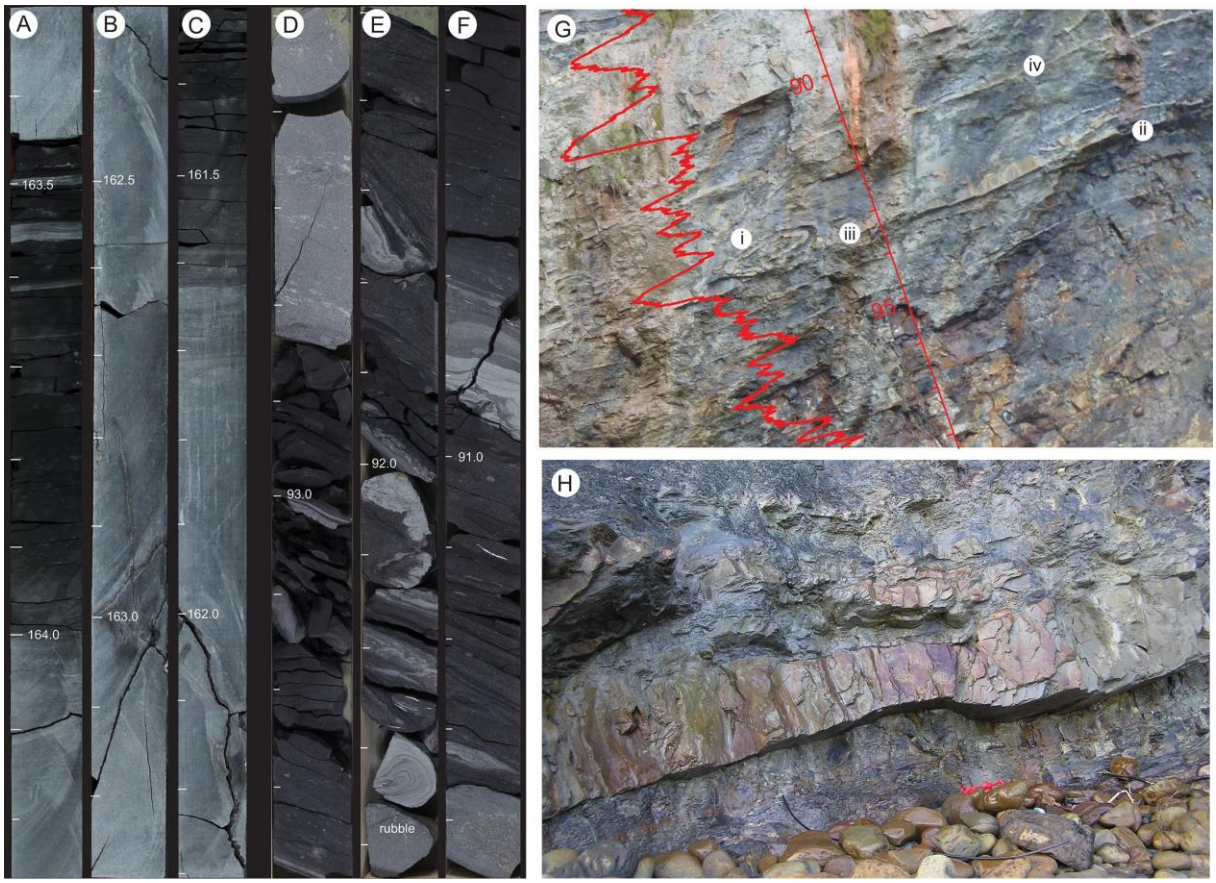
A
B
C
D
E
F
163.5
162.5
161.5
164.0
163.0
162.0
93.0
92.0
91.0
rubble
G
90
95
i
iii
iv
ii
H

Figure 12

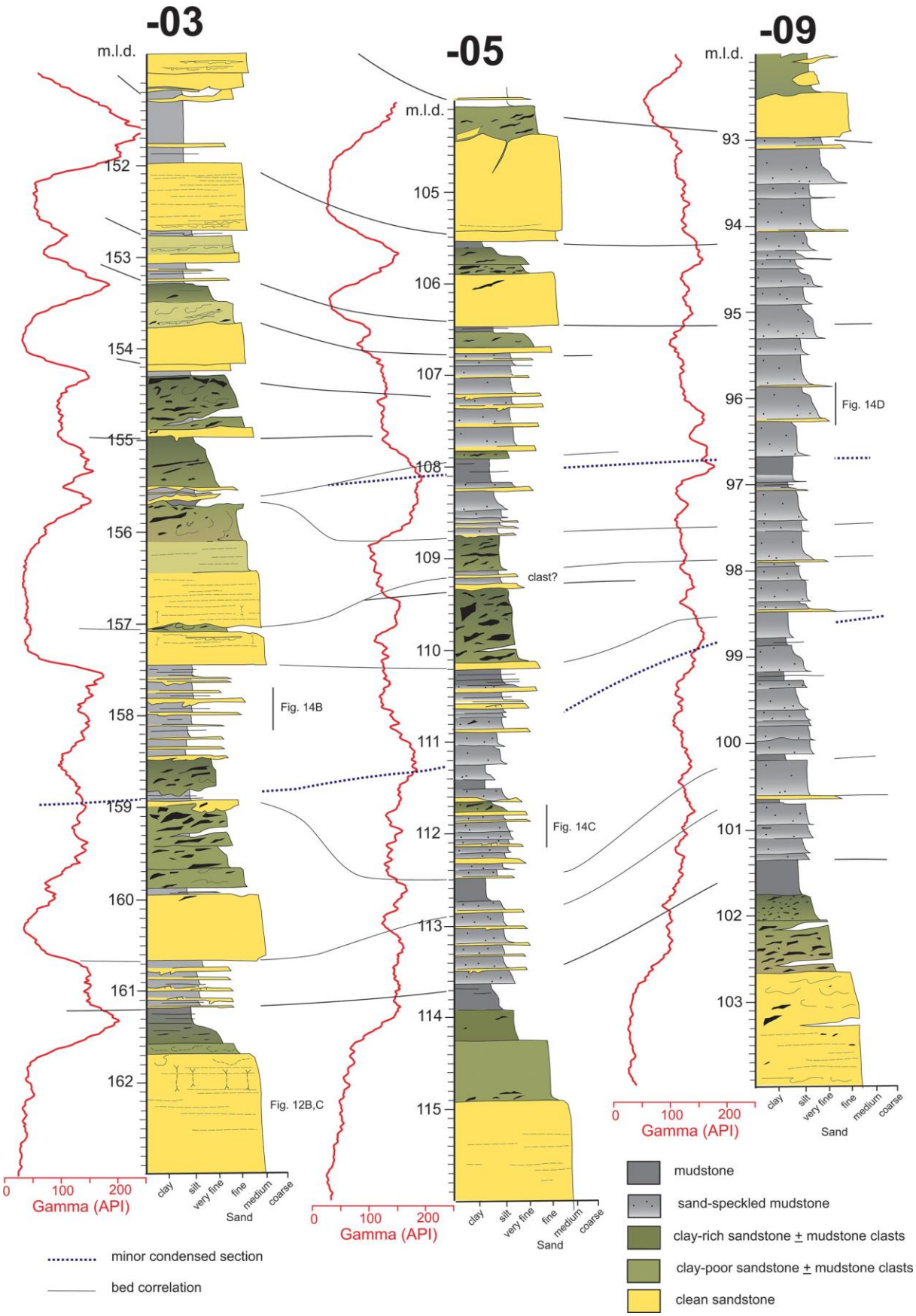
-03
m.l.d.
152
153
154
155
156
157
158
159
160
161
162
Fig. 14B
Fig. 12B,C
0
100
200
Gamma (API)
clay
silt
very fine
fine
medium
coarse
Sand
-05
m.l.d.
105
106
107
108
109
110
111
112
113
114
115
clast?
Fig. 14C
-09
m.l.d.
93
94
95
96
97
98
99
100
101
102
103
Fig. 14D
minor condensed section
bed correlation
mudstone
sand-speckled mudstone
clay-rich sandstone ± mudstone clasts
clay-poor sandstone ± mudstone clasts
clean sandstone

Figure 13

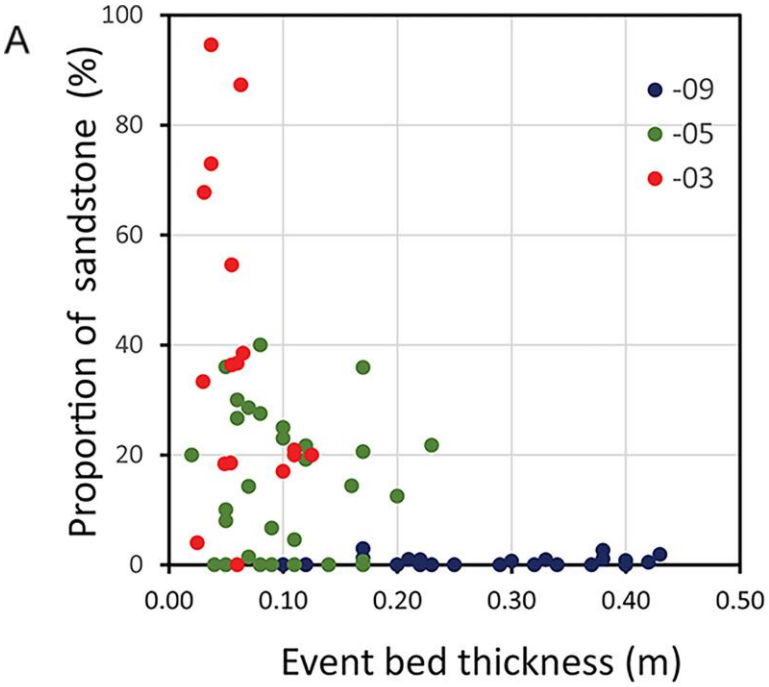
A
Proportion of sandstone (%)
100
80
60
40
20
0
0.00
0.10
0.20
0.30
0.40
0.50
Event bed thickness (m)
-09
-05
-03


B
C
D

Figure 14

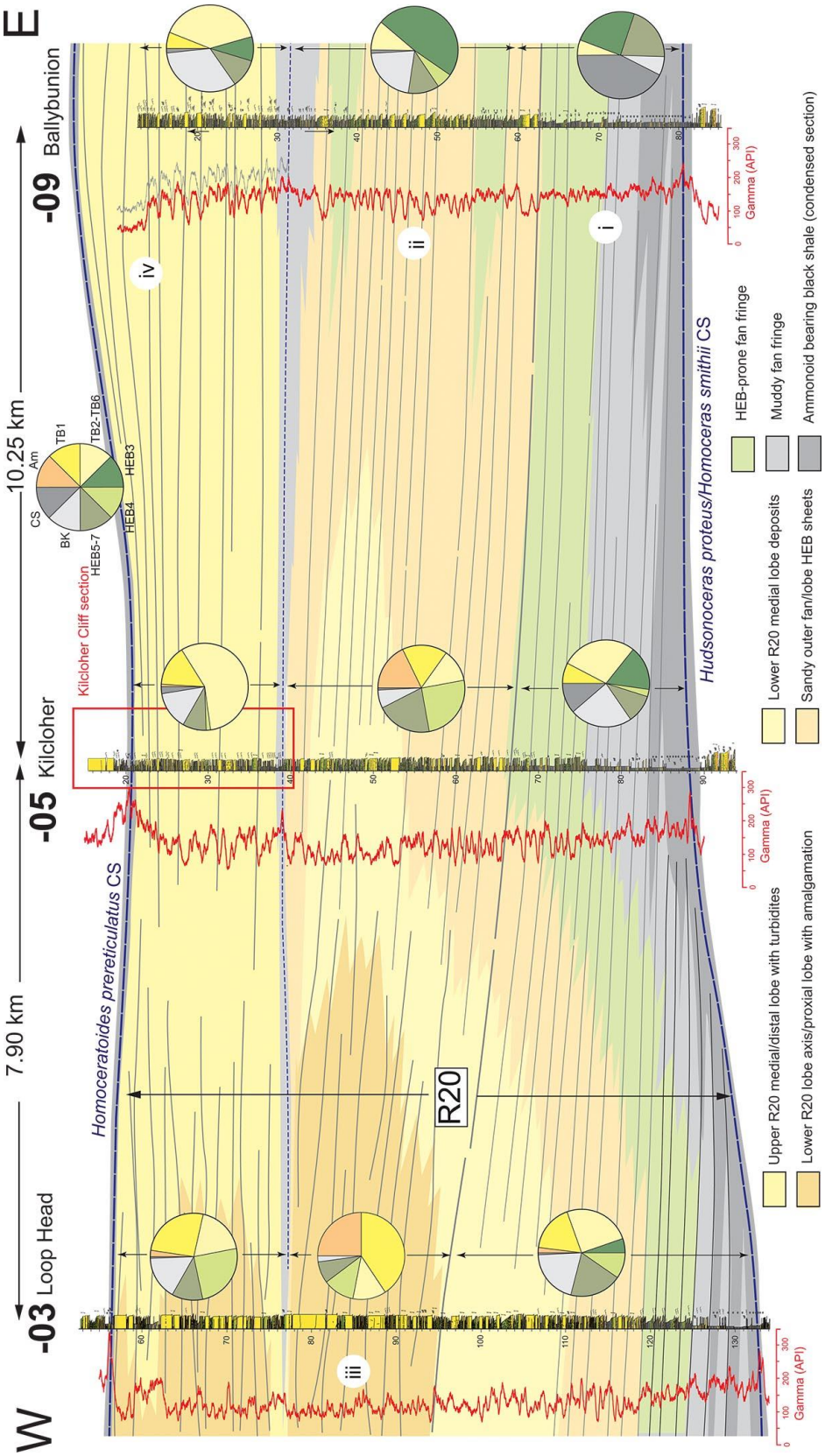
W
E
-03 Loop Head
7.90 km
-05 Kilcloher
10.25 km
-09 Ballybunion
Homoceratoides prereticulatus CS
Hudsonoceras proteus/Homoceras smithii CS
Kilcloher Cliff section
R20
i
ii
iii
iv
CS
Am
BK
TB1
TB2-TB6
HEB3
HEB4
HEB5-7
Gamma (API)
HEB-prone fan fringe
Muddy fan fringe
Ammonoid bearing black shale (condensed section)
Lower R20 medial lobe deposits
Sandy outer fan/lobe HEB sheets
Upper R20 medial/distal lobe with turbidites
Lower R20 lobe axis/proxial lobe with amalgamation

Figure 15

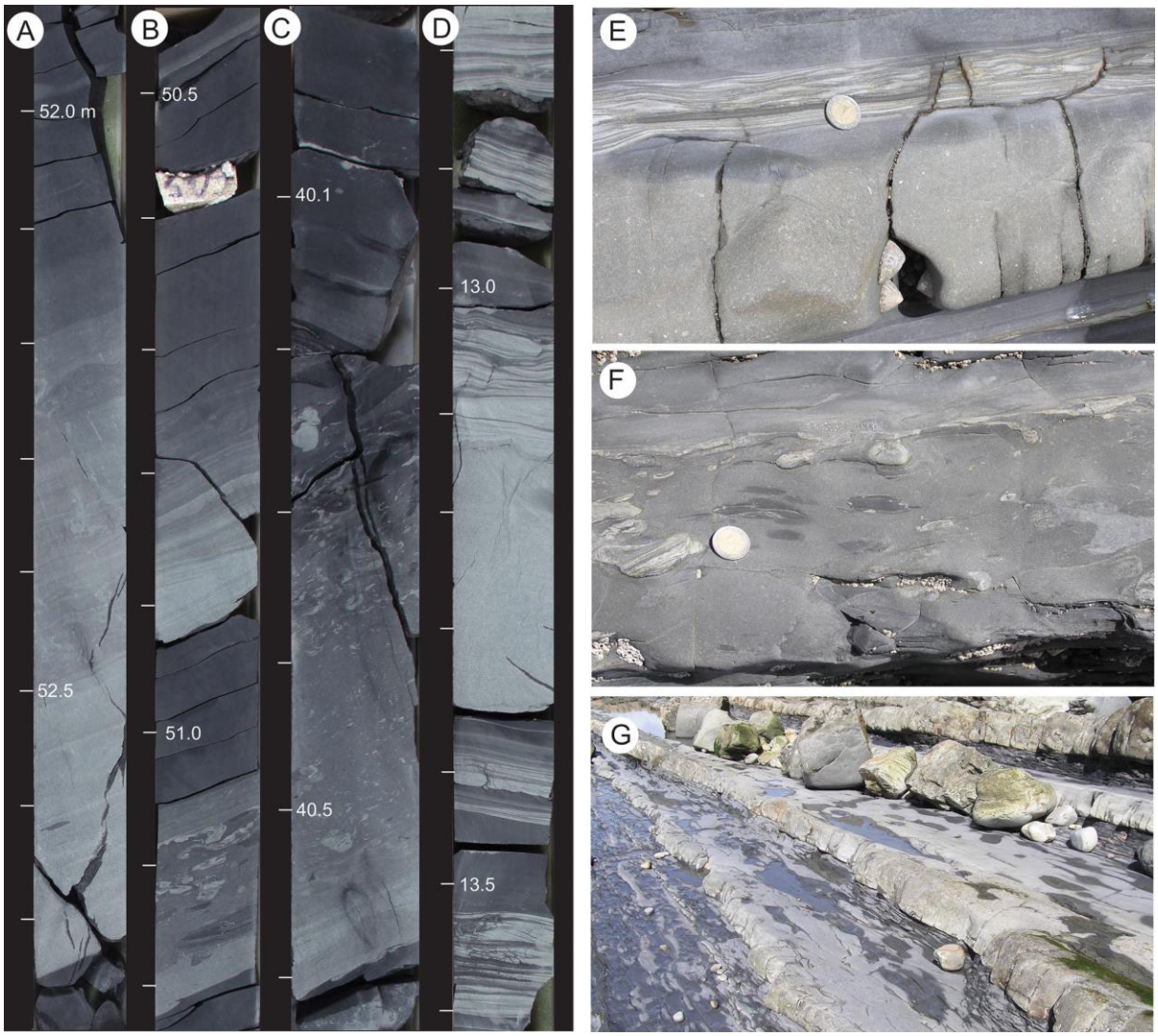

Figure 16

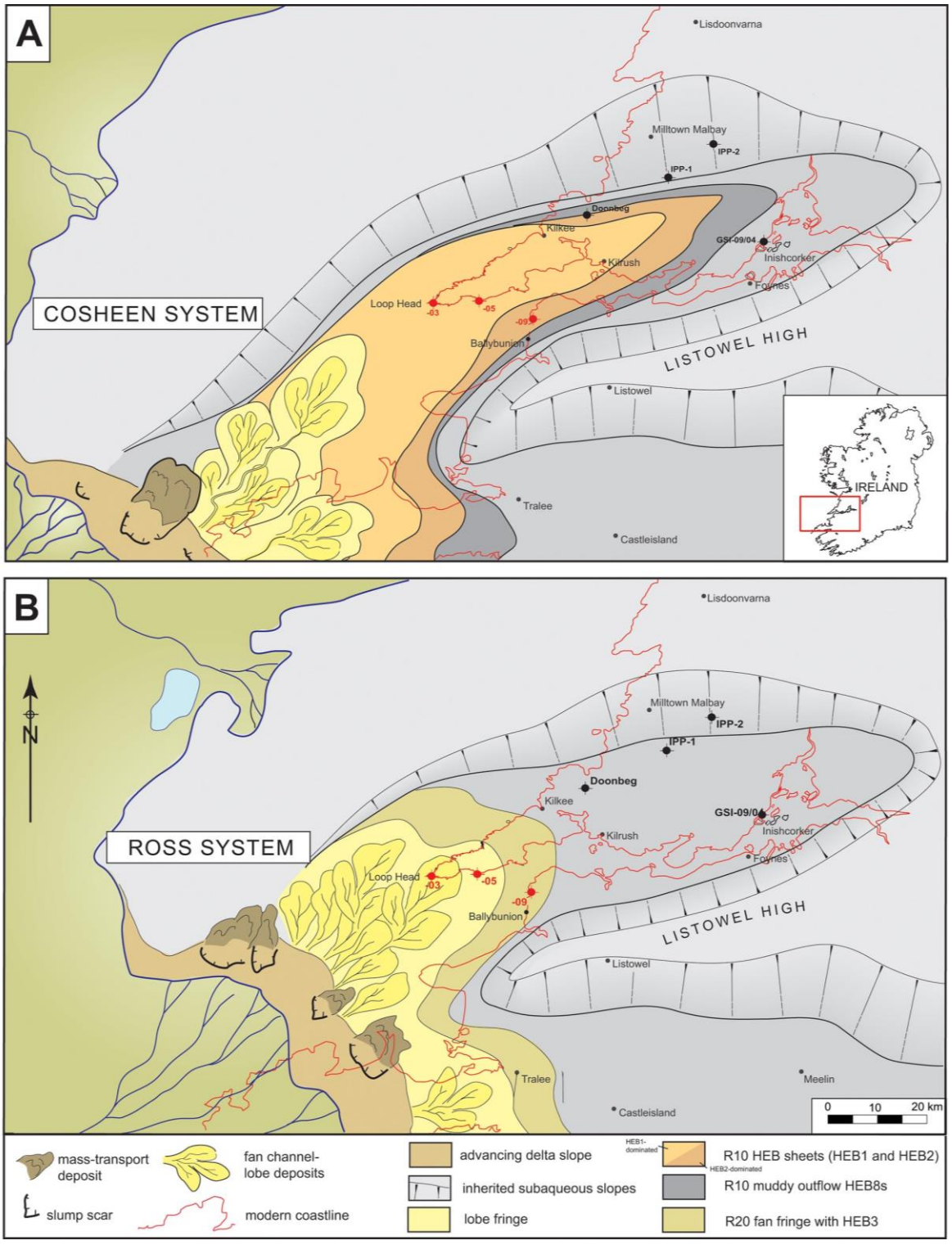
A
Lisdoonvarna
Milltown Malbay
IPP-2
IPP-1
Doonbeg
Kilkee
GSI-09/04
Inishcorker
Kilrush
Foynes
COSHEEN SYSTEM
Loop Head
-03
-05
-09
Ballybunion
LISTOWEL HIGH
Listowel
IRELAND
Tralee
Castleisland
B
N
ROSS SYSTEM
Meelin
0 10 20 km
mass-transport deposit
slump scar
fan channel-lobe deposits
modern coastline
advancing delta slope
inherited subaqueous slopes
lobe fringe
HEB1-dominated
HEB2-dominated
R10 HEB sheets (HEB1 and HEB2)
R10 muddy outflow HEB8s
R20 fan fringe with HEB3

Figure 17

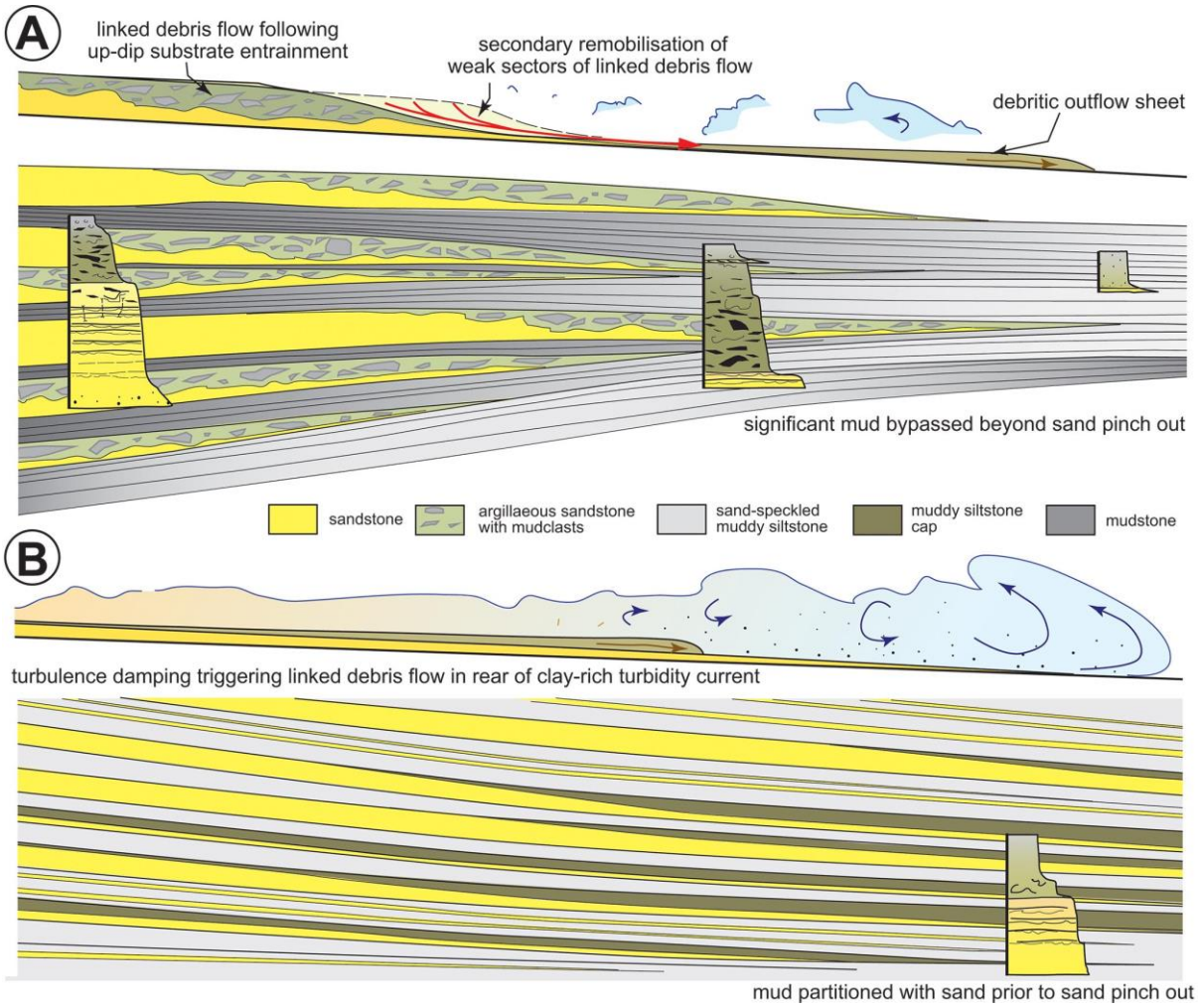
A
linked debris flow following
up-dip substrate entrainment
secondary remobilisation of
weak sectors of linked debris flow
debritic outflow sheet
significant mud bypassed beyond sand pinch out
sandstone
argillaeous sandstone
with mudclasts
sand-speckled
muddy siltstone
muddy siltstone
cap
mudstone
B
turbulence damping triggering linked debris flow in rear of clay-rich turbidity current
mud partitioned with sand prior to sand pinch out

Figure 18

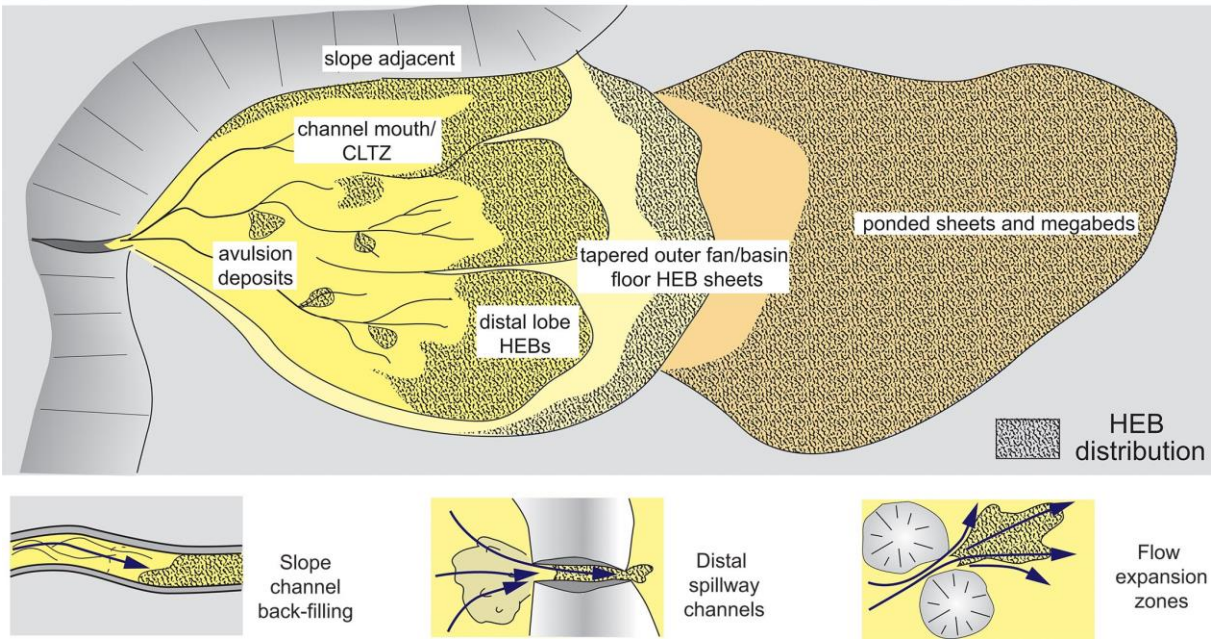
slope adjacent
channel mouth/
CLTZ
avulsion
deposits
tapered outer fan/basin
floor HEB sheets
ponded sheets and megabeds
distal lobe
HEBs
HEB
distribution
Slope
channel
back-filling
Distal
spillway
channels
Flow
expansion
zones

Figure 19

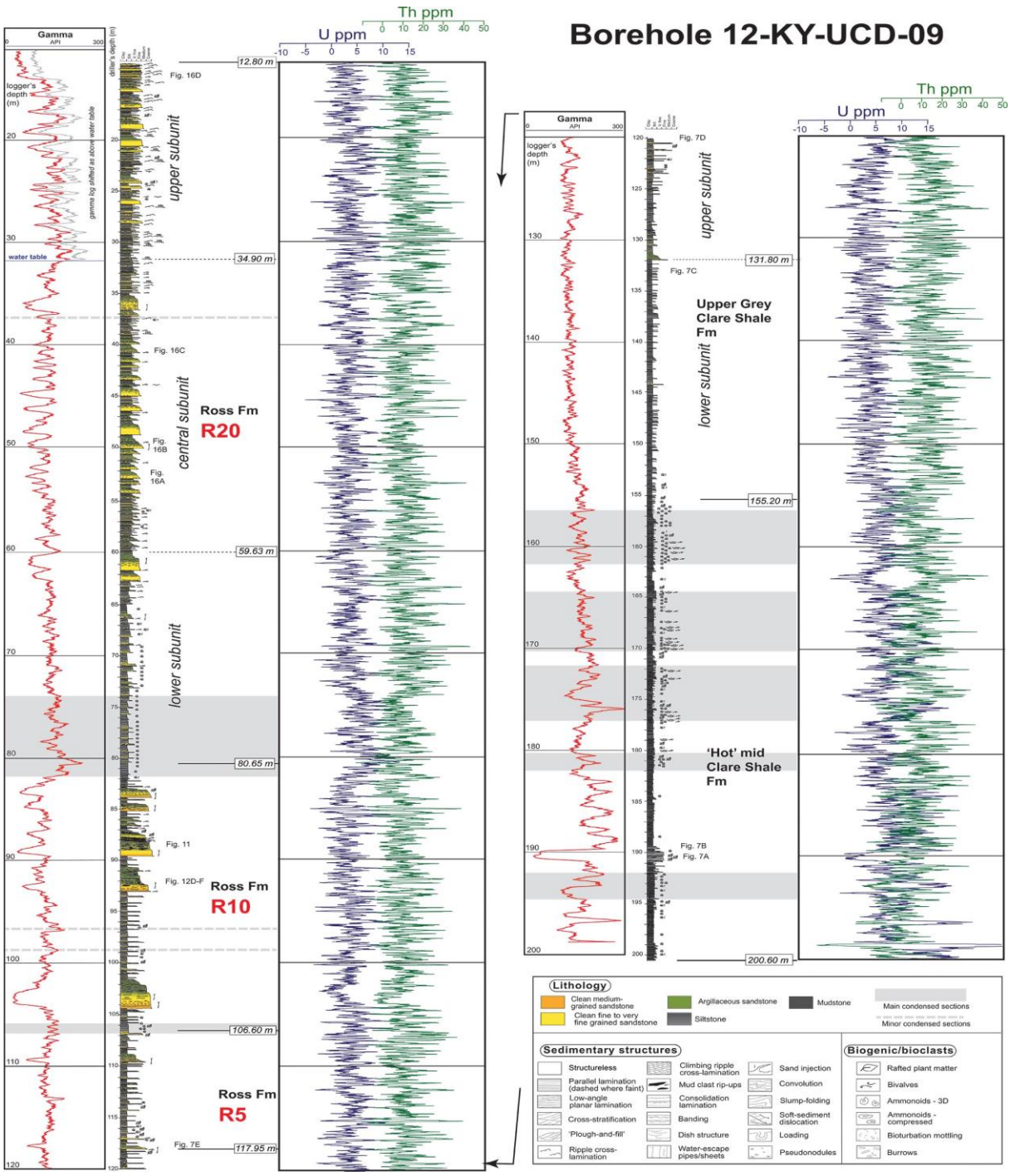

Supplementary Figure 1

Bed Type	Occurrence	Thickness (m)		Grain Size (Range)	Internal divisions	Description
		Range (m)	mean (m)			
HEB1a	R10	0.2-4.1	1.76	silt - c.g sst	H1 < 30%, H2 < 45%, H3 <14%, H5 <2%	H1 grey (N4-5) relatively clean, poorly sorted, structureless, de-watered or diffusely colour-banded graded sandstone with erosional base. H2 is subtly darker grey (N4) and exhibits cm to mm-scale parallel alternation of lighter and darker bands (banding) and dewatering dishes combined with tiered and sheared pipes. H3 has a sharp irregular (erosional and or loaded) base and is a dark grey (N2-3), heterogeneous mix of siltstone and argillaceous sandstone with mudstone clasts some of which show syn-sedimentary folding. Levels of coalified/silicified plant fragments common towards top. H5 is generally thin (cm-scale) grey siltstone and these beds generally lack a H4 division, particularly in the updip -03 and -05 boreholes.
HEB1b	R10	0.2 - 3.7	1.48	silt - c.g sst	H1 <15% , H2 <45%, H3 < 50%, H5 <2%	As for HEB1a, but with a greater proportion of the bed dominated by H3 and reduced proportions of H1. H3 divisions are commonly carbonaceous and the event bed is commonly capped a thin (cm-scale) ripple laminated or banded H4 division and H5 siltstone, the latter with floating sand grains.
HEB2a	R5-R10	0.40 - 3.1	1.25	silt - c.g. sst	H1 / H2 < 15%, H3 <70%, H5 <15%	Relatively thick and coarse-grained event beds with thick H3 as the dominant internal division, with H1 and H2 now typically <15% of the event bed. Basal sandstones are generally medium grained, texturally immature and commonly banded (H2). A sharp internal contact separates the basal sandstone from H3 divisions that are up to 2.1 m thick, dark grey (N2-3) and freighted with abundant mudstone and subordinate sandstone clasts. H3 is overlain by H5 siltstone, or in some cases by a structured H4 sandstone division.
HEB2b	R5-R10	0.5 - 1.7	1.1	silt - m.g. sst	H1 / H2 <8%, H3 <82%, H5 <20%	A subvariant of HEB2 that occurs as thinner and muddier event bed overall. In this case the basal H1 sandstone is very thin (<3%) and may be absent with a a thin banded H2 division sometimes extending to the bed base. The H3 division comprises a highly argillaceous sandstone with pseudonodules and generally lacking or with rare mudstone clasts. The H3 division may have an internal interface distinguishing H3a and H3b (see Hussain et al. 2020). This is capped by a pseudonodular siltsone capping division (H5). H4 is again rare.
HEB3a	R20	0.3 - 1.8	0.85	silt - f.g. sst	H1 <20%, H2 <40%, H3 <20%, H4 <2%, H5 <20%	H1 light grey (N6-7) structureless to dewatered, well-sorted sandstone up to fine sand grade maximum. May contain rare mudstone clasts. H2 divisions relatively well developed with cm-scale banding an prominent darker layers (N4-5). Banding locally soft sediment deformed/contorted/slurried (particlularly at the transition to H3) and grades upwards into sand-speckled mudstone (H3) in which there may be bands of cleaner sandstone, pseudonodules, deformed dewatering structures and/or soft-sediment sheared sandy patches. Mudstone clasts are relatively unimportant at this level but can occur towards top of the division. There is a graded transition to a H5 siltstone division at the top of the event bed that can be relatively thick.
HEB3b	R20	0.11 - 0.3	0.21	silt - f.g.sst	H1 <10%, H2 <30%, H3 <20%, H5 <40%	HEB3b is a thinner and finer grained (max. very fine sand) variant found together with HEB3a in the lower to mid (-09 borehole) part of R20. The basal H1 sandstone is thin or absent with a prominent H2 banded unit, subdued H3 division and a relatively thick H5 siltstone cap.
HEB4a	R20	0.08-0.60	0.35	silt - f.g.sst	H1 >90%, H3 <7%, H4 <2%, H5 <5%	Event bed dominated by a thick H1 division comprising grey-light grey (N6-7), well-sorted, very fine to fine-grained, dominantly structureless sandstone (with occasional faint lamination and water escape features). H2 not obvious but may be cryptic (see XRF bed profiling, Hussain et al. 2020). H3 consists of a homogenous dark grey (N3-4) silty matrix with scattered mudstone clasts and occasional deformed fine-grained sandstone clasts and/or sand-filled fluid escape pipes and is in this case relatively thin. H4 may or may not be present and H5 homogenous dark grey fine grained siltstone (N3-4) is thin (a few cm).
HEB4b	R20	0.20-0.67	0.45	silt - f.g.sst	H1 >70%, H3 <20%, H4 <2%, H5 <5%	A sandstone dominant variant of HEB4 with a more prominent H3 division and reduced proportion of H1. H4 not always present.
HEB5	R20	0.08-0.60	0.12	silt - f.g.sst	H1 >45%, H3 <45%, H4 <5%, H5 <10%	Thinner HEBs in which there is subequal proportions of the H1 (N6-7), cleaner sandy division and argillaceous upper divisions. H1 is very fine to fine grained, subtly normal graded and may be weakly colour banded (H2 equivalent?). H3 (N3-2) is sharp-based muddy sandstone with floating mudstone clasts and deformed sandier patches. This can be capped by a single train of ripple-laminated sandstone (H4) but this may be partly collapsed into H3 or absent. H5 is a sharp-based siltstone (N3-4).
HEB6	R20	0.03 - 0.26	0.07	silt - f.g.sst	H1 <15%, H3 >80% , H4 <5%, H5 <10%	A relatively thin, mud-dominated HEB with a very fine to locally fine grained sandstone H1 division in this case only making up a minor part of the event bed. H3 dominates and is a dark grey (N2-3) well mixed muddy sandstone to sandy mudstone with floating mudclasts and scattered carbonaceous fragments. H3 can include internal interfaces separting subdivisons with different texture and or clast concentrations. H4 is sharp-based and is generally ripple-laminated and the event bed is capped by a thin siltstone.
HEB7	R20	0.01 - 0.64	0.08	silt - v.f.g.sst	H3 >95%, H4 <5%, H5<5%	The distinguished feature of these generally thin HEBs is that they lack a basal H1 or H2 sandstone division. H3 extends to the bed base and dominates. Sand gains entrained in H3 forming pseudonodules are very fine grained and may be vestiges of collapsed H4 divisions that are locally present atop H3 and is very fine grained, very thin and capped by a thin mudstone.

Bed Type	Occurrence	Thickness (m)		Grain Size (Range)	Internal divisions	Description
		Range (m)	mean (m)			
HEB8	CSF, R5, R10	0.01 - 0.4	0.14	silt - v.f.g.sst	N/A	Distinctive, generally thin to very thin HEBs ideally comprising a lower, very fine-grained sandstone, an upper sand speckled mudstone division and a thin capping mudstone. The basal sandstone is not always present and in some cases is just a single laminae. Where thicker it is erosionally based and generally structured, with laminations, ripple lamination or banding (downdip H1 equivalent). It is sharply or in some cases gradationally overlain by sand-speckled mudstone; XRF profiling reveals variable vertical patterns in the sandy mudstones - in some cases they are weakly graded, in others they are ungraded (H3 equivalent). Locally they contain remnants of mudstone clasts but more often they are well mixed. They are capped a sharp change to a minor thin siltstone that completes the event bed.
TB1	R20	0.24 - 0.67	0.40	silt - f.g.sst	Ta >95%, Tc < 3%, Te <2%	Relatively thick sandstone-dominated event beds with mainly structureless, well-sorted lower division (Ta) comprising fine to very fine grained, subtly graded sand (N6-7) with a sharp erosional base and common dewatering pipes and dish structures. Cm-scale mudstone clasts can occur in basal portion of the sandstone and coalified woody material at the top of the event bed with a sharp change to a single train of current ripples in very fine-grained sandstone (Tc). The event bed is topped by a thin siltstone cap (Te) that can contain scattered silicified wood fragments.
TB2	R20	0.28-0.64	0.30	silt - f.g.sst	Ta <10%, Tb>80% , Tc < 5% , Te <5%	Resembling TB1 apart from having more obviously structured fine to commonly very fine-grained sandstone that dominates the event bed in the form of parallel lamination (Tb). There may be a subordinate structureless at the base. Again, the event bed is capped by a single set of ripple cross-laminations (Tc) and a thin mudstone(Te).
TB3	R20	0.16-0.43	0.20	silt - f.g.sst	Ta <40%, Tb <50%, Tc <5%, Td/e<5%	Moderately thickly bedded graded event bed closely resembling a full Bouma-style turbidite with a basal Ta division and parallel-laminated Tb and capping Tc ripple-laminated sandstone (with more than one co-set). Structureless and structured sandstone occur in roughly equal proportions. The event is capped by a thin (cm-scale) laminated (Td) to structureless siltstone (Te).
TB4	R20	0.06-0.15	0.01	silt - f.g.sst	Ta<95%, Te<20%	An uncommon thin event bed comprising a structureless Ta division (N6) directly overlain a silty mudstone cap (Te, N4).
TB5	R20	0.04-0.27	0.06	silt - v.f.g.sst	Tc/d <90%, Te<30%	Thin to moderately thick, fully structured (Ta-absent), very fine-grained sandstones (N6-7) dominated by well-defined parallel (Tb) and ripple-lamination (Tc) and capped by a subordinate siltstone division (Te; N4).
TB6	R20	0.01-0.05	0.02	silt - v.f.g.sst	Tc <60%, Te<40%	Very thin to thin-bedded (cm scale), fully structured, dominantly ripple-laminated, very fine-grained sandy event beds capped by subordinate siltstones commonly arranged in stacks involving multiple very thin TB6 beds.
Am	R20			v.f.to f. sst	N/A	Thicker sandstone intervals in which the sandy divisions of event beds are amalgamated such that without the bed tops it is impossible to know whether the flows were turbidity currents or hybrid flows.
Bk	All			silt	N/A	Structureless to thinly bedded medium to dark grey fine siltstones with mm-scale coarse siltsone/v.fine sandstone laminae.
CS	All			clay-fine silt	N/A	Black, fossilferous, carbonaceous mudstones with ammonoid fauna and local calcite-cemented nodules.

Table 1